الجمهورية الجزائرية الديمقراطية الشعبية
République Algérienne Démocratique et Populaire
وزارة التعليم العالي والبحث العلمي
Ministère de l'Enseignement Supérieur et de la Recherche Scientifique

Université Mohamed Khider – Biskra
Faculté des Sciences et de la technologie
Département : Génie Civil et Hydraulique
Ref : ……

جـــامعة محمد خـيـضر بـــسكرة
كـلية الـعلـــوم و التكـــنولوجـيا
قسـم : الهنـدسـة المـدنيـة و الــري
المـرجع : .....

Thèse présentée en vue de l'obtention

Du diplôme de

Doctorat LMD en Génie Civil

Option : Modélisation numérique en génie civil

Estimation des pressions de terre dynamique sur les structures de soutènement

---

Présentée par :

DRAM Abdelkader

Soutenue publiquement le : 23/09/2021

Devant le jury composé de :

Pr. BELOUNAR Lamine	**Professeur**	**Président**	**Université de Biskra**
Pr. BENMEBAREK Sadok	**Professeur**	**Rapporteur**	**Université de Biskra**
Pr. KHEMISSA Mohamed	**Professeur**	**Examinateur**	**Université de M'Sila**
Dr. HOUHOU Mohamed Nabil	**Maitre de Conférences 'A'**	**Examinateur**	**Université de Biskra**

ACKNOWLEDGEMENTS

First and foremost, I wish to give all the praise to Almighty God for giving me the strength and time to complete this research.

I wish to express my deepest gratitude to my supervisor and co-supervisor, Professor Sadok Benmebarek, and professor Umashankar Balunaini for their constant encouragement, wisdom guidance, and helpful advice, comments, and suggestions during the undertaking of this research. They provided me with all kinds of support during my PhD study.

First, I would like to express my sincere gratitude to Prof. B. Umashankar; Dr. S.M. Sravanam, and Prof. M. R. Madhav, Department of Mechanical and Aerospace Engineering, IIT Hyderabad, for their insightful suggestions and support throughout my work. I learned a lot from them. Their approach to problem-solving has inspired me a lot. Also, I am proud to say that I am associated with Prof. B. Umashankar.

I wish to express my sincere thanks to the Algerian Ministry of Higher Education and Scientific Research for funding his Ph.D. program. He also thanks to the Indian Institute of Technology Hyderabad for co-hosting his Ph.D. research work.

I would also like to thank Professor BELOUNAR Lamine of the University of Biskra, for having done me a great honor by accepting to chair the jury of this thesis.

I also thank Professors KHEMISSA Mohamed (Université of M'Sila), and HOUHOU Mohamed Nabil (University of Biskra), first of all for doing me honor by agreeing to participate in the jury for this thesis, and also for the time and interest they took in this research by agreeing to examine this work.

I would like to express my deepest gratitude to my father, my mother, my brothers, my sisters for their unflinching support, encouragement and love. Without them, this would not have been possible.

Finally, my deepest appreciation goes to all members and friends of both the Department of Civil Engineering and Hydraulic, NMISSI Laboratory, Biskra University, and Department of Civil Engineering, IIT Hyderabad, Kandi, Telangana, 502285, India, who supported me in all respects during my PhD research.

ABSTRACT

Earth retaining structures represent an essential component of many civil engineering works. These structures are used in numerous infrastructure projects and are often exposed to a differential settlement problem in the backfill area of the structures because of the different characteristics of the settlement between the structures and backfill soils. However, seismic mitigation techniques are becoming matters of interest of reducing the lateral earth pressures of the earth retaining structures, lightweight (compressible) novel materials have entered the practice that effectively serves the purpose where civil engineering projects can positively subscribe to a sustainable society.

This thesis presents the finite element program PLAXIS 2D investigating the performance of the seismic behavior of two retaining wall types – a cantilever retaining wall, made up of compressible tire shreds as a cushion between the wall and the backfill, and connected and unconnected back-to-back mechanically stabilized earth walls.

The use of recycled tire shreds as a compressible inclusion behind cantilever retaining wall is one of the novel ways to reduce the seismic earth pressures acting on the wall. The response of a typical cantilever retaining wall, consisting of compressible tire shreds (CTS) as a cushion, under earthquake ground motion applied at the wall base. The numerical model was first validated against experimental shake table test results available in the literature. To quantify the benefit of CTS cushion, a comparison was made in the behavior of wall without and with cushion in terms of horizontal displacement and rotation, the maximum shear force and bending moment, the seismic earth thrust, and its point of application on the wall. The results from the analysis indicate that the dynamic earth thrust against the wall reduced considerably due to the presence of cushion made up of compressible tire shreds.

The behavior of connected and unconnected back-to-back mechanically stabilized earth walls under earthquake loading is also analyzed. The numerical model was first validated with the results from the full-scale dynamic centrifuge tests on reinforced soil retaining walls. The behavior of connected and closely-spaced unconnected walls (BBMSE) were compared in terms of tensile forces mobilized in geogrids, and the lateral earth pressures and maximum displacements of the wall. The total seismic earth thrusts at the end of the reinforced zone and at the facing of BBMSE walls and their points of application were presented. These results were compared with the widely used Mononobe-Okabe method. The connected walls were found to significantly reduce the dynamic loads on the walls compared to those on unconnected walls.

Keywords: Seismic earth pressure; Reinforced soil; Geogrid; Back-to-back walls; Tire shreds; Compressible inclusion; Retaining walls; Finite element analysis.

RÉSUMÉ

Les structures de soutènement en terre représentent une composante essentielle de nombreux travaux de génie civil. Ces structures sont utilisées dans de nombreux projets d'infrastructure et sont souvent exposées à un problème de tassement différentiel dans la zone de remblai des ouvrages en raison des différentes caractéristiques de tassement entre les ouvrages et les sols de remblai. Cependant, les techniques d'atténuation sismique deviennent des sujets d'intérêt pour réduire les pressions latérales de la terre des structures de soutènement de la terre, de nouveaux matériaux légers (compressibles) sont entrés dans la pratique qui sert efficacement l'objectif où les projets de génie civil peuvent souscrire positivement à une société durable.

Cette thèse présente le code éléments finis PLAXIS 2D pour étudier la performance du comportement sismique de deux types de murs de soutènement – un mur de soutènement cantilever, composé de pneus déchiqueter (lambeaux de pneus) compressibles comme coussin entre le mur et le remblai, et connectés et non connectés des murs à double parement en sol renforcé par géosynthétique.

L'utilisation de lambeaux de pneus recyclés comme inclusion compressible derrière le mur de soutènement en porte-à-faux est l'un des nouveaux moyens de réduire les pressions sismiques de la terre agissant sur le mur. La réponse d'un mur de soutènement cantilever, constitué de lambeaux de pneus compressibles (CTS) comme coussin, sous un mouvement du sol sismique appliqué à la base du mur. Le modèle numérique a d'abord été validé par rapport aux résultats des tests expérimentaux sur table vibration disponibles dans la littérature. Pour quantifier le bénéfice du coussin CTS, une comparaison a été faite dans le comportement du mur sans et avec coussin en termes de déplacement horizontal et de rotation, la force de cisaillement maximale et le moment de flexion, la poussée sismique de la terre et de point d'application sur le mur. Les résultats de l'analyse indiquent que la poussée dynamique de la terre contre la paroi s'est considérablement réduite en raison de la présence d'un coussin constitué de lambeaux de pneus compressibles.

Le mur de soutènement en sol renforcé à double parement (murs opposés) des connectés et non connectés est également analysé. Le comportement des murs non reliés connectés (BBMSE) et a été comparé en termes de forces de traction dans les géogrilles, et les pressions latérales de la terre et les déplacements maimaux de la mur. Les poussées sismiques totales de terre à l'extrémité de la zone renforcée et au parement des murs BBMSE et points d'application ont été présentés. Ces résultats ont été comparés à la méthode Mononobe-Okabe largement utilisée. On a constaté que les murs connectés réduisaient considérablement les charges dynamiques sur les murs par rapport à ceux des murs non reliés.

Mots clés: pression sismique de la terre; Sol renforcé; Geogrid; murs à double parement; Lambeaux de pneus; Inclusion compressible; Murs de soutènement; Analyse des éléments finis.

ملخـــــــــص

تمثل هياكل الاحتفاظ بالأرض عنصرًا أساسيًا في العديد من أعمال الهندسة المدنية. تُستخدم هذه الهياكل في العديد من مشاريع البنية التحتية وغالبًا ما تتعرض لمشكلة تسوية في منطقة ردم الهياكل بسبب الخصائص المختلفة للتسوية بين الهياكل وتربة الردم. ومع ذلك ، أصبحت تقنيات التخفيف من الزلازل من الأمور ذات الأهمية للحد من ضغوط الأرض الجانبية للهياكل الاحتفاظ بالأرض ، وقد دخلت المواد الجديدة خفيفة الوزن (القابلة للضغط) في الممارسة التي تخدم بشكل فعال الغرض حيث يمكن لمشاريع الهندسة المدنية الاشتراك بشكل إيجابي في مجتمع مستدام.

تقدم هذه الرسالة برنامجًا فريدًا من عناصر PLAXIS 2D المحدودة التي تبحث في أداء السلوك الزلزالي لنوعين من الجدران المحتجزة - جدار احتفاظ ناتئ ، مكون من شظايا إطارات قابلة للضغط كوسادة بين الجدار والردم ، متصلة وغير متصلة من ظهر إلى ظهر بجدران أرضية مستقرة ميكانيكيًا.

يعد استخدام شظايا الإطارات المعاد تدويرها كإدراج قابل للضغط خلف جدار الاحتفاظ الكابولي إحدى الطرق الجديدة لتقليل ضغوط الأرض الزلزالية التي تعمل على الجدار. استجابة جدار احتفاظ ناتئ نموذجي ، يتكون من شظايا إطار مضغوط كوسادة (CTS) ، تحت حركة أرضية زلزال مطبقة على قاعدة الجدار. تم التحقق من صحة النموذج العددي لأول مرة مقابل نتائج اختبار طاولة الاهتزاز التجريبية المتوفرة في الأدبيات. لتقدير فائدة وسادة CTS ، تم إجراء مقارنة في سلوك الجدار بدون ومع وسادة من حيث الإزاحة الأفقية والدوران ، وقوة القص القصوى ولحظة الانحناء ، ودفع الأرض الزلزالي ، ونقطة التطبيق على الجدار. تشير نتائج التحليل إلى أن الدفع الأرضي الديناميكي على الجدار قد انخفض بشكل كبير بسبب وجود وسادة مكونة من شظايا الإطارات القابلة للضغط.

يتم أيضًا تحليل سلوك الجدران الأرضية المستقرة ميكانيكيًا والمتصلة وغير الموصلة تحت تحميل الزلزال. تم التحقق من صحة النموذج العددي أولاً بالنتائج من اختبارات أجهزة الطرد المركزي الديناميكية واسعة النطاق على الجدران الاستنادية للتربة. تمت مقارنة سلوك الجدران (BBMSE) المتصلة و المتقاربة من حيث قوى الشد التي تم حشدها في الشبكات الجيولوجية ، وضغوط الأرض الجانبية والحد الأقصى من عمليات النزوح للجدار. تم تقديم دفعات الأرض الزلزالية الإجمالية في نهاية المنطقة المقواة وفي مواجهة جدران BBMSE ونقاط تطبيقها. تمت مقارنة هذه النتائج مع طريقة Mononobe-Okabe المستخدمة على نطاق واسع. تم العثور على الجدران المتصلة لتقليل الأحمال الديناميكية على الجدران بشكل كبير مقارنة بتلك الموجودة على الجدران غير المتصلة.

كلمات مفتاحية: ضغط الأرض الزلزالي، من الخلف إلى الخلف الجدران، شظايا الإطارات إدراج قابل للضغط الجدران الاستنادية؛ تحليل العناصر المحدودة.

CONTENTS

LIST OF ABBREVIATIONS

LIST OF FIGURES

LIST OF TABLES

First Part: Literature Review

Chapter 1

Analytical approach in order to estimate the seismic earth pressure

Chapter 2

Scrap tire-derived and geosynthetic geomaterials for geoengineering applications

Second Part: Numerical Modeling

Chapter 3

Performance of retaining walls with compressible inclusions under seismic loading

Chapter 4

Seismic performance of cantilever retaining walls with tire shreds as compressible inclusion

Chapter 5

Earthquake response of connected and unconnected back-to-back

LIST OF ABBREVIATIONS

a	acceleration
g	acceleration due to gravity
f_{max}	maximum frequency of the seismic input motion
f	frequency of the seismic input motion
f_n	natural frequency of soil mass
λ_{min}	wavelength of shear wave
α, β	Rayleigh damping parameters
K	stiffness matrix of the system
M	mass matrix of the system
F_h	horizontal inertial force
F_v	vertical inertial force
H	height of the retaining wall
h	application point locations of the dynamic thrust

Δx	lateral displacement of the stem
z	height of the stem
t	thickness of tire shreds cushion
γ	unit weight of the soil
E	Young's modulus
φ	friction angle of backfill
ψ	dilatancy angle
δ'	interface friction angle
c	cohesion
ν	Poisson's ratio
v_s	shear wave velocity
R_{inter}	interface strength-reduction factor
EA	elastic stiffness
EI	flexural rigidity
θ	rotation of the stem
N^*	normalized shear force
M^*	normalized bending moment
σ^*_E	normalized seismic earth pressure
σ_h	effective vertical pressure
σ_v	effective lateral confining pressure
P_{stem}	seismic earth pressure thrust at the stem
P_{heel}	seismic earth pressure thrust at the vertical section the heel
L	reinforcement length
D	distance between two opposing walls
$Tmax$	maximum tensile force in each reinforcement
S_H	horizontal spacing between reinforcement
S_V	vertical spacing between reinforcement
K_A	earth pressure coefficient
P_A	static active earth pressure
K_{AE}	total (static and dynamic) earth pressure coefficient
ΔK_{AE}	incremental dynamic earth pressure coefficient
P_{AE}	total thrust (static and dynamic)

ΔP_{AE}	incremental dynamic earth thrust
M-O	Mononobe-Okabe
S-W	Seed and Whitman
2D	two-dimensional
LVDT	linear variable displacement transformers
STD	scraps tire-derived
TDA	Tire Derived Aggregate
STC	sand–tire chips
EPS	expanded polystyrene
BBMSE	Bak-to-back mechanically stabilized earth
FHWA	Federal Highway Administration

LIST OF FIGURES

Chapter 1

Analytical approach in order to estimate the seismic earth pressure

Chapter 2

Scrap tire-derived and geosynthetic geomaterials for geoengineering applications

Chapter 3

Performance of retaining walls with compressible inclusions under seismic loading

Chapter 4

Seismic performance of cantilever retaining walls with tire shreds as compressible inclusion

Chapter 5

Earthquake response of connected and unconnected back-to-back geosynthetic reinforced soil walls

LIST OF TABLES

GENERAL INTRODUCTION

The problem of earthquake-induced lateral earth pressures on retaining structures has received considerable attention from researchers over the years. Lateral earth pressures were originally calculated using the methods of Coloumb (1776) where an active wedge was mobilized in order to generate an active pressure, the value of which could be computed using geometric properties and basic equations of equilibrium. Lateral seismic pressures for retaining walls originated using this approach, Okabe (1926) and Mononobe and Matsuo (1929) did a pioneering work to propose by these authors and currently known as the Mononobe-Okabe (M-O) method. This theory used primitive shake table experiments, to calculate seismic earth pressures for displacing retaining walls founded in cohesion less soils. This theory has since been applied to numerous different wall conditions, and apart from modifications to the original coefficients by Seed & Whitman (1970), has remained largely unchanged since its inception. Subsequent studies provided design methods primarily based on analytical, numerical, and experimental methods and solutions to understand the development of seismic earth pressure behind retaining structures.

Among numerous parameters that need to be considered in the design of retaining structures, lateral earth pressures and horizontal displacements resulting from the supported backfill are the most effective and the same are the influencing parameters on the performance of retaining walls under static and seismic loading conditions depends on the kind of backfill soil. However, the increased thrust of the backfill on the retaining walls can be mitigated by a lightweight, compressible material with high vibration absorption capacity, such as scrap tire derived)STD(materials)tire shreds, tire chips(, and geosynthetics (*e.g.*, Ahmed and Lovell 1993; Humphrey and Sandford 1993; Tweedie et al. 1998; Ghazavi and Sakhi 2005; Balunaini et al. 2009; Xiao et al. 2012; Reddy and Krishna 2015; Mashiri et al. 2016; Shrestha and Ravichandran 2018; Reddy and Krishna 2019; Dhanya et al. 2019; Li et al. 2020; etc.). The earthquake mitigation techniques are becoming matters of interest, to achieve stability. It has been found that these tire shreds often at a great benefit to engineers and society as a whole. Many studies have been reported a reduction of lateral earth pressures against retaining walls under dynamic loads through the inclusion of compressible material between the wall and the backfill, and

geosynthetic soil reinforcement, which are being examined as a reinforcement technique for retaining wall structures. These materials are beneficial in reducing the earth pressures and lateral displacements of the retaining walls.

RESEARCH OBJECTIVES

The main objective of this thesis is the finite element analysis based on PLAXIS 2D was used to study the different types of retaining walls viz., a cantilever type retaining wall, and back-to-back mechanically stabilized earth walls under earthquake loading. The first type of recycled tire shreds is used as a compressible inclusion behind the cantilever retaining wall to investigate the performance of the retaining wall against dynamic loading. For the second type, a numerical model was developed to study the seismic performance of connected and unconnected back-to-back walls under seismic loading using real-time earthquake data.

ORGANIZATION OF THE THESIS

The thesis titled "Estimation of dynamic earth pressures on retaining structures" consists of five Chapters. The thesis outline is presented below:

Chapter 1 presents a thorough literature review of past studies pertinent to the present research. The major focus of this chapter is on the many analytical, numerical and experimental methodologies that have been developed for the seismic analysis of retaining walls.

Chapter 2 details literature review discusses the work performed previously in the field of scrap tire-derived in civil engineering applications. This chapter also includes the literature available back-to-back walls, related to the estimation of lateral pressures which is mostly presented here.

Chapter 3 deals with the numerical model developed using the finite element software PLAXIS 2D was validated against the shaking table tests available in the literature reported by Kloukinas et al. (2015). The effects of the thickness of cushion made up of compressible shredded tires behind the retaining wall under cyclic harmonic motion and the backfill friction angle on the seismic performance of the retaining walls were analyze.

Chapter 4 details the results and discussion of the finite element-based numerical model were developed to study the seismic response of acantilever wall without and with a cushion composed of compressible tire shreds (CTS) between the wall and the backfill. To quantify the benefit of CTS cushion, a comparison was made in the behavior of wall without and with

cushion in terms of horizontal displacement and rotation, the maximum shear force and bending moment, the seismic earth thrust, and its point of application on the wall and draw important and unique conclusions.

Chapter 5 describes the results of the seismic response of reinforcement in back-to-back walls for both connected and unconnected BBMSE walls under seismic loading was investigated through numerical modeling. The model was validated with the centrifuge test results reported in the literature)Takahashi et al. 1999(. The effect of earthquake ground motion on seismic earth pressures, total seismic earth thrust coefficients)K_{AE}), incremental seismic earth thrust coefficients (ΔK_{AE}), the locations of the point of action of resultant seismic earth thrust)P_{AE}), and the acceleration amplification at the end of the reinforcement zone and the facing of the wall were mainly analyzed. The findings reported in the study can provide a rational and economical design of back-to-back mechanically stabilized earth walls (MSE) in earthquake-prone areas.

FIRST PART

LITERATURE REVIEW

Chapter 1

Approaches for estimating dynamic pressures on retaining walls

1.1 Introduction

This chapter presents a review of the literature of previous studies proposed to study the seismic performance of retaining walls. It provides a discussion of previous analytical, numerical, and experimental methods related to dynamic earth pressure and force-displacement design methods of retaining walls. This chapter summarizes research carried out by highlighting only some relevant work for this study.

1.2 Retaining Walls

Retaining walls are the structures that are built to retain vertical or nearly vertical earth banks or any other materials (Murthy, 2002). Some of the earliest and fundamental principles of soil mechanics were developed to allow the rational design of retaining walls as the problem of retaining soil is one of the oldest in geotechnical engineering (Kramer, 1996). Retaining walls are usually constructed of masonry or sheet piles and may retain water or earth and also the earth retained may be natural or fill. The different types of retaining walls generally used are shown in Figure 1.1. These walls have to withstand the lateral pressure either from earth or any other materials on the face regardless of whatever may be the type of wall. The pressure due to the soil acting on the wall tries to move the wall away from its position, hence the wall should be designed in such a way that the wall remains stable in the place and do not move from its position (Murthy, 2002).

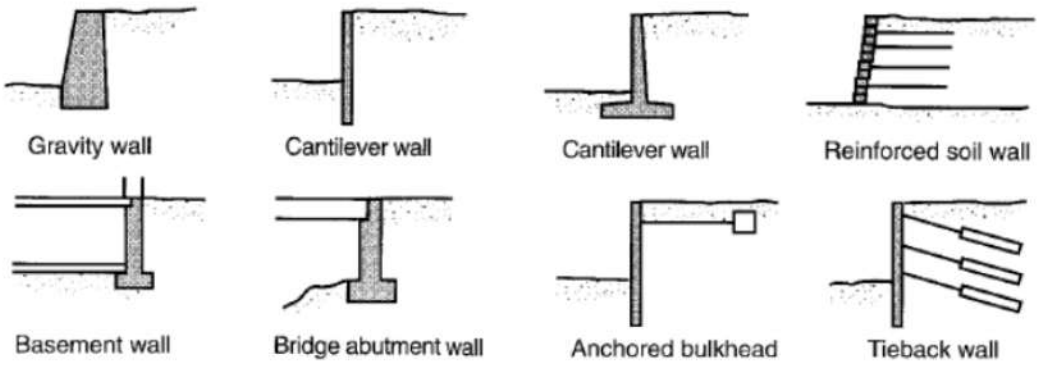

Figure 1. 1. Different types of retaining walls (Kramer, 1996).

1.3 Methods for determining dynamic earth pressure

After the pioneering work of Mononobe and Matsuo (1929) and the analytical work of Okabe (1926), researchers developed a variety of analytical and numerical models to predict the dynamic behavior of retaining walls or performed various types of experiments to study the mechanisms under the development of seismic earth pressures on retaining structures.

1.3.1 Analytical methods

Great work was performed using an analytical approach to estimate seismic earth pressure. Retaining walls that can move sufficiently to develop minimum active and/or maximum passive earth pressures are referred to as walls. The analytical approach can be divided into pseudo-static and pseudo-dynamic methods.

1.3.2 Pseudo-static methods

The most common approach based on limit state methods is pseudo-static analysis in which the effects of the seismic action are expressed by a constant horizontal and vertical acceleration attached to the mass. The common form of pseudo-static analysis estimates the effects of earthquakes by pseudo-static accelerations that produce inertial forces, the horizontal inertial force (F_h) and vertical inertial force (F_v) act at the center of the failure mass, and the magnitudes of these forces are:

$$F_h = \frac{a_h.W}{g} = k_h.W \tag{1.1}$$

$$F_v = \frac{a_v.W}{g} = k_v.W \tag{1.2}$$

Where, F_h and F_v are horizontal and vertical pseudo-static forces; ah and av are horizontal and vertical pseudo-static accelerations; k_h and k_v are dimensionless horizontal and vertical pseudo-static coefficients; W is weight of the failure mass.

Related to static limit equilibrium design methods, pseudo-static analyzes provide a safety factor against failure. The vertical pseudo-static force has less effect on the safety factor, it can reduce or increase (depending on the direction) both the driving force and the resistance force. Thus, the influence of vertical acceleration is ignored in pseudo-static analysis (Kramer, 1996). The most commonly used rigid plastic methods are the Mononobe-Okabe (1929) and Steedman-Zeng (1990) methods.

1.3.2.1 Mononobe-Okabe (M-O) method:

The "General Theory of Earth Pressure" proposed by Mononobe and Matsuo (1929), and Okabe (1926). The experiments were carried out using a shake table. results of these experiments and Okabe (1924) analysis led to the development of the Mononobe-Okabe method (M-O). The M-O method is an extension of Coulomb's static earth pressure theory to include the inertial forces due to the horizontal and vertical backfill accelerations. In the M-O method, the total seismic active and passive earth pressure are computed by applying pseudo-static acceleration forces on the static forces acting on the soil wedge in both the horizontal and vertical directions. The magnitude of these pseudo-static forces depends on the acceleration level in the horizontal and vertical directions and the mass of the soil wedge.

***Seismic active earth pressure*:** Figure 1.2 shows the forces acting on the dry cohesionless backfill wedge. In addition to the static forces, the wedge is also under the effect of the pseudo-static forces that are a function of the mass of the wedge and pseudo-static accelerations ($a_h = k_h \times g$ and $a_v = k_v \times g$). where, k_h = ratio between the horizontal seismic acceleration (a_h) and gravity acceleration (g), and k_v = ratio between the vertical seismic acceleration (a_v) and gravity acceleration (g). The total seismic active earth pressure force can be computed similarly to that calculated by the Coulomb method:

$$P_{AE} = \frac{1}{2} K_{AE} \gamma H^2 (1 - k_v) \tag{1.3}$$

where, γ = unit weight of the soil, and H = height of the wall. The total (static plus dynamic) earth pressure coefficient (K_{AE}) is calculated using the Mononobe-Okabe equation given by:

$$P_{AE} = 0.5\gamma H^2 \frac{(1 \pm k_v)\cos^2(\varphi - \theta - \beta)}{\cos^2\theta \cos\beta \cos(\delta + \theta + \beta)\left[1 + \sqrt{\dfrac{\sin(\delta + \varphi)\sin(\varphi - \alpha - \beta)}{\cos(\delta + \theta + \beta)\cos(\theta - \alpha)}}\right]^2} \tag{1.4}$$

where, φ = peak soil friction angle, α = backfill surface slope angle from the horizontal, δ = interface friction angle at the back of the wall-soil (or back of the reinforced soil zone), β = seismic inertial angle given by $\beta = tan^{-1}(k_h/1 \pm k_v)$, and k_h and k_v are the peak horizontal and vertical seismic coefficients, respectively.

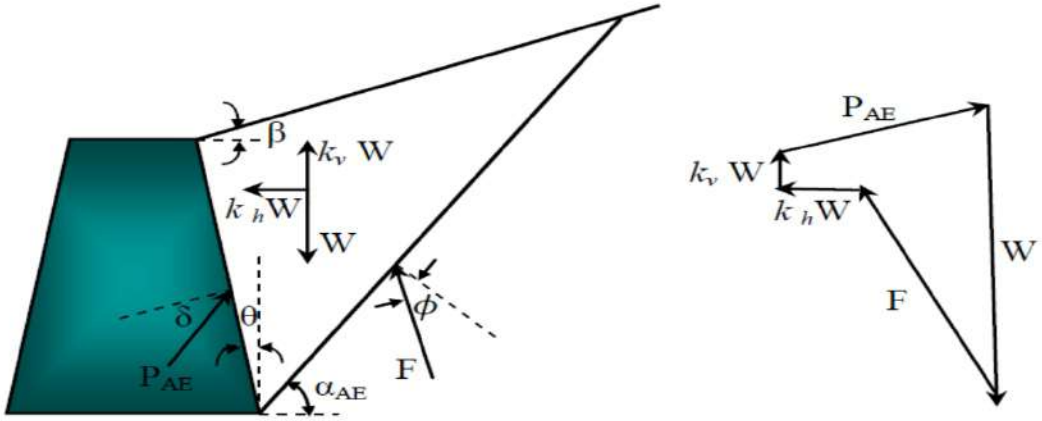

Figure 1. 2. Forces acting on a soil wedgr for an case in the M-O analysis.

Seismic passive earth pressure: Figure 1.3 shows the forces acting on the dry cohesionless backfill wedge. The total seismic passive earth pressure force can be computed by:

$$P_{PE} = \frac{1}{2} K_{PE} \gamma H^2 (1 - k_v) \tag{1.4}$$

where, K_{PE} = seismic passive earth pressure coefficient and it can be calculated by:

$$K_{PE} = \frac{\cos^2(\varphi + \theta - \beta)}{\cos^2\theta \cos\beta \cos(\delta - \theta + \beta)\left[1 - \sqrt{\frac{\sin(\delta + \varphi)\sin(\varphi + \alpha - \beta)}{\cos(\delta - \theta + \beta)\cos(\theta - \alpha)}}\right]^2} \tag{1.5}$$

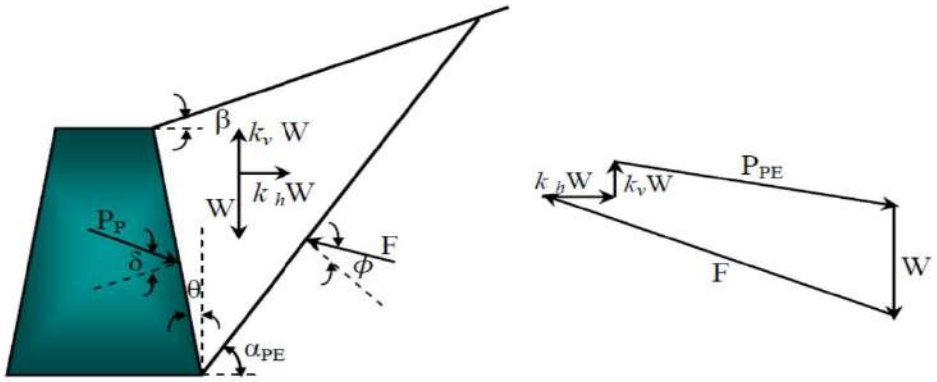

Figure 1. 3. Forces acting on soil wedge for a passive case in the M-O analysis.

The M-O method gives the total active thrust acting on the wall and the point of application of the thrust is assumed to be at $H/3$ above the base of the wall.

1.3.2.2 Seed and Whitman (1970) (S-W) method:

Seed and Whitman (1970) proposed modifications to M-O theory based upon their parametric study performed to evaluate the lateral earth thrust acting on the retaining wall. They reported that the total seismic earth pressure, P_{AE}, consisted of two parts: the static earth pressure and interment of dynamic earth pressure due to seismic load, ΔP_{AE}, as follows:

$$P_{AE} = P_A + \Delta P_{AE} \tag{1.6}$$

$$K_{AE} = k_A + \Delta K_{AE} \tag{1.7}$$

Where the changes in dynamic pressure are calculated as:

$$\Delta K_{AE} \cong \frac{3}{4} k_h \tag{1.8}$$

$$\Delta P_{AE} = \frac{1}{2} \gamma H^2 \frac{3}{4} k_h \tag{1.9}$$

Seed and Whitman (1970) suggested that the resultant pressure due to both seismic and static thrusts be moved from the initial value calculated by Mononobe (1929), based on the triangle distribution assumed by Coulomb Theory, the point of application should be at 1/3 the height of the wall above the base to a value approximately 0.6 of the total height of the wall above the base of the retaining wall (refer Figure 1.4). Thus, the point of application of the total thrust under seismic conditions is calculated using the subsequent equation:

$$h = \frac{\frac{P_A H}{3} + P_{AE}(0.6H)}{P_{AE}} \tag{1.10}$$

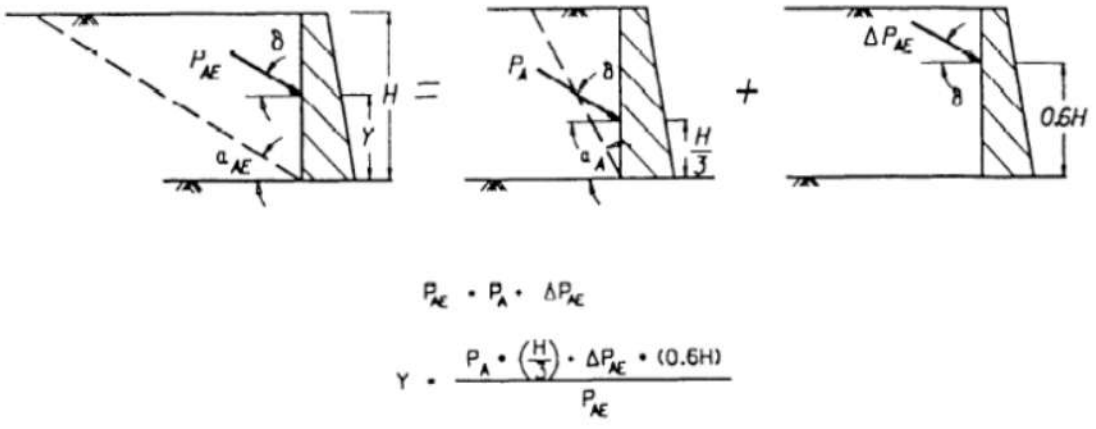

Figure 1.4. Forces considered in Seed-Whitman analysis.

1.3.3 Pseudo-dynamic methods

In the pseudo-static approach, the progress over the previous approach is that the dynamic nature of the seismic load is considered in an approximate and simple way. The phase difference and the amplification effects within the mass of the soil are considered along with the accelerations to the inertia.

1.3.3.1 Steedman-Zeng (1990) method:

Steedman and Zeng (1990) proposed an analytical solution to estimate the seismic active earth pressure considering finite shear wave propagation within backfill soil. A fix-base vertical cantilever wall of height H is assumed to support a cohesionless backfill material with definite soil friction, as shown in Figure 1.5. The backfill soil is considered horizontal in the analysis. The base of the backfill soil is assumed to be subject to harmonic horizontal acceleration of amplitude a_h. The horizontal seismic acceleration acting in the backfill soil is not constant, but it is dependent on the time, frequency and phase difference in a shear wave (v_s) propagating in the vertical direction within the backfill soil (Bakr, 2018). The horizontal seismic acceleration at any depth z below soil surface and time can be expressed as:

$$a_h(z,t) = a_h \sin w\left[t - \frac{H - z}{v_s}\right] \tag{1.11}$$

where, t = time elapsed, ω = frequency of sinusoidal earthquake acceleration and v_s shear wave velocity. The planar rupture surface, inclined at an assumed angle α to the horizontal, is considered in the analysis along with the seismic force and weight of failure block. The total seismic active force on the wall , as shown below:

$$P_{AE}(t) = \frac{Q_h(t)\cos(\alpha - \phi) + W\sin(\alpha - \beta)}{\cos(\delta + \phi - \alpha)} \tag{1.12}$$

$$Q_h(t) = \frac{\lambda\gamma\alpha_h}{4\pi^2 g\tan\alpha}\left[2\pi H\cos\omega\zeta + \lambda(\sin\omega\zeta - \sin\omega t)\right] \tag{1.13}$$

Where,

$$\lambda = \frac{2\pi v_S}{\omega} \text{ and } \zeta = 1 - \frac{H}{v_S} \tag{1.14}$$

The point of application of the total seismic active force is hd from the base of the wall and given by,

$$h_d = H - \frac{2\pi^2 H^2 \cos\omega\zeta + 2\pi\lambda H \sin\omega\zeta + \lambda^2(\cos\omega\zeta - \cos\omega t)}{2\pi H \cos\omega\zeta + \pi\lambda(\sin\omega\zeta - \sin\omega t)} \tag{1.15}$$

This point of application of the seismic force for very low frequency motions (small H/λ, so the backfill moves essentially in phase) is at $h_d = H/3$. For higher frequency motions, hd moves pwards from base of the wall. This solution accounts for non uniformity of acceleration within the soil mass but disregards dynamic amplification.

More recently, the Steedman and Zeng method was extended by Choudhury and Nimbalkar (2005 and 2006), Ghosh (2010), and Bellezza et al. (2012). Choudhury and Nimbalkar (2005) modified the pseudo-dynamic method by considering seismic vertical acceleration and extended for determining seismic passive earth pressure. Choudhury and Nimbalkar (2006) include vertical acceleration, showing the effects of various factors such as the shear resistance angle and the soil-wall friction angle on the distribution of seismic active soil pressure. Ghosh (2010) proposed a solution for the seismic active thrust acting on a battered retaining wall supporting a dry, cohesionless, inclined backfill. Bellezza et al. (2012) applied the pseudo-dynamic method to submerged backfill including both horizontal and vertical acceleration and amplification effects.

The pseudo-dynamic method was also extended to passive case (Choudhury and Nimbalkar 2005; Ghosh 2007) and the same framework was utilized to estimate seismic displacements (Choudhury and Nimbalkar 2007, 2008) and design retaining structures also with reinforced backfill (Ahmad and Choudhury 2008a, b, 2009; Choudhury and Ahmad 2008; Nimbalkar and Choudhury 2007; Nimbalkar et al. 2006).

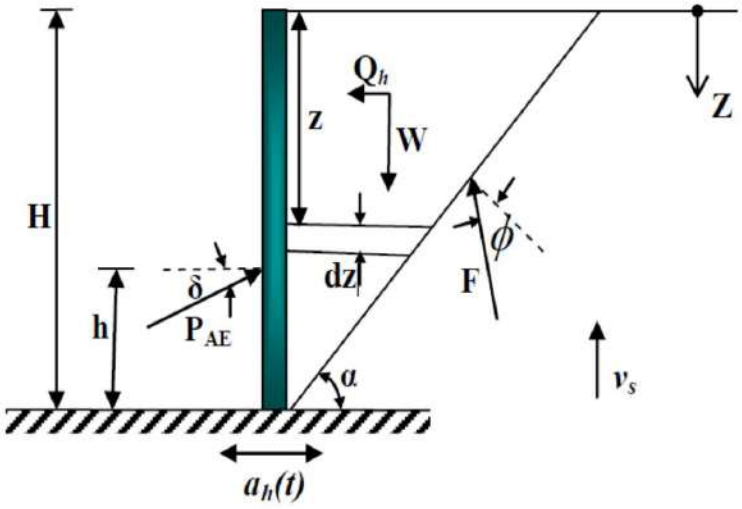

Figure 1. 5. Wall geometry con sidered in the Steedman and Zeng (1990) model.

1.4 Numerical methods

Numerical modeling efforts have been applied to verify the seismic design methods in practice and to provide new insights to the problem. A variety of numerical codes have been used to analyze the problem of the retaining structure numerically like PLAXIS, ABAQUS, FLAC, ANSYS, etc. Thus, it is necessary to discuss some remarkable numerical research on the seismic response of retaining walls. This section discusses the numerical methods that have been adopted to investigate the problem of earth seismic pressure.

Wood (1973) used finite elements to study the static and dynamic response of non-yielding walls and the effects of bonded walls and non-uniform soil stiffness. Recently, a combination of theoretical, numerical and experimental studies on engineering matters has been a dominant research trend, as shown in Figure 1.6. He showed that the smooth and bonded wall contacts had no significant influence on the frequency response or the earth pressure distributions.

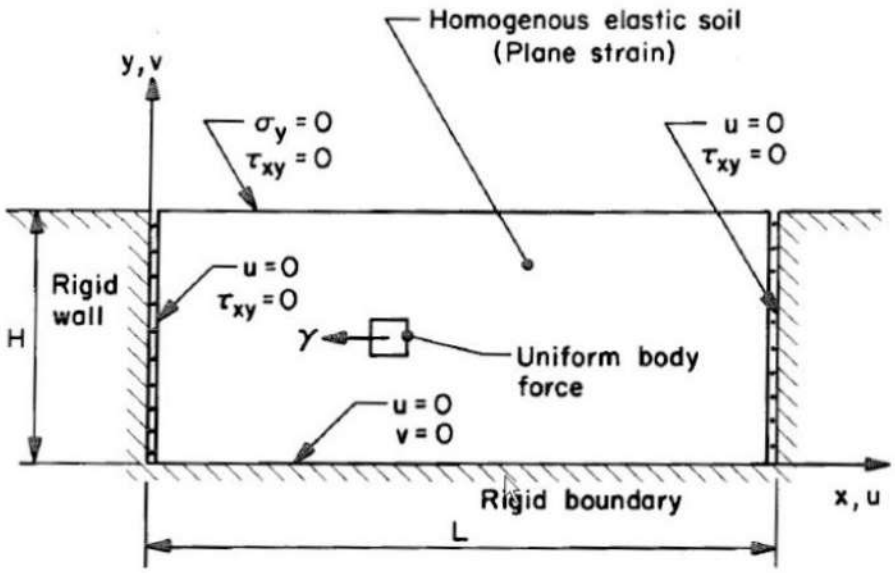

Figure 1.6. Wood (1973) rigid problem.

Aggour and Brown (1973) performed 2D plane strain analyzes on a 20-ft-tall cantilever retaining wall to investigate the effects of wall flexibility and backfill length and shape. On the dynamic distribution of soil pressure. Siddharthan and Maragakis (1989) suggested a finite element model to investigate the seismic response of a flexible cantilever retaining wall. They used an incrementally elastic approach to model soil nonlinear hysteretic behavior and validated their model by comparing its results to recorded responses from a dynamic centrifuge experiment. This study investigated the effect of wall flexibility and relative density of soil on the dynamic response of the wall.

Green et al. (2002) studied the seismic response of a cantilever retaining wall with cohesionless backfill using the finite difference code FLAC (ITASCA, 2001). For low intensity ground accelerations, they calculated earth pressure coefficient comparable to the M-O method; however, they suggested an upper bound closer to Wood's (1973) solution (Candia, 2013).

Green et al. (2003) performed a series of nonlinear dynamic response analyzes of the cantilever retaining wall-soil system using FLAC modeling. The M-O method was evaluated for estimating the seismic earth pressure induced on the shank of the wall. The results of the analysis show that the computed seismic earth pressures were in general agreement with those predicted by the M-O method at low acceleration levels. However, when the acceleration level increased, the computed seismic earth pressures were larger than those predicted by the M-O method. Gazetas et al. (2004) used finite elements to model the seismic behavior on several types of flexible restraint systems subjected to moderately strong excitations. They found that the dynamic ground pressures are lower than M-O.

To investigate the characteristics of the lateral seismic soil pressure on building walls, Ostadan (2005) performed a series of soil-structure interaction analyses using SASSI. Using the concept of a single degree-of-freedom, Ostadan (2005) proposed a simplified method to predict maximum seismic soil pressures for building walls resting on firm foundation material. This proposed method resulted in dynamic earth pressure profiles comparable to or larger than the Wood (1973) solution, with the maximum earth pressure occurring at the top of the wall (Al Atik and Sitar , 2008).

Pathmanathan (2007) conducted a series of finite element models to determine the seismic earth pressure on a flexible diaphragm, a flexible cantilever wall and gravity wall. It was concluded that the magnitude of the earth pressure resultant matched predictions by the M-O method when the levels of shaking were small. When the levels of shaking were large, the magnitude of the earth pressure resultant was lower than that predicted by the M-O method and the point of application of the dynamic increment was around $0.6H$ as proposed by Seed & Whitman (1970).

Green et al. (2008) used the same finite difference dynamic analysis to investigate the structural and global stability of the cantilever retaining wall under seismic condition, as shown in Figure 1.7. It was found that at very low levels of acceleration, the induced pressures were in general agreement with those predicted by the MononobeOkabe method. However, as the

accelerations increased to those expected in regions of moderate seismicity, the induced pressures are larger than those predicted by the Mononobe-Okabe method.

Jung & Bobet (2008) performed a parametric study to assess the effects of the relative stiffness of a retaining structure and the base constraint on the pressure distribution. They conclude that the wall flexibility has a large effect on the magnitude and ddistribution of the dynamic earth pressure, whereas the base rotation has a large effect on the magnitude of the pressure and a modest effect on the distribution.

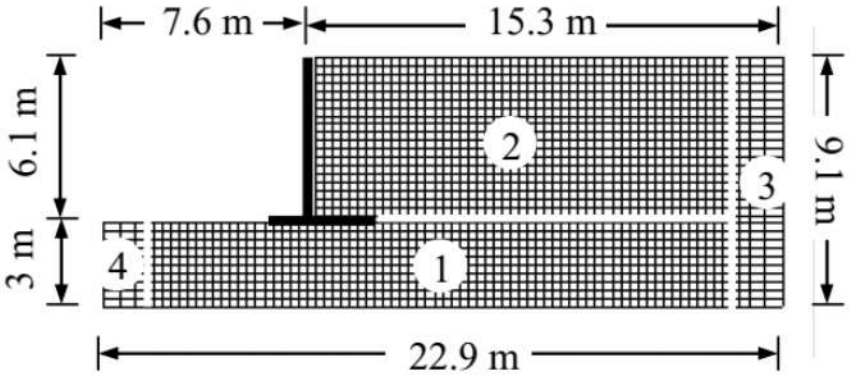

Figure 1.7. Finite difference model of a retaining wall proposed by Green et al. (2008).

Al Atik and Sitar (2008) developed a 2D nonlinear finite element model by using the OpenSees program to evaluate the ability of a numerical model to simulate the seismic response of retaining structures observed in centrifuge experiments. The finite element model was developed to estimate seismic earth pressure behind two U-shaped cantilever retaining walls, one flexible and one stiff. The result shows that the seismic earth pressure depends on the magnitude and intensity of the shaking and flexibility of the retaining wall. The distribution of dynamic earth pressure can be approximated to a triangular shape. The dynamic earth pressure and inertial forces did not act in the same phase. The seismic earth pressure can be neglected at acceleration levels below 0.4g. The finite element analysis for denser soil backfill soil shows that the seismic earth pressure reduced by about 23-30% (Bakr, 2018). Al Atik & Sitar (2010) used finite elements and Mikola & Sitar (2013) used finite differences to model displacing and non-displacing walls on a sand foundation with a sand backfill, and calibrated the models with centrifuge experiments. Also, Candia & Sitar (2013) used finite differences to model the same walls as Mikola & Sitar (2013) on a clay foundation with a clay backfill to investigate the effects of cohesion on the dynamic earth pressure. These studies concluded that a numerical model can

capture essential responses of a soil-wall system provided that a constitutive model calibrated against experimental data is used for the soil model.

Geraili et al. (2016) presented a finite difference analysis by using FLAC 2D to simulate two centrifuge experiments. The retaining walls were modelled to simulate the basement wall type and cantilever retaining wall type to support dry medium-dense sand backfill. The data show that seismic earth pressure increments increase with depth consistent with the static earth pressure distribution and consistent with that implicit in the M-O solution which forms the upper bound for the experimental results.

Bakr and Ahmad (2018) presented a finite element PLAXIS 2D model to investigate the relationship between the seismic active earth pressure and the movement of a rigid retaining gravity wall. They observed that the seismic active earth pressure is independent of the seismic input motion and hence does not depend upon the wall movement during an earthquake, while on the contrary the seismic passive earth pressure is significantly affected by it. Comparison of the results of the present study with the Mononobe-Okabe and pseudo-dynamic methods (see Figure 1.8) clearly highlights that the latter overestimates the seismic earth pressure.

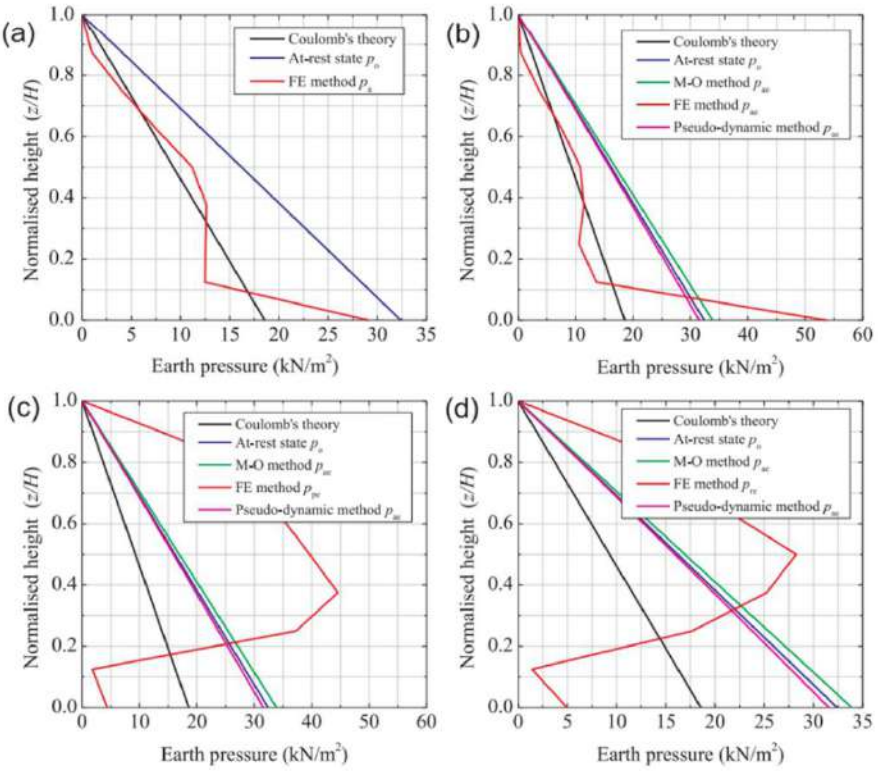

Figure 1.8. (a) Static active earth pressure at t = 0s, (b) seismic active earth pressure at t = 3.8s , (c) seismic passive earth pressure at t = 4.5s, and (d) seismic residual earth pressure at t = 30 s (Bakr and Ahmad, 2018).

After that, Bakr and Ahmad (2019) used the same finite difference dynamic analysis to investigate the deformation mechanism of the cantilever-type retaining wall under the effect of seismic loading. A new and robust approach is proposed to compute the seismic earth pressure behind the stem and along a virtual plane passing the heel of the wall, as shown in Figure 1.9. The results show that under different earthquake characteristics and wall geometries, the seismic earth pressure forces may be out of phase, leading to different seismic responses of the wall.

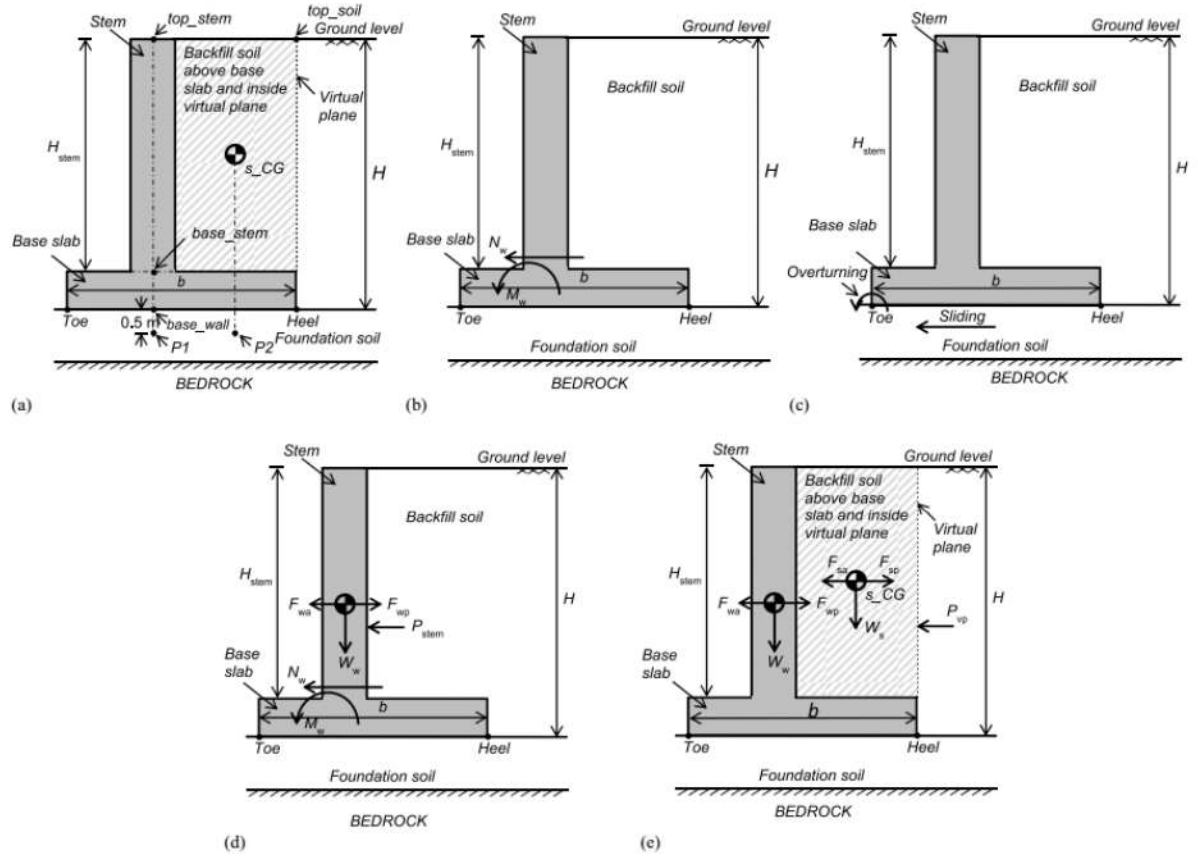

Figure. 1.9. Typical cantilever-type retaining wall–soil system (Bakr and Ahmad (2019).

Salem et al. (2020) performed a series of twodimensional finite element methods for analyzing the seismic response of cantilever retaining walls. The sensibility of the system response to the soil constitutive model was studied. A Rigid perfectly plastic (M-C) and an advanced nonlinear elastoplastic model (HSSMALL) were used. Results of the analysis quantified seismic earth pressure in terms of magnitude and point of application. A relationship has also been proposed to relate the horizontal seismic inertial coefficient with a representative lateral seismic active earth pressure coefficient.

1.5 Experimental methods

Two types of experimental tests have been used for evaluating the dynamic response of retaining walls the first type is performed under the shaking table experiments (1g model test) and dynamic centrifuge experiments of the second type. They are generally considered a very useful method to identify important phenomena and verify numerical and analytical models. The focus of this review is to identify the previous experimental studies conducted using a force-based design method.

1.5.1 Shaking table tests

Following the great Kwanto earthquake of 1923, Mononobe and Matsuo (1929) conducted experimental shaking table studies of seismic earth pressures acting on retaining walls. The shaking table experiment consisted of a rigid base box mounted on rails and driven by a conical drum winch connected through a crankshaft to the base of the box (Figure 1.10). The seismic loads measured in the experiments were in agreement with Okabe's (1926) analytical work. Also, verify the analytical method proposed by Okabe (1926).

The results of various later experimental programs aimed at determining the dynamic pressures on retaining walls have been reported in the literature. The results from the 1-g shaking table experiments were reported by Matsuo (1941), Matsuo and Ohara (1960), Bolton and Steedman (1982), Steedman (1984), Bolton and Steedman (1985) and Ishibashi and Fang (1987). Generally, all of these experiments report seismic loads similar to the M-O method, but the general observation was that the earth pressure distribution was non-linear and the resultant was applied at a point much higher than H/3.

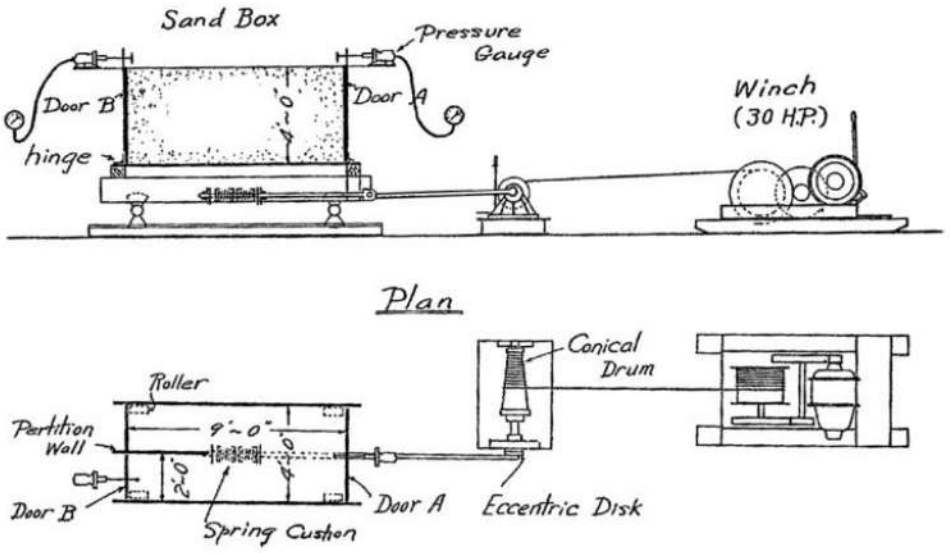

Figure 1.10. Shaking table arrangement used by Mononobe and Matsuo (1929).

Watanabe et al. (2003) and Watanabe et al. (2011) developed a three part gravity wall consisting of two outer sections and a central section of plates attached to load cells to interpret the earth pressure distribution along the entire depth of the wall. The backfill was sand and the foundation soil was either sand or a thin layer of gravel (to force sliding failure before overturning failure). The inertia loads from the plates were explicitly measured and accounted for in the analysis of the load cell data when computing the dynamic earth pressure resultant. Based on the results of the experiments, an analysis procedure was proposed wherein a critical yield acceleration was computed for stability (either sliding or overturning) using a pseudo-static analysis. This yield acceleration was then used as an input for the M-O equation to calculate a maximum total seismic load. Higher total seismic loads due to higher accelerations would be "capped" at this maximum value, essentially prescribing design loads based on the stability of the wall instead of the input motion characteristics (Wagner (2016)).

Kim et al (2004) evaluated the force components acting on gravity type quay wall during earthquakes by using analytical and experimental studies. Modified Mononobe-Okabe method and Westeergard method as analytical studies are used to define dynamic forces and small and large scale shaking table tests as experimental studies are performed to compare the results. They tried to obtain the forces with low and high excess pore pressure ratio and they found that the modified Mononobe-Okabe method could not simulate the phase relationship between the wall inertia force and the dynamic thrust.

Kloukinas et al. (2015) conducted a shaking table experiment and theoretical analyzes to investigate the seismic response of a cantilever retaining wall conducted at the University of Bristol (EERC-EQUALS). The shaking table experiment was conducted by scaling the retaining wall model and assuming the retaining wall has a compliant base under different geometries of the wall and input shaking, as shown in Figure 1.11. The backfill and foundation soil was considered to be dry silica sand. The shaking table results show that the rotation of the retaining wall is more sensitive to the strong seismic shaking than the sliding mechanism.

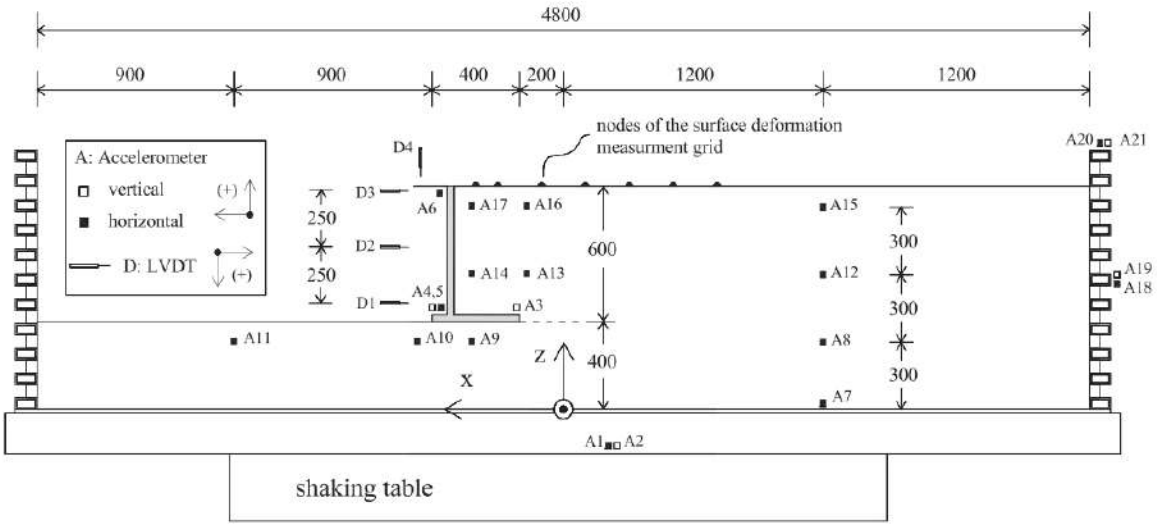

Figure 1.11. Geometry and instrumentation of the shaking table model used by Kloukinas et al. (2015).

1.5.2 Centrifuge tests

Ortiz et al. (1983) performed a centrifuge test to investigate the seismic response of a cantilever retaining wall supporting medium-dense sand, as shown in Figure 1.12. The results of the tests show that the total seismic pressure is in reasonable agreement with those computed by the M-O method but the bending moment can be different. The seismic earth pressure distribution along the height of the wall is nonlinear.

Steedman (1984) conducted centrifuge experiments of micro concrete cantilever walls retaining a dry cohesion less backfill. Sinusoidal excitation with amplitude up to 0.22 g was applied, and the dynamic pressure resultant was observed to act at one-third of the wall height in agreement with M-O predictions. They also suggested that the dynamic earth pressures act at H/3 and that the wall inertial forces must be taken into account in addition to M-O earth pressures.

Nakamura (2006) performed a series of dynamic centrifuge experiments to study the seismic behavior of gravity retaining walls in order to assess the M-O method (Figure 1.13). Centrifuge acceleration of 30 g was applied, horizontal shaking was performed using different types of base earthquake acceleration. He observed that when the walls are excited in the active direction the ground motion was transmitted instantly to the wall and then to the backfill. Moreover, the distribution of earth pressures was nonlinear and changed with time.

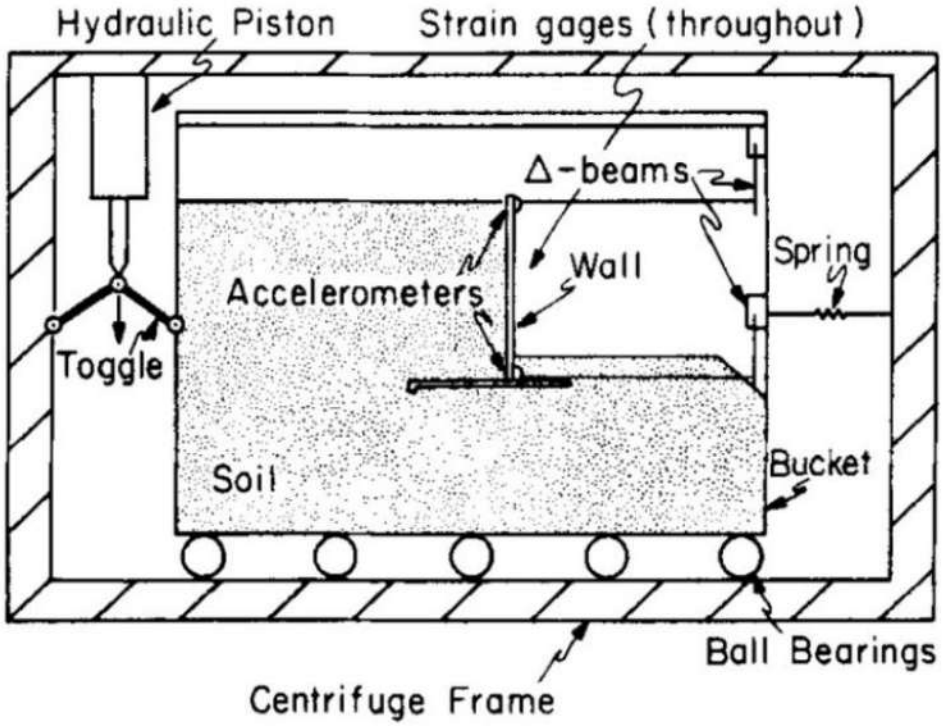

Figure 1.12. Centrifuge experiment set up of Ortiz (1983).

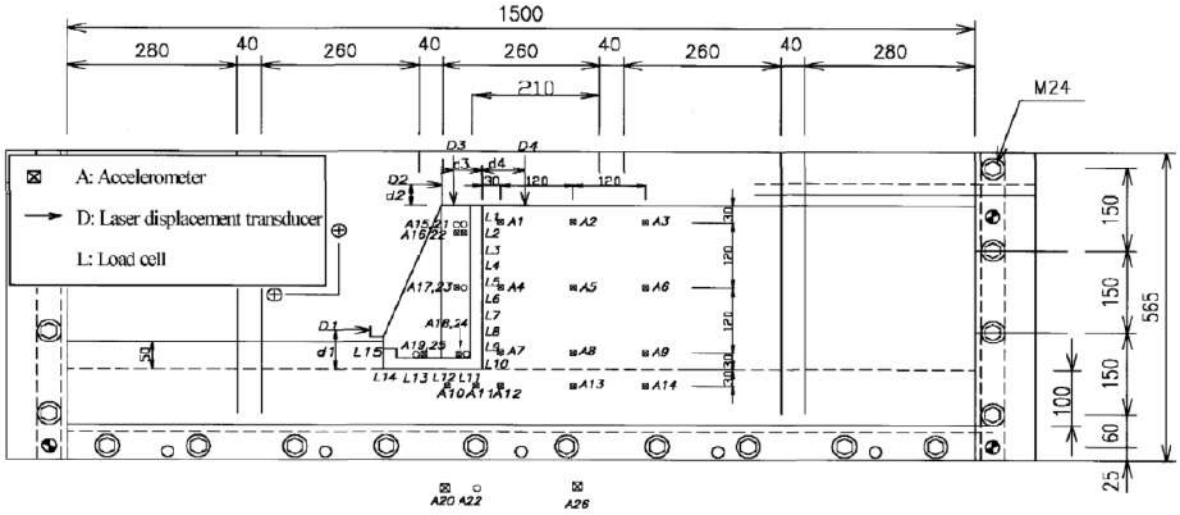

Figure 1.13. Nakamura (2006) test configuration.

Al Atik and Sitar (2008) conducted two sets of dynamic centrifuge tests to estimate the magnitude and distribution of seismic earth pressure induced behind two U-shaped cantilever-retaining structures, one flexible and one stiff, which were constructed to support dry sand backfill material. The result shows that the seismic earth pressure depends on the magnitude and intensity of the shaking and flexibility of the retaining wall. The distribution of dynamic earth pressure can be approximated to a triangular shape. The dynamic earth pressure and

inertial forces did not act in the same phase. The seismic earth pressure can be neglected at acceleration levels below 0.4g (Bakr, 2018). After that, Al Atik and Sitar (2010) and Mikola and Sitar (2013) (see Figure 1.14), used the centrifuge to model the behavior of fixed base U-shaped walls, basement walls and freestanding cantilever walls supported in medium dense sand. The experiments used a flexible shear beam container that deforms horizontally with the soil. They concluded that the M-O method was conservative, especially at high accelerations above 0.4g. They also observed that earth the seismic pressures increase approximately linear with depth, and that the Seed and Whitman method (Seed and Whitman, 1970) with the resultant applied at 0.33H is a reasonable upper bound to the total seismic earth pressure increment.

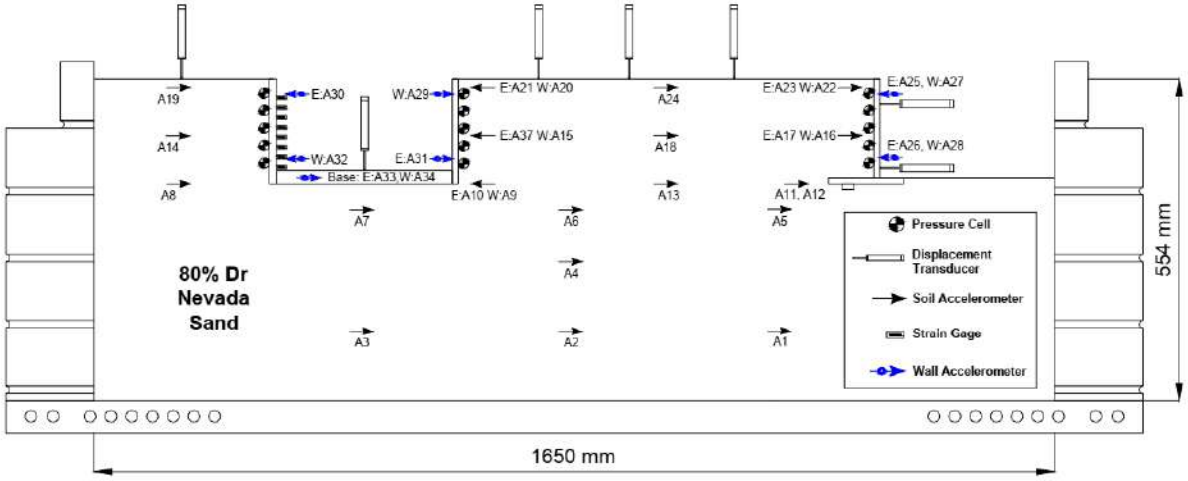

Figure 1.14. Centrifuge experiment set up of Mikola and Sitar (2013).

Mikola et al. (2016) recorded distribution of the seismic earth pressures on cantilever retaining structures using centrifuge tests. Jo et al. (2017) carried out two dynamic centrifuge tests were designed and conducted to evaluate the magnitude and distribution of the dynamic earth pressure and the inertial effect of the wall itself on an inverted, T-shape, stiff retaining wall with a dry medium sand backfill. Results from two sets of dynamic centrifuge experiments show that the dynamic earth pressure has a triangular shape for critical states during the earthquake and that the inertial force of the wall significantly influences the structural moment. Moreover, the deformation pattern, the rigidity of the retaining wall, and the frequency contents of the input motions cause the phase difference between the wall and the soil. Correspondingly, this phase difference influences the dynamic earth pressure.

1.6 Displacement-based methods

A retaining structure subjected to earthquake motion will vibrate with the backfill soil and the wall can easily move from the original position due to an earthquake. An effort has been made to suggest design methods for predict the permanent retaining wall displacement and design a retaining wall based on the allowable displacement. This design technique is called the 'displacement-based method'. Several analytical, numerical and experimental methods have been proposed in the literature to estimate the permanent displacement of the retaining wall.

1.6.1 Analytical methods

Several analytical methods have proposed to estimate the displacement-based methods are generally developed for retaining walls and are mainly based on different concepts such as one block analysis concept.

1.6.1.1 Richards-Elms method (1979):

The model proposed by Richards and Elms (1979) is based on the basic Newmark's model, developed originally for evaluation of seismic slope stability, modified for the design of gravity retaining walls, as shown in Figure 1.15. Richards and Elms recommended that the dynamic active earth force calculated using Mononobe-Okabe method, and it can be expressed as:

$$P_{AE} = 0.5\gamma H^2 \frac{(1 \pm k_v)\cos^2(\varphi - \theta - \beta)}{\cos^2\theta \cos\beta \cos(\delta + \theta + \beta)\left[1 + \sqrt{\frac{\sin(\delta + \varphi)\sin(\varphi - \alpha - \beta)}{\cos(\delta + \theta + \beta)\cos(\theta - \alpha)}}\right]^2} \tag{1.16}$$

The level of acceleration that is required to cause the wall to slide on its base is the yield acceleration, and it can be expressed as:

$$a_y = \left[\tan\phi_b - \frac{P_{AE}\cos(\delta + \beta) - P_{AE}\sin(\delta + \beta)}{W}\right] g \tag{1.17}$$

where, ya = yield acceleration, W = weight of the wall, and Pae = seismic active earth pressure and is calculated using the M-O method as recommended by Richards and Elms. They also proposed the following formula to calculate permanent block displacement:

$$d_{perm} = 0.087 \frac{V^2_{\max} a^3_{\max}}{a^4_y} \tag{1.18}$$

where v_{max} = peak ground velocity, a_{max} = peak ground acceleration, and a_y the yield acceleration for the wall-backfill system.

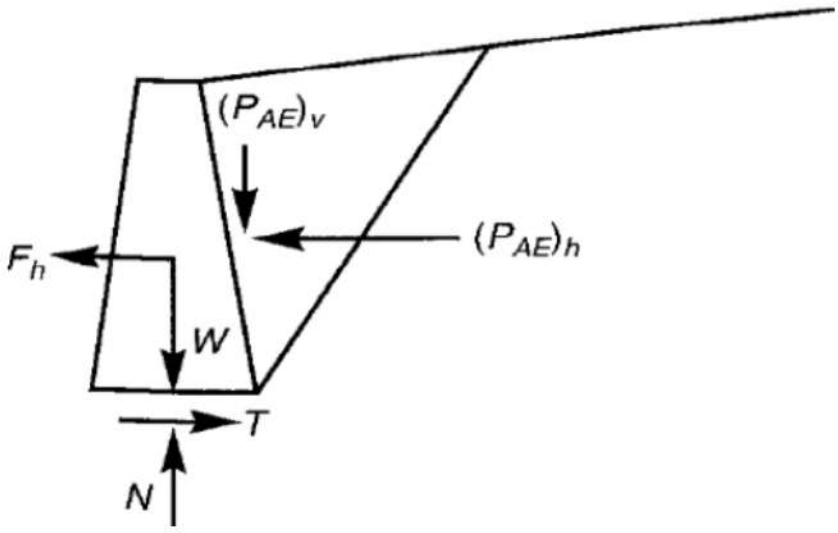

Figure 1.15. Forces acting on a wall-soil system proposed by Richards and Elms (1979).

Similar to sliding block methods, Nadim and Whitman (1983), Steedman (1984), Whitman and Seed (1984) proposed a procedure using a one-block method to compute the displacement of the retaining wall. Zarrabi (1979) improved this method by taking into account vertical acceleration: this normally renders a slightly lower displacement value than the R-E model. Zeng and Steedman (2000) established a method for a rotational displacement of gravity retaining walls. Corigliano et al. (2011) have proposed a novel procedure to improve the applicability of the Newmark method in computing the permanent displacement of gravity earth-retaining structures induced by earthquake loading introducing the effects of the double-support seismic excitation in the foundation layer and backfill retained soil. The results predicted from the modified Newmark procedure show that the standard Newmark method underestimates residual displacement (Bakr, 2018).

1.6.2 Numerical methods

Several numerical methods have been proposed to estimate the seismic response of retaining structures using the displacement-based design method. A variety of numerical codes has been used to analyze the problem of the retaining structure. The main results of the numerical models based on the displacement-based design method will be discussed as follows.

Madabhushi and Zeng (1998) carried finite element analysis to investigate the seismic response of a rigid retaining wall under earthquake loading. Special slip elements were used at the interface between the quay wall and soil body to improve the numerical predictions. They found that the numerical modeling results agreed quite well with the experimental data for the dry and saturated tests.

Moghadam et al. (2009) conducted a finite difference analysis to investigate the seismic response of caisson quay walls under harmonic base motions are used with constant frequency and amplitude. The mitigation results show that the deformable panels can significantly decrease the seaward movement, settlement, and inclination of a wall as well as the total pressure recorded behind the caisson wall. Bhattacharjee and Krishna (2009) proposed that a gravity retaining wall be modeled using FLAC 3D, to study the dynamically induced displacement, as shown in Figure 1.16. The results obtained from the numerical model were compared with the results obtained according to the analytical model of Richard and Elms (1979). Notice that the displacement of the model increase with acceleration and acceleration decreases with an increase in damping of the material.

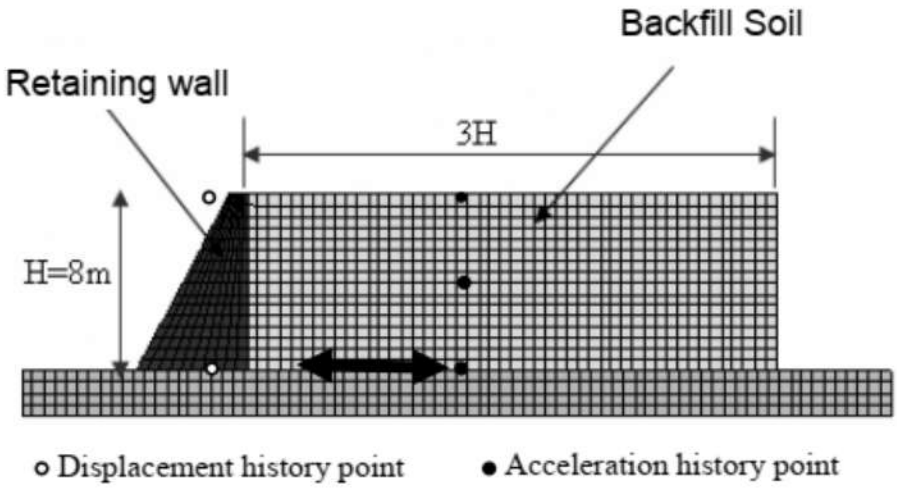

Figure 1.16. Numerical grids of retaining wall model proposed by Bhattacharjee and Krishna (2009).

Tiznado and Rodríguez-Roa (2011) carried out a series of two-dimension finite element analyses by using PLAXIS software to investigate the seismic behavior of a gravity retaining wall. The results showed that seismic amplification effects in the soil foundation and backfill have a significant role in determining the permanent displacements of these walls.

Ibrahim (2015) conducted finite-element analyses were carried out to study the seismic behavior of gravity retaining walls on normally consolidated granular soils. It is also found that seismic wall displacement is directly proportional with the positive angle of inclination of the back surface of the wall, soil flexibility, and with the earthquake maximum ground acceleration.

Jadhav and Prashant (2020) carried out a series of two-dimension finite element analyses of cantilever retaining wall with different locations of the shear key has been performed in

Chapter 2

Scrap tire-derived and geosynthetic geomaterials for geoengineering applications

2.1 Introduction

In the construction of a retaining wall, the backfill material has a significant impact on the behavior and proper functioning of the structure. For this, innovation in technology requires judicious consideration of cost-saving and the mitigation capability of materials that do not affect the performance of retaining walls under static and seismic loading conditions. The materials used in these techniques are scrap tire-derived (STD) geomaterials and geosynthetics for retaining walls. The literature review is presented in two parts: a) Geoengineering applications with the use of scrap tire-derived recycled materials. b) back-to-back geosynthetic reinforced soil retaining walls. This chapter presents the literature review according to the general objective of the study.

2.2 Geoengineering applications with the use of scrap tire-derived recycled materials

The rapid expansion of the transportation industry around the world has produced a huge amount of waste tires generated yearly. The annual production rate of scrap tires has been reported to be 200-300 million in the United States, 104 million in Japan, 112 million in India. Most of these used tires are stored, dumped in landfills, or thrown away illegally, creating serious fire, health, and environmental hazards. The making safe disposal of this waste material a dire necessity and extreme challenge, thus, alternative approaches to using large quantities of scrap tires have captured the attention of the engineering community.

The use of scrap tires in civil engineering projects is an encouraging method to recycle this waste. Scrap tires can be used in geotechnical engineering applications in lieu of soils as namely lightweight fill material, good insulation properties, high vibration absorption capacity, good long-term durability, and high elastic compressibility. Scrap tires are shredded for use in these applications,used alone, or mixed with soil. The grain size and distribution of shredded tires may differ. These materials are called geomaterials scrap tire derived (STD). However, American Society for Testing and Materials ASTM D6270-08 (2012) (ASTM 2008) and Yasuhara (2007)

suggests using the terms based on the particle sizes: granulated rubber (maximum size of 12 mm), tire chips (between 12 and 50 mm) and tire shred (between 50 and 305 mm) as depicted in Figure 2.1.

Many researchers have explored the use of waste tires in various civil engineering applications (e.g., Ahmed and Lovell 1993; Humphrey and Sandford 1993; Tweedie et al. 1998; Ghazavi and Sakhi 2005; Balunaini et al. 2009; Xiao et al. 2012; Reddy and Krishna 2015; Shrestha and Ravichandran 2018; Reddy and Krishna 2019; Li et al. 2020; etc.).

Figure 2. 1. Scrap tire derived geomaterials (Modified after Hazarika and Yasuhara (2007)).

2.2.1 Use of (STD) in retaining wall backfill

Cecich et al. (1996) used tire chips alone as a backfill in retaining structures and obtained high factors of safety against sliding and overturning compared to that when sand was used as backfill. Tweedie et al. (1998) constructed and instrumented a full scale 4.88 m high retaining wall with tire shreds as backfill. A cross-section of the retaining wall is shown in Figure 2.2. They observed that

the lateral pressures with tire shreds as backfill were reduced by about 45% and 35% compared to conventional granular backfill at at-rest and active conditions.

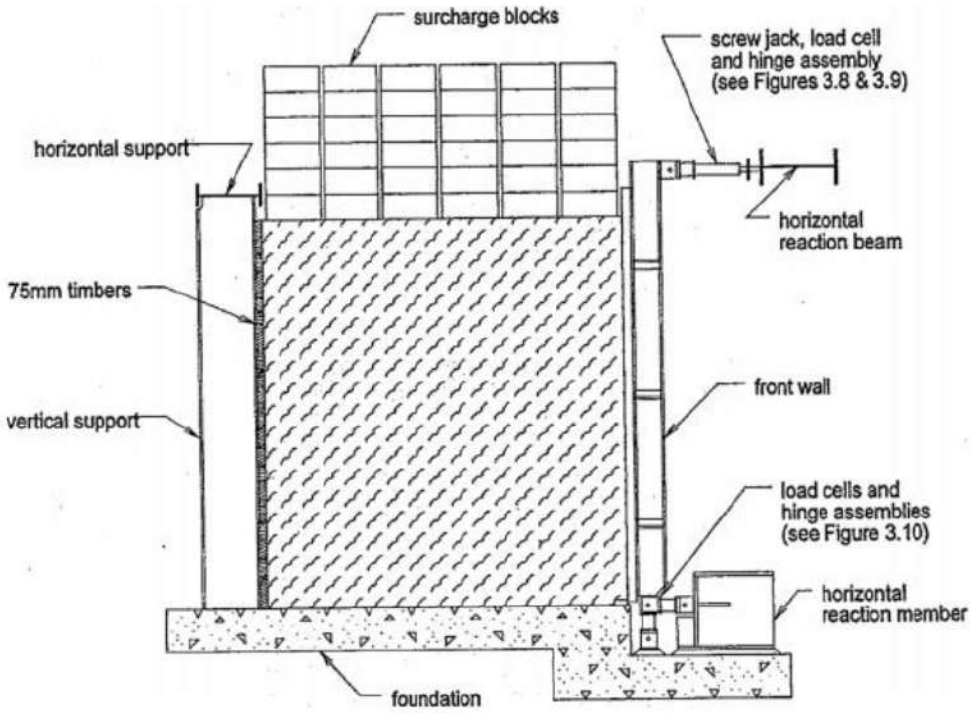

Figure 2. 2. Longitudinal cross section of retaining wall at university of maine proposed by Tweedie et al. (1998).

Humphrey et al. (1997) constructed a 300 m long abutment using the STD geological materials for a bridge in Tubham. Four types of instruments were installed to monitor lateral earth pressure against the abutment wall (Figure 2.3). It was observed that the total compression of the tire shred fill was 520 mm, which was 13% greater than the 460 mm that was anticipated based on laboratory compression tests. Xiao et al. (2012) used shake table experiments to evaluate the seismic efficiency of geogrid-stabilized retaining walls constructed with Tire Derived Aggregate (TDA) (Figure 2.4), noted that wall displacements, accelerations, and dynamic backfill stresses were reduced noticeably by the use of TDA compared to that of conventional sand backfill.

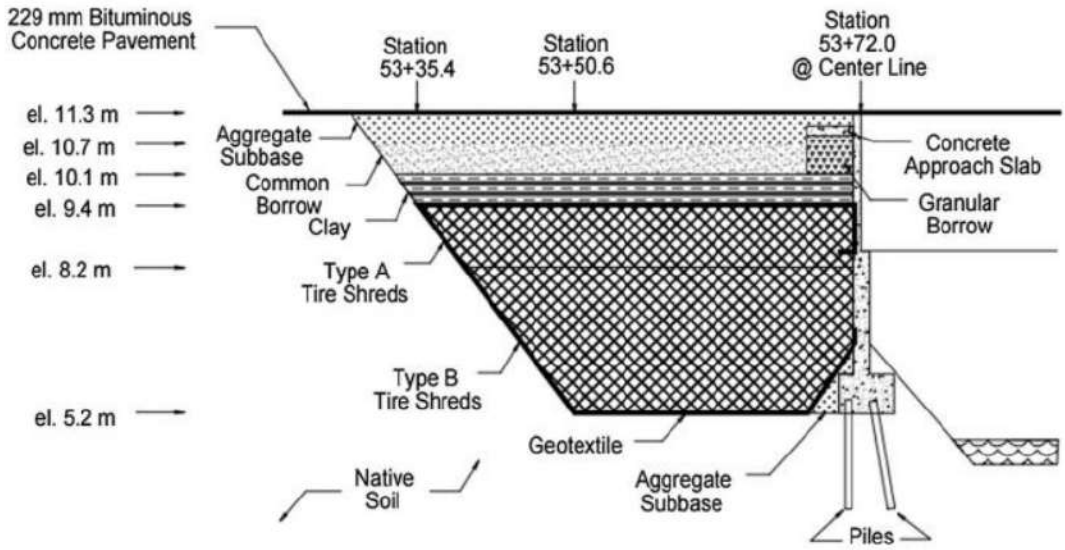

Figure 2. 3. North abutment of the 300m long Merrymeeting Bridgr proposed by Humphrey et al. (1997).

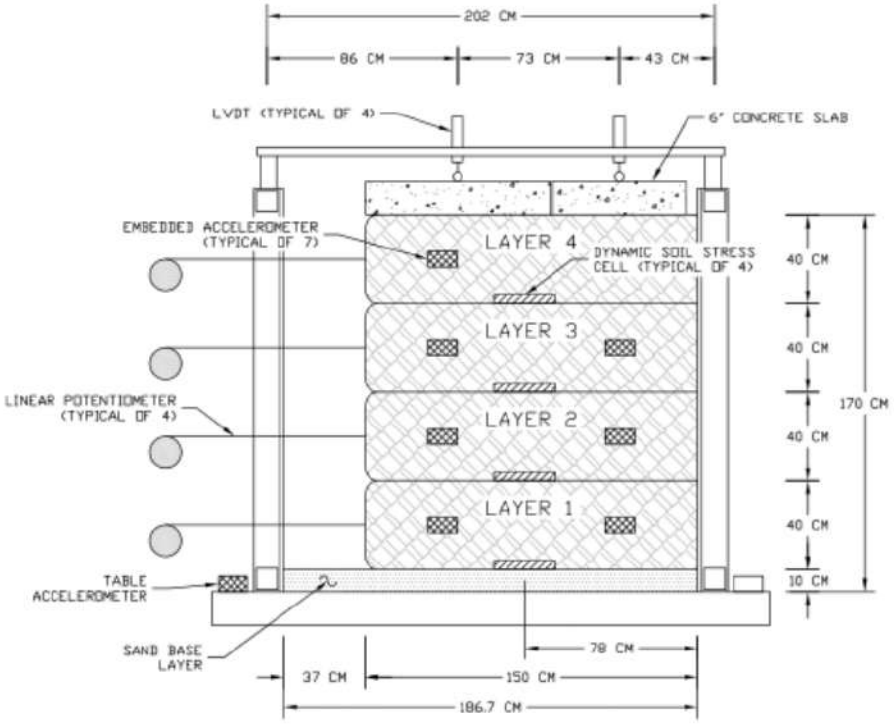

Figure 2. 4. Test configurations.

Hazarika et al. (2008) conducted induced model studies using a mixture of tire chips and sand as backfill for retaining walls in order to study the effect of sand and sand-tire aggregate mixtures on the seismic behavior of caisson walls. They observed that the use of sand mixed with tire chips reduces soil liquefaction. The additional dynamic ground pressures on soil structures have been reduced by about 60% as shown in Figure 2.5.

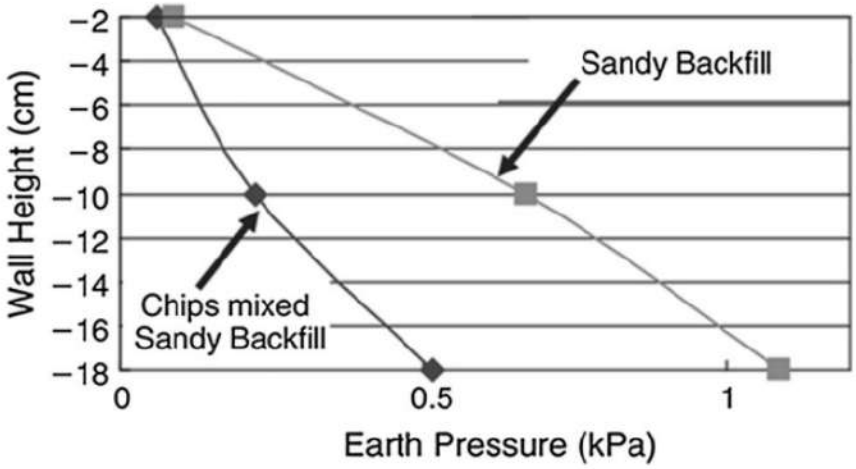

Figure 2. 5. Incremental seismic earth pressure proposed by Hazarika et al. (2008).

Reddy and Krishna (2015), and Dammala et al. (2015) investigated the static and the seismic behavior of retaining wall backfilled with sand-tire aggregate mixtures (STC) as backfill materials. Reddy and Krishna (2019) conducted a shaking table experiment to investigate the seismic response of retaining wall models backfilled with different types of sand–tire chips (STC) mixtures. The STC mixtures with different tire chip proportions, such as STC10, STC20, STC30, STC40, STC50, and STC0 (control test) were considered as backfill materials, as shown in Figure 2.6. They concluded that the tyre chips content in sand, up to 50% to 65% reduction in wall displacements and 70% to 80% lowering of dynamic earth pressures were observed compared with the control test (STC0) conventional backfill model wall.

Based on full-scale shake table testing, Ahn and Cheng (2014) reported that TDA backfill experienced significant shear deformation; however, the dynamic earth pressures exerted on the wall due to TDA backfill were considerably less than those compared to soil backfill.

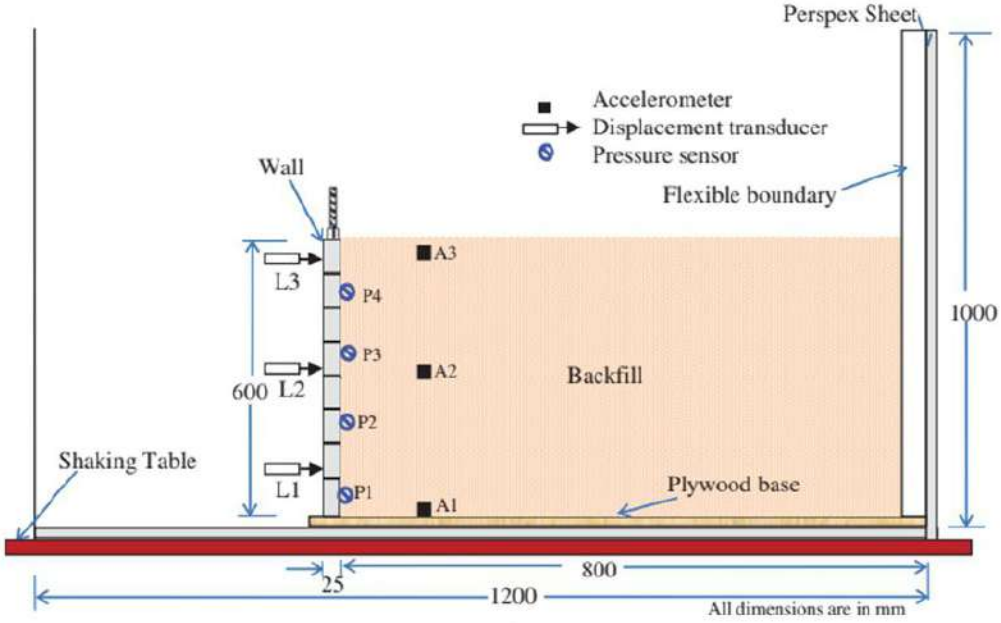

(a)

(b)

Figure 2. 6. (a) schematic diagram of retaining wall model for dynamic tests; (b) different STC mixtures used by Reddy and Krishna (2019).

Numerical studies and field tests of concrete culverts backfilled with tire chips and expanded polystyrene by Lee and Roh (2007) showed that the use of tire combination resulted in a lower dynamic earth pressure due to its lower modulus of elasticity and its higher damping ratio can efficiently reduce the dynamic earth pressure induced by the compaction load due to the effects of wall movement and enhance the characteristics of compacted soils compared to expanded polystyrene. Lee and Roh (2007) compared the performance of tire chips and expanded polystyrene (EPS) boards as cushions materials in reducing the dynamic earth pressures acting on the culvert walls. Based on numerical modeling and field studies, they showed that the dynamic earth pressures on the culvert reduced by 70% due to cushion made up of tire chips compared to a reduction of 23% for the case of EPS board. This is because of low modulus of elasticity and high damping ratio of tire chips compared to those of EPS material.

Ravichandran and Huggins (2014), and Shrestha et al. (2016) performed a numerical investigation on the seismic behavior of cantilever retaining walls backfilled with tire shreds and clean sand using a finite element software (PLAXIS 2D). Figure 2.7 shows the PLAXIS model with mesh. The studies showed a significant decrease in the maximum bending moments, shear forces, and displacements of the walls when the tire aggregate backfill was used. The maximum bending moments and shear forces, for sand and tire chips backfills were compared in Figure 2.8. Sand backfill had undergone maximum bending moments and shear forces of 1105.4 kNm/m, and 421.78 kNm/m while that of tire chips was 790.93 kNm/m, and 224.01 kN/m. It was reported that the reduction in maximum bending moments and shear forces was due to the absorption of acceleration by the tire chips. After, Shrestha and Ravichandran (2018) studied the static and dynamic behaviors of a retaining wall backfilled with tire aggregate using finite element simulations. They found that the geotechnical designs and computer simulations show significant reductions in structural demand in terms of maximum shear force and bending moment, and construction cost in terms of excavation behind the wall, material required for constructing a retaining wall, and the volume of backfill material when tire aggregate is used as the backfill. The results of a parametric study indicate that the economic advantage is significant even with the highest and the lowest values of the key properties and the parameters of input motion.

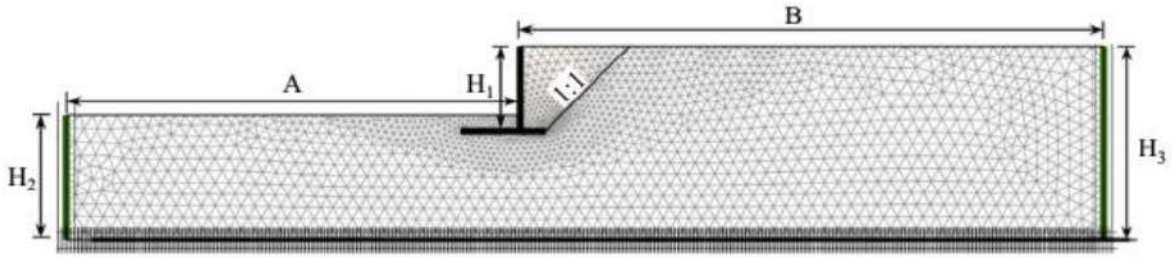

Figure 2. 7. Simulation domain with sample finite element mesh.

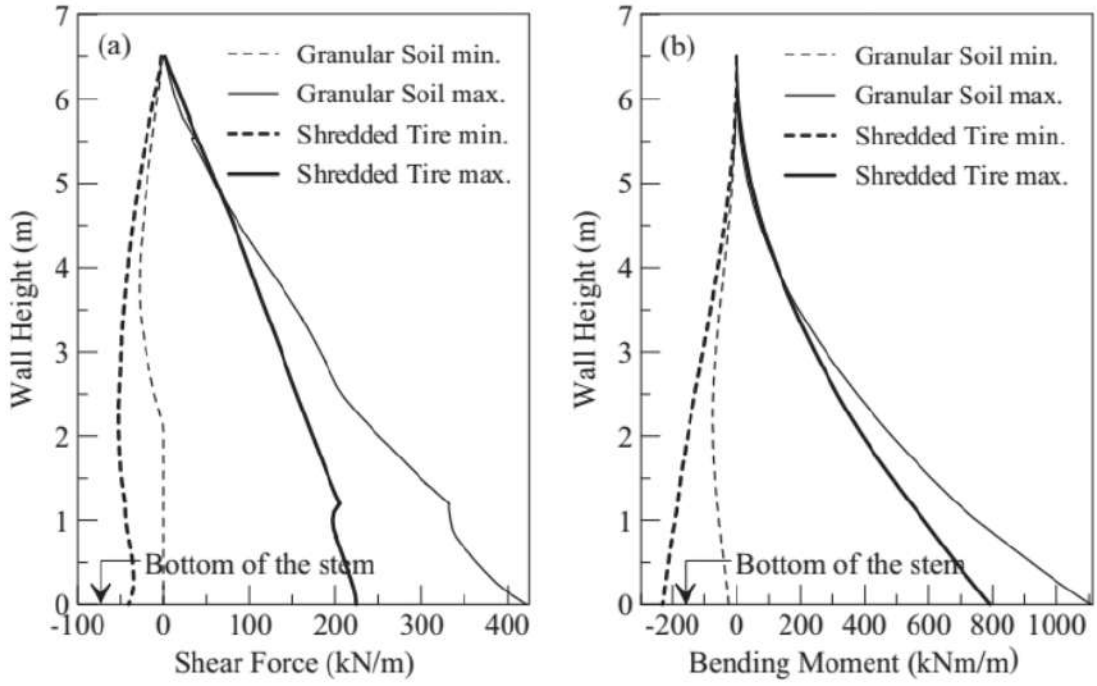

Figure 2. 8. Comparison of computed maximum shear force and bending moment.

Djadouni et al (2019) studied a cantilever retaining wall (CRW) with different STC mixtures, as lightweight backfill materials were evaluated and analyzed numerically using the finite element software, RS2. It was found that cases with STC0 and cases with STC100, as presented in Figures 2.9, the use of sand alone or pure tire chips as backfill materials influences the response of the wall significantly resulting in a complex interaction between wall and backfill. In both cases, the vertical joint section was turned red indicating that this entire section of the joint has slipped, and this is the opposite of what happened in the cases with sand–tire chips mixture in which a small failure

was observed; this suggests that the STC mixture is successfully preventing slip/separation from occurring.

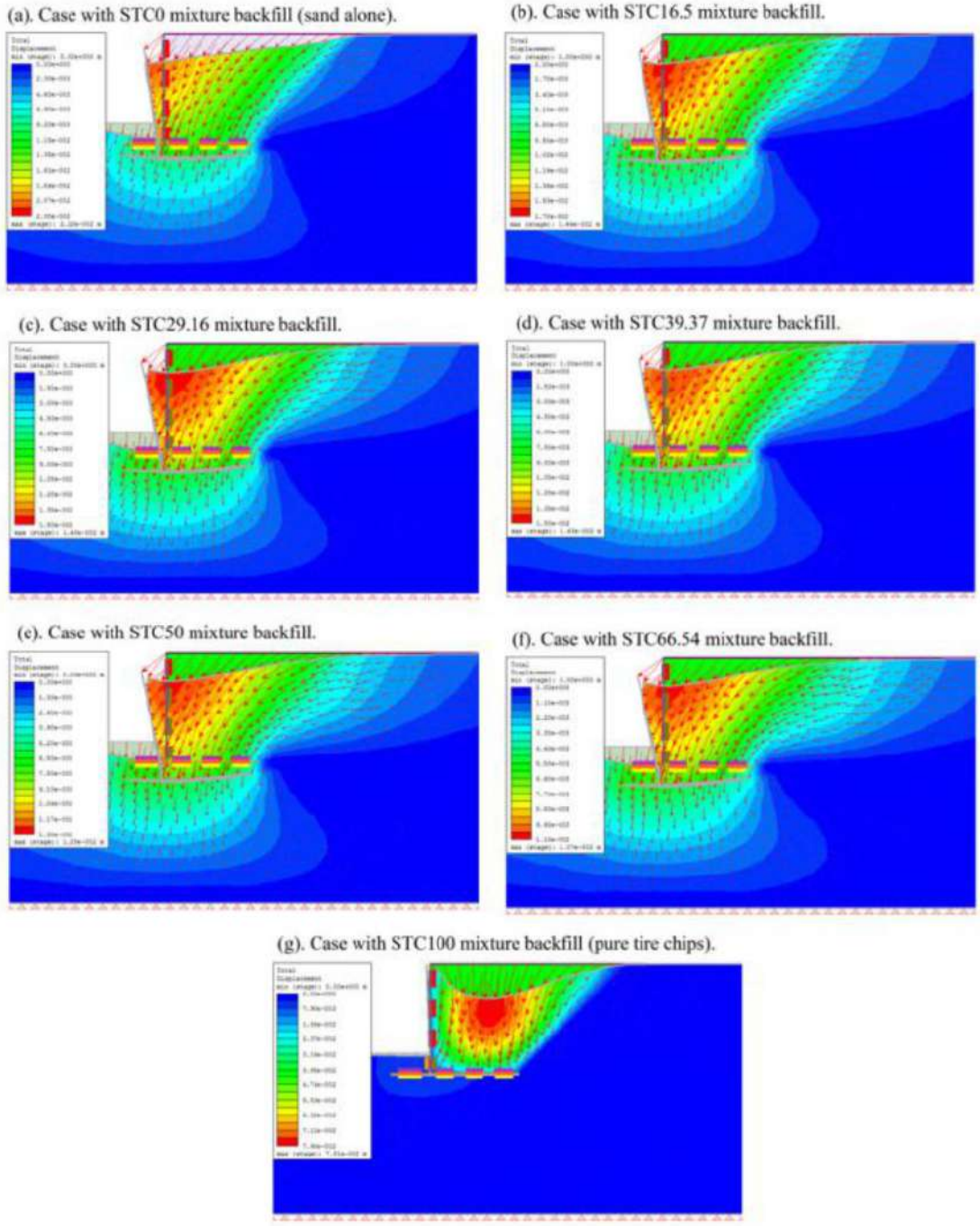

Figure 2. 9. Total displacements of the soil and the retaining wall for each case proposed by Djadouni et al (2019).

2.2.2 Compressible Inclusion (Cushion) Behind Retaining

The use of 1.00 m wide tire shreds behind the rigid frame structure has been reported by Humphrey et al. (1997). slope indicators, soil strain meters, pressure cells, and temperature sensors were installed to monitor the lateral pressures of the earth on the wall, as well as the temperature and movement inside the tire shred area (Figure 2.10). They observed that the presence of tire shreds in the backfill reduced the pressure to less than half the pressure with the soil backfill.

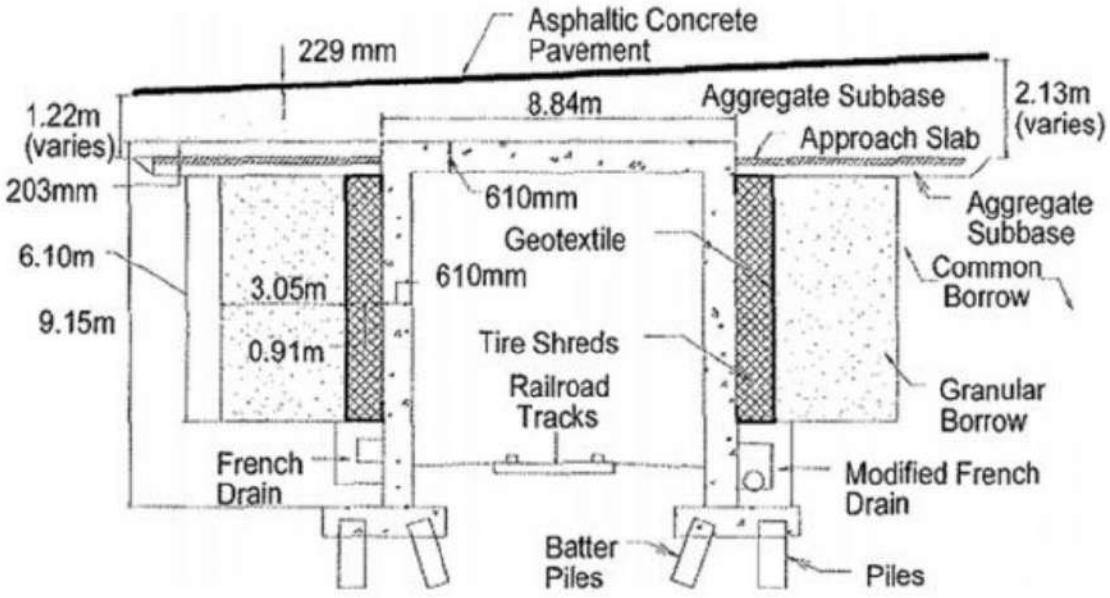

Figure 2. 10. Rigid frame structure with three-foot wide vertical strip of tire shreds proposed by Humphrey et al. (1997).

Field tests were carried out by Hazarika et al. (2004) using a 1.5 m high rigid retaining wall against which the variation of static at rest pressure was measured for a week (refer to Figure 2.11). Figure 2.12 shows the results of the earth pressure distribution tests for two cases; conventional retaining wall and retaining wall with compressible tire shreds cushion (thickness = 30 cm). It can be observed from the figure that the soil pressure is very reduced by using tire chips as a compressible inclusion. Kaneda et al. (2008) performed a numerical investigation on retaining wall by using compressible tire chips between the wall and backfill. The numerical simulation results show that the static at-rest earth pressure against the retaining wall could be brought to a quasi-active state by using compressible inclusion behind the wall.

Shaking table tests have been conducted by Hazarika et al. (2008) on gravity-type model caisson shielded by cushioning tire chips. The caisson model was made 700 mm high and the compressible thickness layer was considered 300 mm using tire slats average size of tire chips 20 mm as shown in Figure. 2.13. The soil structure system was subjected to three different seismic loads and measured the respective responses. The results showed that the earthquake load against the caisson quay wall was reduced using the cushion. However, the presence of the tire chip cushion considerably reduced the displacement of the caisson quay wall.

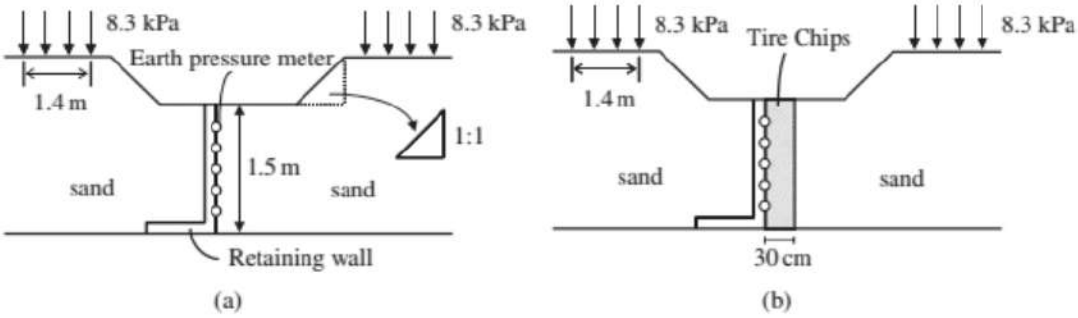

Figure 2. 11. Field-tests: (a) Sand alone, (b) Tire chips as compressible inclusion (after Hazarika et al. 2004).

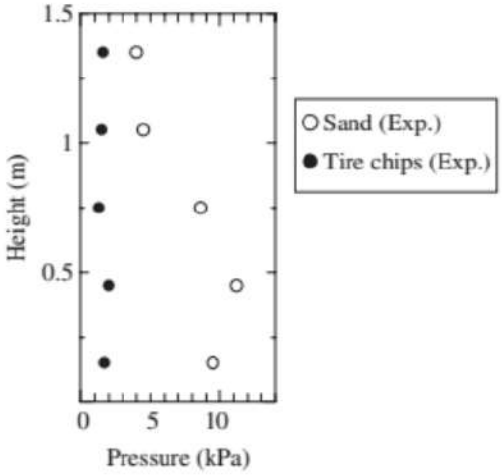

Figure 2. 12. Reduction of earth pressure (after Hazarika et al. 2004).

Reddy and Krishna (2017) investigated using tire chips as a compressible inclusion between wall and backfill under different dynamic excitations. A diagram of the model wall with a compressible inclusion is shown in Figure 2.14. reported using their experimental investigation that the horizontal displacements and lateral earth pressures were reduced to about 70–80%, compared to those without compressible inclusion.

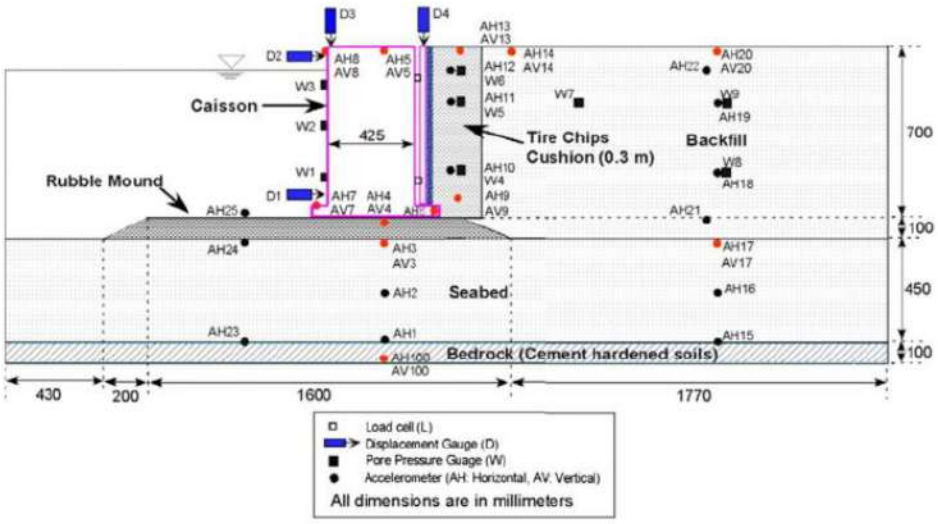

Figure 2. 13. Cross section of caisson model proposed by Hazarika et al (2008).

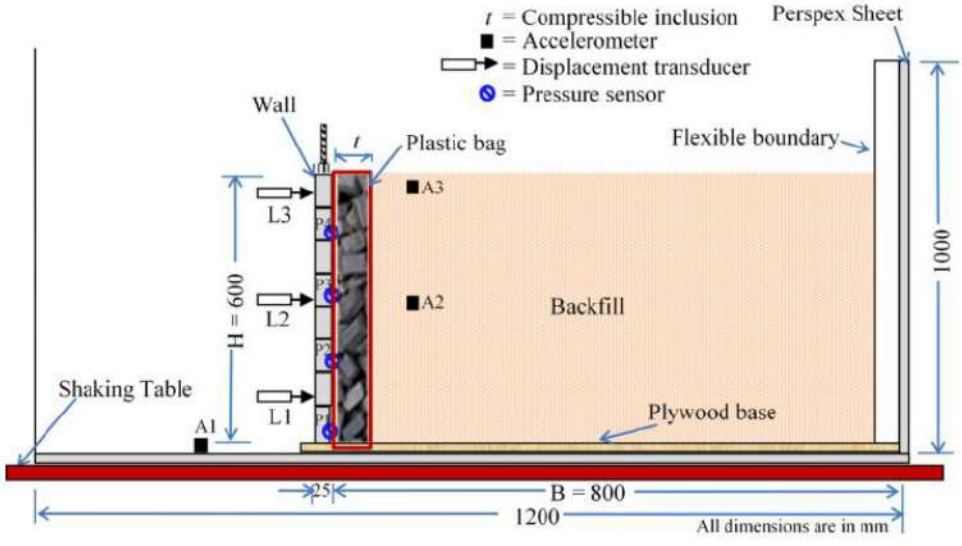

Figure 2. 14. Schematic diagram of the model wall proposed by Reddy and Krishna (2017).

2.3 Back-to-back geosynthetic reinforced soil retaining walls

Bak-to-back mechanically stabilized earth (BBMSE) walls are widely used in various projects. In the Federal Highway Administration (FHWA) design guidelines on reinforced soil walls (Berg et al. (2009)), recommendations on the lateral earth pressures against BBMSE walls under static loading were highlighted. However, numerical model studies on the seismic behavior of BBMSE are very limited or nonexistent.

2.3.1 Back-to-back retaining walls

Back-to-back walls are often used for highway ramps. For walls which are built back-to-back as shown in Figure 2.15, a modified value of lateral pressure influences the external stability calculations. As indicated in Figure 2.15, two cases can be considered and are discussed below.

Case I: For Case I, the overall base width is large enough so that each wall behaves and can be designed independently. In particular, there is no overlapping of the reinforcements. Theoretically, if the distance, D, between the two walls is shorter than $D = H_1 \tan(45° - \phi°/2)$ where H_1 is the taller of the parallel walls, then the active wedges at the back of each wall cannot fully spread out and the active thrust is reduced. However, for design it is assumed that for values of $D > H_1 \tan(45° - \phi°/2) \approx 0.5H_1$ then full active thrust is mobilized (Berg et al. (2009)).

Case II: For Case II, there is an overlapping of the reinforcements such that the two walls interact. When the overlap, L_R, is greater than $0.3H_2$, where H_2 is the shorter of the parallel walls, no active earth thrust from the backfill needs to be considered for external stability calculations. For intermediate geometries between Case I and Case II, the active earth thrust may be linearly interpolated from the full active case to zero (Berg et al. (2009)).

For Case II geometries with overlaps (L_R) greater than $0.3H_2$, the following guidelines should be used:

- $L1/H1 \geq 0.6$ where L_1 and H_1 is the length of the reinforcement and height, respectively, of the taller wall.
- $L_2/H_2 \geq 0.6$ where L_2 and H_2 is the length of the reinforcement and height, respectively of the shorter wall.
- $W_b/H_1 \geq 1.1$ where Wb is the base width as shown in Figure 2.15 and H_1 is the height of the taller wall.

The above guidelines are valid for static load conditions or in areas where the seismic horizontal accelerations at the foundation level are less than 0.05g (Berg et al. (2009)). Back-to-back walls in seismically active areas should be designed based on a more detailed analysis that includes effects of potential non-uniform distribution of seismic and inertial forces within the wall.

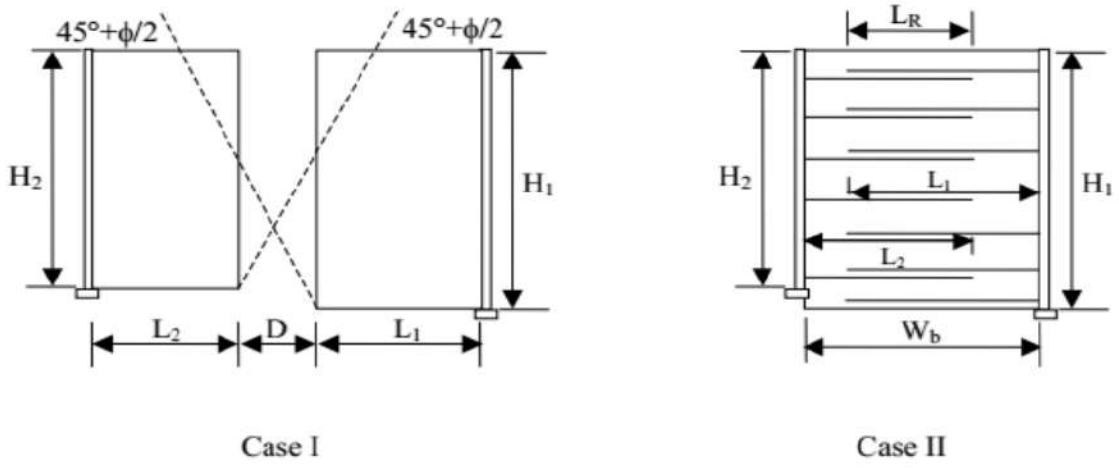

Figure 2. 15. Back-to-back MSE walls.

Ling et al. (2003) had simulated an overpass in Turkey, using FLAC. Tensions in reinforcements and lateral displacements were computed for seismic loading. However, the model was basic which may simulate the exact field conditions. Hardianto and Truong (2010) had studied the effect of the aspect ratio of back-to-back walls on tensile forces under seismic loading. Lower aspect ratios were also analyzed using FLAC 6.00. However, the study was elementary as it did not consider the staged constriction and compaction stresses (Mouli and Umashankar (2019)).

Han and Leshchisnskv (2010) studied back-to-back MSE retaining walls using FLAC and ReSSA (limit-equilibrium-method based software). The effects of the ratio of the distance between the walls to the height of the walls (*W/H* ratio) and quality of backfill on the critical failure surface required the tensile strength of reinforcement, and lateral pressures at the end of the reinforced zone were analyzed. The analysis was performed at limit state condition using FLAC. Limit equilibrium analysis was performed for only single walls and results were comparerd with the back-to-back walls. Walls of 6-m height were simulated. The angle of shearing resistance of the backfill (ϕ) of 25° and 34° and *W/H* ratio of 1.4, 2.0, and 3.0 were considered for the study. The critical failure surface was dictated to pass through the toe of the walls by providing the weaker bond strength at the bottom blocks of the facing. The shape and location of critical failure surfaces were analyzed

for various *W/H* ratios and various angle of shearing resistance of the backfill. The critical failure surface of one wall interferes into the reinforced zone of the other wall in low *W/H* ratios. Figure 2.16 shows the interaction of critical failure surfaces in *W/H* = 1.4 and 2.0 for ϕ = 25° and 34°. It was observed that the interference of failure extended to the greater depths as the angle of shearing resistance was decreased. In *W/H* = 1.4, and ϕ = 25°. the interaction between the failure surfaces extends up to about half the depth of the walls. As per FHVVA guidelines, for ϕ= 34°, walls with *W/H* = 2.0 should behave independently. However, the interaction of critical slip surfaces was observed for this configuration. In *W/H* = 1.4, lateral force at the end of the reinforcement zone reduced to about 70% mid 85% of theoretical active Kankine lateral force in ϕ = 25°. and ϕ = 34° respectively. The percentage reduction of lateral force with W\H ratio is more significant in ϕ = 25° than ϕ = 34°. The distribution of maximum tension in reinforcements with the depth of the wall in the unconnected walls was reported as linearly increasing up to a certain depth and then constant till the bottom of the wall. However, in connected walls maximum tension was constant all through the depth of the wall. A limit state, connected walls mobilize lesser tensions than that of unconnected walls. The value of maximum tension in reinforcement increases with a decrease in the angle of shearing resistance of the backfill. The maximum reinforcement tensions in walls with ϕ = 25° were 67% and 100% higher than those of walls with ϕ = 34° in connected and unconnected walls respectively. However, the model had not simulated staged construction and compaction stresses (Mouli and Umashankar (2019)).

Katkar and Viswanadham (2011) analyzed back-to-back walls using finite element. software-PLAXIS 2D. the study aimed in examining the effect of distance between the ends of the reinforcements of the walls (*D*) and angle of shearing resistance of backfill on the lateral displacements and maximum tensions in the reinforcements. A wall of 6-m height was considered. Four cases were considered with different *D/H* ratios ranging from 0 to 1.6. The connection of reinforcements was also studied. Lateral displacements and the maximum tension in the reinforcements were studied. Lateral displacements reduced drastically in the case of connected reinforcements. However, the maximum tension in the reinforcement in the connected case was found to be higher than that for the unconnected case. However, the model was a basic model which did not consider staged construction (Mouli and Umashankar (2019)).

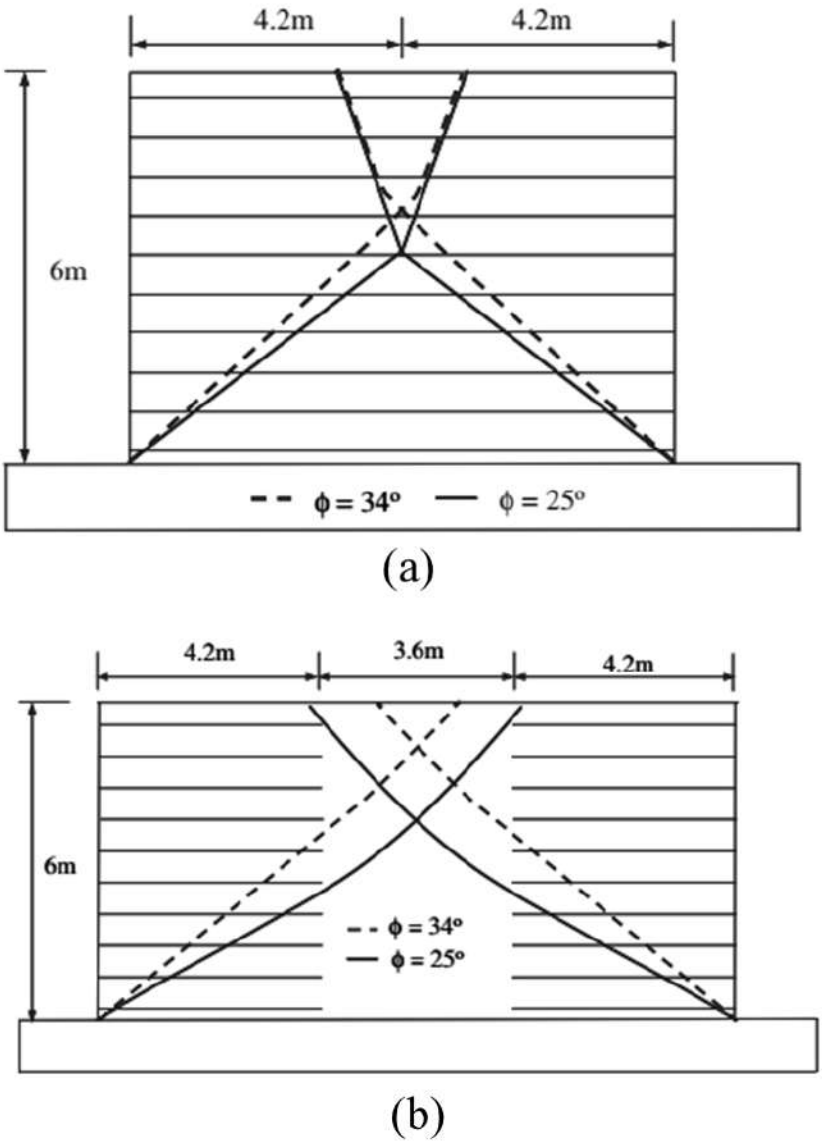

Figure 2. 16. Influence of angle of shearing resistance of backfill on ceitical failure surface in back-to-back walls in (a) $W/H = 1.4$, and (b) $W/H = 2$.

Anubhav and Basudhar (2011) studied the response of footing placed on a double-faced, wrap-around reinforced walls using numerical modeling in PLAXIS 2D. Authors have presented the influence of number of reinforcing layers and overlap length on load-deformation behavior, the ultimate bearing capacity of footing, and lateral deformations. The numerical results were validated using experimental data. Experiments were conducted in a small-scale tank. The numerical model could predict the experimental data with minimum error. However, the numerical and experimental

model was simulated a wall of height 0.5m and the results might be affected with full-scale wall (Mouli and Umashankar (2019)).

Katkar and Viswanadham (2012) conducted centrifuge model tests to study the behavior of single vertical wall, and back-to-back geogrid reinforced walls constructed using the wrap-around technique. The effect of reinforcement connection in the middle of the wall was also analyzed. In this study, three cases were considered. Single reinforced wall, back-to-back walls with unconnected reinforcement, and back-to-back walls with reinforcement connected in the middle were considered. Lateral deformations, strains in the reinforcements, and surface settlements were studied. Loading was given from 10g to 60g. It was found that the connected walls had lesser lateral deformations than those of unconnected walls. However, the peak strains in the reinforcements were highest in the connected walls at 45g (Mouli and Umashankar (2019)).

El-Sherbiny et al. (2013) used the finite element method (PLAXIS) to simulate a back-to-back walls model. Effect of distance between the walls on the lateral pressures, lateral displacements, and the maximum tensions in the reinforcement was studied under working-stress condition. The formation of the critical slip surface and overall factor of safety of the back-to-back walls were analyzed under limit-state condition. It was found that as the distance between the walls decreases from 0.5H to zero, the lateral earth pressures decreases by approximately 25% and the maximum tensile force in the reinforcement reduces by 5% -10%. The length of reinforcement was also varied to investigate the effect in reducing the length to less than 0.7H. The reduction in the length of reinforcement increased the horizontal deformation and the maximum tensile forces. However, the study did not mention about the interfaces used and the study did not consider the compaction stresses (Mouli and Umashankar (2019)).

Benmebarek et al. (2016) modeled back-to-back walls incorporating staged construction using Finite Element Program (PLAXIS). Critical failure surfaces, lateral pressures at the end of the reinforcement zone, lateral displacements and maximum tension profile along the height of the wall were investigated for various *W/H* ratios. The study concluded that interaction between the walls exist even when the *W/H* ratio is more than two for an internal angle of shearing resistance of backfill of 35° (as per FHWA guidelines, both the walls should behave independently for *W/H* > = 1.93). *W/H* ratio had a significant influence on the lateral pressures at the end of the reinforcement zone. Influence of cohesion in the backfill material was also analyzed. A small

reduction in the lateral pressures was observed. Djabri and Benmebarek (2016) analyzed back-to-back walls using limit state approach. Effect of W/H ratio on the lateral earth pressures, maximum tension profiles and critical failure surface was dealt. Djabri and Benmebarek (2016) analyzed *W/H* ratio effect on lateral displacements and the maximum tension line. In both the above studies, the effect of reinforcement stiffness was not considered. Model did not consider the surcharge loads also (Mouli and Umashankar (2019)).

Balunaini et al. (2017) studied the effect of compaction and surcharge loads on both connected and unconnected BBMSE walls. Benmebarek and Djabri (2017a) investigated the effect of overlap length in the back-to-back walls using PL AXIS (refer to Figure 2.17). The influence of overlapping length on the factor of safety, lateral displacements, maximum tension in the reinforcement, potential failure surface for internal stability was studied. It is found that the factor of safety was increasing by 50% with an increase in overlapping length from $0.1L_R/H$ to $0.4L_R/H$. Lateral displacements decreased by more than 20% when overlapping length increases. Reinforcement tension had minimal effect with the overlap length. The effect of the height of the walls was also studied. However, the interface between the facing panel was simulated as hinges which might not simulate the exact interaction of the facing panels.

Benmebarek and Djabri (2017b) investigated for simple cyclic harmonic loading in back-to-back MSE walls. It concluded that the lateral deformations and maximum tensile force in the reinforcements were affected by the variation of *W/H* ratios in this loading condition. When the *W/H* ratio is decreased, the amplitude displacement decreases drastically. The stability of back-to-back walls significantly depended on peak ground acceleration and frequency of loading. The study concluded that lateral displacements and maximum reinforcement tension forces were not linearly related to the characteristics of loading. However, a detailed study in back-to-back walls with respect to the compaction stresses and surcharge loads was required. The reinforcement stiffness effect was not studied in any of the above studies (Mouli and Umashankar (2019)).

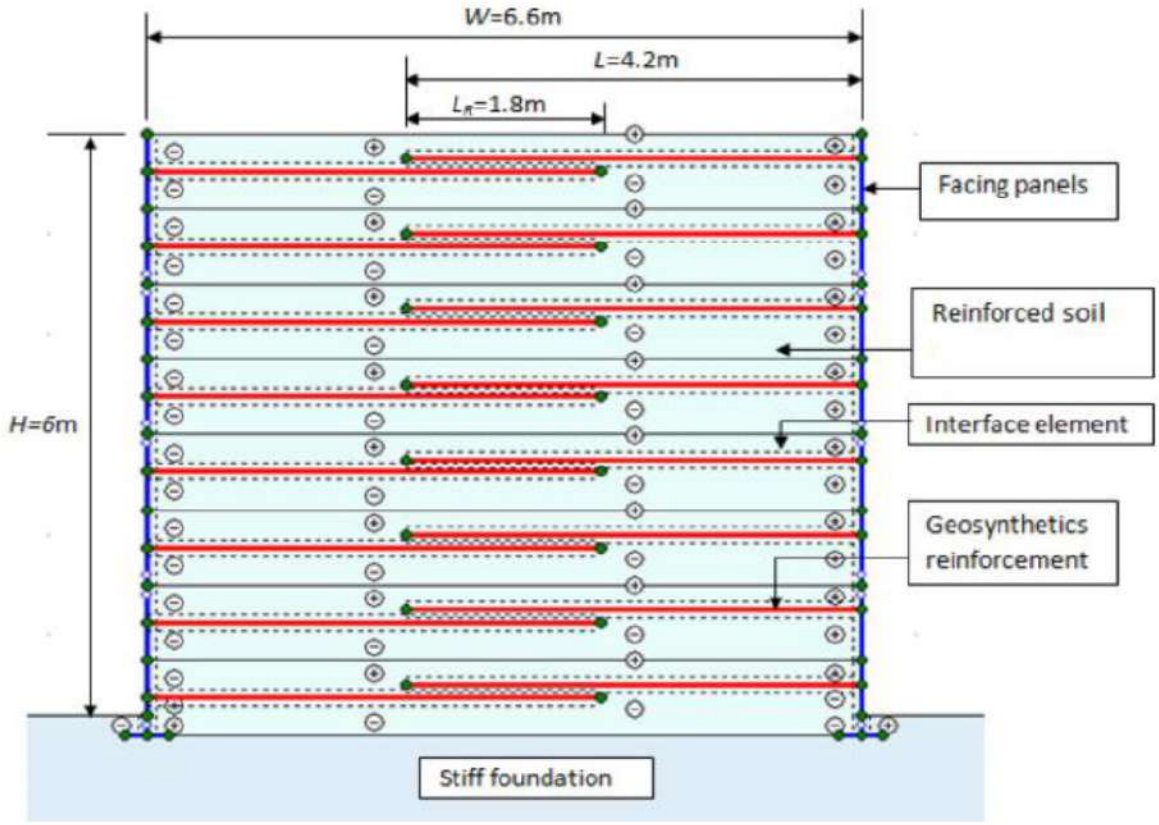

Figure 2. 17. The geometry of the basic model proposed by Benmebarek and Djabri (2017a).

Djabri and Benmebarek (2020) used the finite element method PLAXIS 2D to simulate a back-to-back (BBMSEWs) walls model. The effect of backfill type, wall facing type, reinforcement stiffness, and distance between opposing walls was studied under the static and dynamic response of an idealized 6 m high BBMSEW with 12-m width. It is found that by decreasing the distance between opposing walls to zero, the reinforcements from both sides would meet in the middle and the magnitude of the displacement has been significantly reduced. also, it was revealed that connecting two opposing walls reduces only the maximum horizontal displacement, while the effect of axial rigidity of reinforcement was found to be negligible.

Sravanam et al. (2019) studied the back-to-back MSE walls with full-length panel facing are modeled using finite difference-based software (Fast Lagrangian Analysis of Continua). presented the lateral pressures at the facing and at the end of the reinforcement zone under compaction and surcharge loads on BBMSE walls in various configurations (*W/H* ratios). The influence of these loads on the maximum tensile loads in the reinforcement was also analyzed. Both connected and

unconnected BBMSE walls were analyzed to study the various design parameters (mainly tensile profiles of reinforcement) under working stresses (Sravanam et al. (2020)). The effect of the stiffness of the reinforcement was also examined.

2.4 Summary

This chapter described the properties of different materials (sand, tire chips, and STC mixtures) used on laboratory model tests numerical simulations and field studies, and discussed briefly in order to provide critical insight into various behavioral aspects of these structures. Generally, scrap tire-derived geomaterials and their mixtures showed excellent performance benefits when compared to conventional sand fills. By observing the variation of void ratio and shear-strength values of various mixtures. Which can reduce the demand for a huge volume of sand material in any geotechnical application. This optimum shredded tire and mixture will provide better compressibility characteristics due to the lesser void ratio and high load-carrying behavior due to high shear strength. In addition, the results showed that the dynamic load against the structure retaining can be considerably reduced through the proposed techniques in the field of shredded tire backfills and compressible inclusion just behind the retaining wall.

A review of numerical, and experimental methods proposed to investigate the seismic response of back-to-back mechanically stabilized earth (BBMSE) walls was presented. The literature on back-to-back walls for different parameters like reinforcement stiffness, types of wall facia, loading conditions, and battered angle of the facia was limited. Hence, an extensive study on back-to-back walls is needed to study the intricacies of the problem. However, there are very limited numerical modeling and experimental studies on the behavior of back-to-back mechanically stabilized earth walls in seismic conditions.

The next chapter will discuss the finite element method that will be adopted for this research. All steps required for building up the numerical model will be presented in detail in order to fill the knowledge gaps discussed previously.

SECOND PART

NUMERICAL MODELING

Chapter 3

Performance of retaining walls with compressible inclusions under seismic loading

3.1 Introduction

This chapter present investigates the possible application of recycled tire shreds as compressible inclusion behind retaining walls under dynamic loading. A numerical model to analyze the behavior of retaining walls with compressible cushion was developed in PLAXIS 2D, a two-dimensional finite element analysis-based software. The results were validated by comparison with experimental findings from physical models. A parametric study is also presented in order to the effects of the thickness of the compressible cushion and the friction angle of the backfill on the seismic performance of retaining walls. The following sections discuss the effect of each of these parameters on the seismic response of the wall models in terms of horizontal displacements, lateral earth pressures to bring out the effectiveness of tire chips as compressible inclusions.

3.2 Development and Validation of Numerical Model

3.2.1 Details on Physical Model Study

Physical model tests conducted in the container by Kloukinas et al. (2015) were adopted as the reference case models for developing the numerical model. The target physical model wall was 4.8m long ×1 m wide and 1.15 m deep, constructed in a flexible laminar container. The apparatus was kept on the shake table of aluminium of 3 × 3 m size and a payload capacity of 3.8 tons were used in the tests. The shaking can be equipped with various frequencies from 1 Hz to 100 Hz. The overall device is provided with 21 1-D accelerometers to determine accelerations, 4 LVDT (linear variable differential transducer) to capture dynamic response and permanent displacement, and 32 strain measures to observe the wall bending. Figure 4.1 shows the dimensions of the model and the position of instrumentation used in the experiment. The model comprised of L-shaped retaining walls with a 0.6 m deep backfill resting on a 0.4 m deep soil layer. Configuration 1 comprised of wall heel of 300 mm with 50 mm toe. In Configurations 2 and 3, the wall heel was shortened by 50 mm making it 250 mm in both cases and the toe was removed after increasing the frictional

resistance of the base interface from 23.5° to 28°, by gluing with a rough sandpaper. The interface friction angles were measured in-situ through static pull tests on the wall. The foundation layer and backfill were both made up of Leighton Buzzard (LB) sand (Fraction B) prepared at different compaction levels. Based on the relative densities, D_r, of sand prepared, the peak friction angles of the foundation layer and the backfill were estimated from empirical correlations as 42.5° and 33.5°, proposed by the experimental work of Cavallaro et al. (2001). Figure 4.2 shows the overall sand layers specified in two different sections with different frequencies (f_{1n}) and a shear modulus (G_0). The retaining wall model was made of aluminium alloy 5083 plates of thickness 32 mm with properties: unit weight $\gamma = 27 kN/m^3$, Young's modulus $E = 70$ GPa and Poisson's ratio $\nu = 0.3$. The harmonic acceleration was loaded by a sinusoidal excitation composed of 15 stable cycles. An excitation frequency of 7 Hz was then chosen for a series of sinusoidal seismic excitations with increasing amplitude Kloukinas et al. (2015).

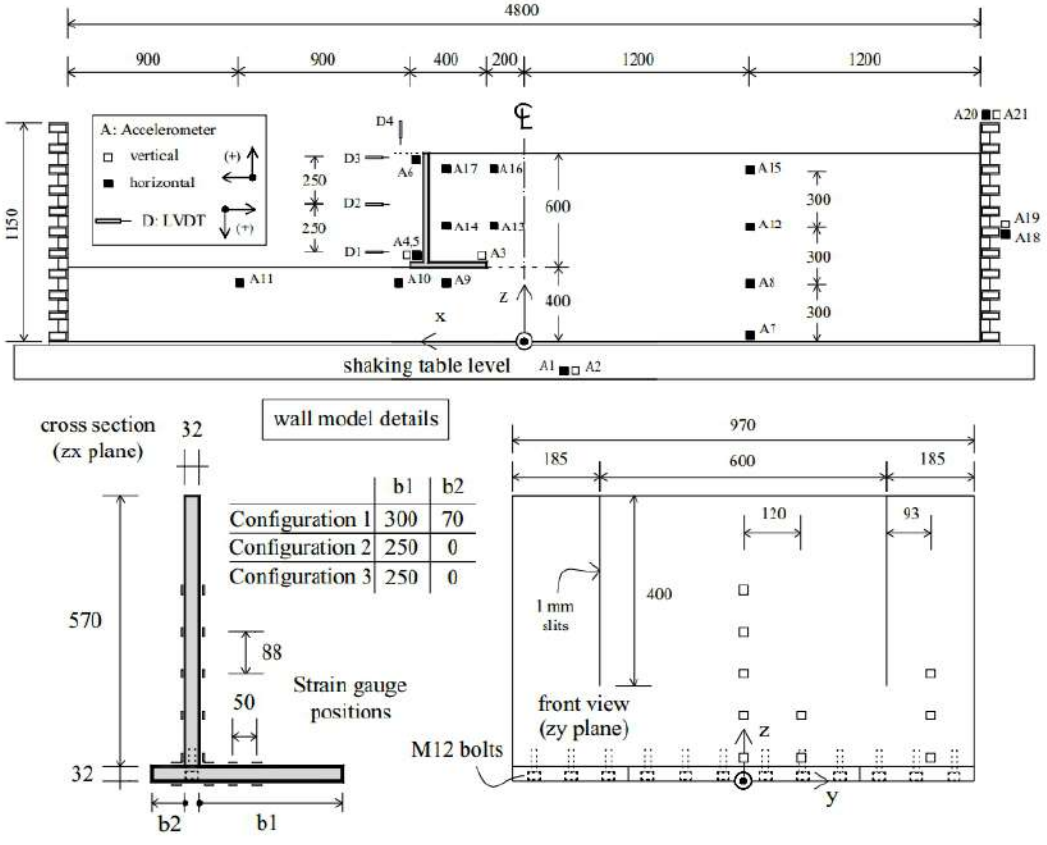

Figure 3. 1. Geometry and instrumentation of shake test table (2015) (dimensions in mm).

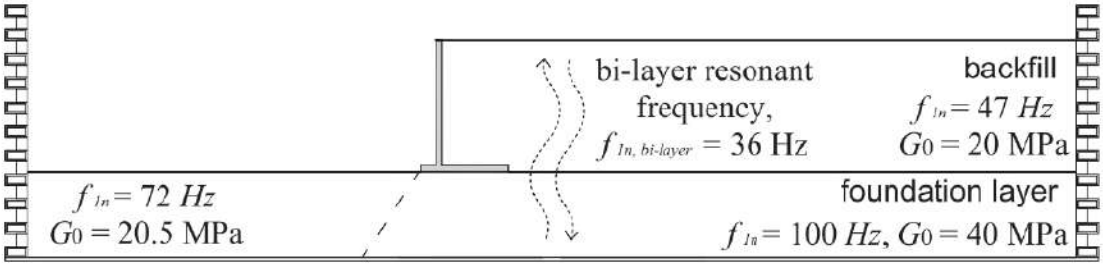

Figure 3. 2. Frequencies and shear modulus for different sand layers (2015).

3.3 Numerical modelling

In this study, same size as the physical shaking table test model 4.8 m wide and 1 m high, was simulated numerically using PLAXIS 2D. The size of a retaining wall was taken for Configuration 3 with height of 600 mm and a base width of 250 mm. Three node points D1, D2 and D3 along the height of the wall were taken to record the displacement histories of the wall (refer to Figure 3.3).

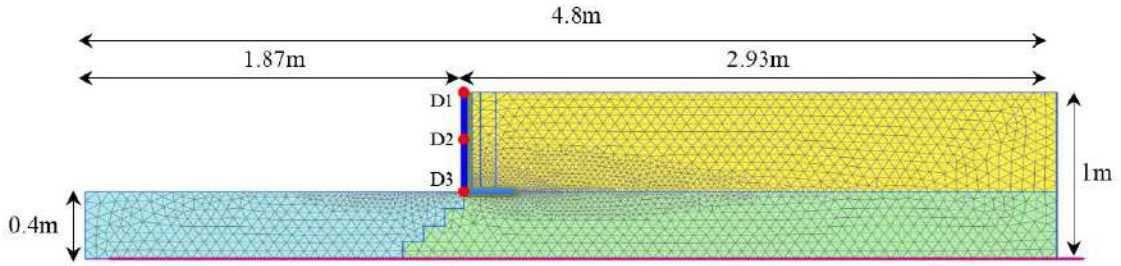

Figure 3. 3. Finite element mesh used in the numerical model in PLAXIS for shake table test.

3.3.1 Case analysis

Figure 3.4 shows the two series of analyses carried out in the study. In first series (Case A), a retaining wall model with a medium dense backfill was used (Control case). In another series (Case B), tire shreds were placed vertically in the form of compressible inclusions with three different thicknesses, chosen as follow: 25 mm, 50 mm and 100 mm (t/H = 0·04, 0.08 and 0·16), behind the model wall as a buffer cushion, in which t denotes thickness of tire shreds and H denotes the wall height. To better comprehend the behavior of compressible inclusions under harmonic cyclic loading conditions, parametric studies were conducted on different models (as presented in Table

4.1), which expresses the dynamic response of each model in terms of the lateral earth pressures and displacements.

Table 3. 1. Parameters of the different models for finite element analysis.

Thickness of compressible inclusion (t) (mm)	Code t/H	Input acceleration (g)	Excitation
0.00	0.00 (Control Case)	0.1	
25	0.04	0.2	
50	0.08	0.3	
100	0.16		
	Backfill ϕ (30, 40°)		Sinusoidal, 7 Hz 15 cycles
0.00	0.00 (Control Case)		
25	0.04	0.3	
50	0.08		
100	0.16		

3.3.2 Materials models used

The numerical study was performed for 15 nodes elements and plane deformation condition. The material parameters for the sand and retaining wall have been taken similar to those from the shake table test. In this research, the Mohr-Coulomb elastoplastic model was used to illustrate the stress-strain behavior of foundation, soil and backfill materials, especially when subjected to dynamic loads (see Table 3.2).

The tire shreds material was modelled as a linear elasto-plastic material. The cushion layer consisted of pure tire shreds (grain size 50–150 mm). The tire shreds properties obtained are shown in Table 3.2, which are in the range of the results reported by Shrestha et al. (2016).

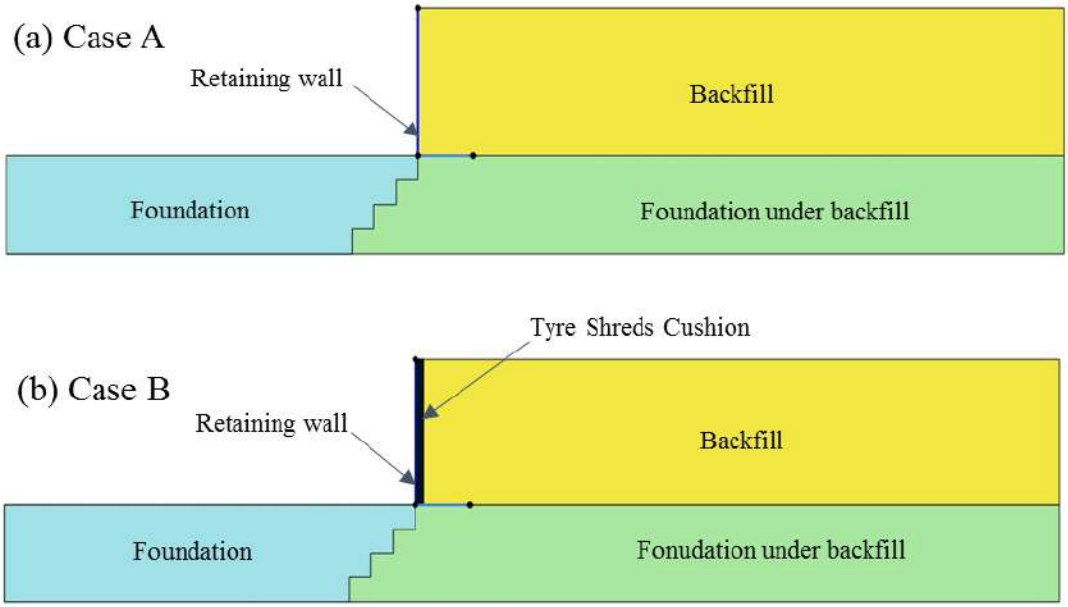

Figure 3. 4. Model cases considered: (a) Case A: sandy backfill, and (b) Case B: compressible cushion used between sandy backfill and retaining wall.

3.3.3 Properties of structural components

The retaining wall was modelled as a linear-elastic material. In PLAXIS input, the properties of the wall are defined by its elastic stiffness (EA), flexural rigidity (EI), unit weight (γ), Poisson ratio (ν) and its weight (W). The properties utilized in the modelling are shown in Table 3.3.

Table 3. 2. Material properties used in numerical simulations [Shrestha et al. (2016) and Shrestha et al. (2016)].

Material	γ (kN/m^3)	E (kN/m^2)	c (kN/m^2)	ϕ (°)	ν	R_{inter}
Foundation (dense sand)	16.14	53.3×103	1	42	0.3	0.6
Foundation (dense sand) under backfill	16.14	104×103	1	42	0.3	0.6
backfill (medium dense sand)	15.11	52×103	1	34	0.3	0.6
Tire shreds	6.313	1363	6.8	23	0.29	0.6

Table 3. 3. Material properties of the retaining wall.

Parameter	Symbol	Value	Unit
Elastic stiffness	EA	2.24×10^6	(kN/m)
Flexural rigidity	EI	191	(kN/m^2/m)
Unit weight	γ	27	(kN/m^3)
Weight of wall	W	0.86	(kN/m/m)
Poisson ratio	ν	0.3	-

3.3.4 Dynamic analysis

3.3.4.1 Damping

In PLAXIS, the dynamic calculations depend on the fundamental equation of the movement of a volume as a function of time under the influence of a dynamic load (2017). The relative damping of mass and stiffness is computed as given in Eq. (3.1).

$$C = \alpha_R M + \beta_R K \tag{3.1}$$

where C, M, and K are the damping matrix, the mass matrix, and the stiffness matrix, respectively. α and β are the Rayleigh coefficients. Given the Rayleigh damping, a relationship can be established between the damping ratio ξ and Rayleigh damping parameters α and β:

$$\alpha_R + \beta_R \omega^2 = 2\omega\xi, \text{with } \omega = 2\pi f \tag{3.2}$$

In Eq. (3.2), ω is the angular frequency [rad/s] and f the frequency [Hz]. Resolving (3.2) for two different target frequencies and corresponding target damping ratios give the required Rayleigh damping coefficients:

$$\alpha_R = 2\omega_1\omega_2 \frac{\omega_1\xi_2 - \omega_2\xi_1}{\omega_1^2 - \omega_2^2} \tag{3.3}$$

$$\beta_R = 2\frac{\omega_1\xi_1 - \omega_2\xi_2}{\omega_1^2 - \omega_2^2} \tag{3.4}$$

In PLAXIS 2D, the target frequencies and damping ratios can be specified after the Rayleigh coefficients are automatically calculated through Eqs. (3.3) and (3.4), where ξ is the target damping of 5.0 %. Hudson and Beirkae (1994) and Hashash and Park (2002) explain that the first target

frequency can be taken as the first natural frequency f_1 and the second target frequency is taken as the closest odd integer larger than the ration f_p/f_1, the ratio of the predominant frequency of the input motion to the natural frequency of the soil. The natural frequency of soil deposition of thickness H is related to its geometry and its stiffness by this equation:

$$f_1 = \frac{v_s}{4H}, v_s = \sqrt{\frac{V_s}{\rho}} \tag{3.5}$$

where, v_s is the shear wave velocity in the soil deposition, a function of the shear stiffness modulus G. The values of the Raleigh damping coefficients and the dynamic soil properties were calculated using Eqs. (3.4-3.5) and are shown in Table 3.4.

Table 3. 4. Rayleigh damping coefficients for backfill and foundation materials.

Soil	H (m)	V_s (m/s)	f_1 (Hz)	α	β
Foundation (dense sand)	0.4	115.9	72.438	4.103	0.0001524
Foundation (dense sand) under backfill	0.4	111.6	69.750	3.997	0.0002074
backfill (medium dense sand)	0.6	113.8	47.416	3.832	0.0002925
Tire shreds	0.6	28.65	11.937	2.772	0.0008404

3.3.5 Element size

For the finite element model, the size of the mesh elements discretizing the soil profile of the dynamic calculation is a major importance to ensure a correct propagation of the waves in the model. The maximum element size can be determined according to Kuhlemeyer and Lysmer (1973). In this theory, the maximum size of the elements in a layer is limited by the maximum frequency and the shear wave velocity of a layer as given in Eq. (3.6):

$$\text{Average Element size} \leq \frac{\lambda}{8} = \frac{V_{S,\min}}{8 \times f_{\max}} \tag{3.6}$$

3.3.6 Interface properties

In order to model the interaction between soil and structural units, it is necessary to identify interfaces. This is done to specify a lower resistance between a structured surface and the soil. Without interface elements, no slipping or gapping is allowed, which in most cases is a non-physical assumption for the interaction between structure and soil. Strength and stiffness reductions are introduced through the use of interfaces, by the parameter R_{inter}. The interface strength was reduced by using the strength reduction factor of 0.60 < 1 in these analyses.

3.3.7 Boundary conditions

A standard absorbent boundary applied to the model as suggested in the user's manual (2017) for dynamic analysis. The absorbent boundaries are applied at x-min and x-max of the model to absorb the increments of stress on the boundaries due to the dynamic loading and the base of the model domain against translation in both x and y directions. The fixed base has been applied with a horizontal prescribed displacement to the numerical model.

3.3.8 Excitation

The finite element model was subjected to a basic excitation representing a harmonic motion of variable amplitude. The frequency of the applied harmonic input base acceleration was the agent of a typical predominant frequency of medium-to-high frequency content earthquake as suggested by Bathurst and Hatami (1998) and Matsuo et al. (1998). The constant frequency cyclic load was modelled by employing the prescribed displacement feature of the program at the base of the wall, as shown in Figure 3.3. The varied-amplitude harmonic excitation was chosen so that the gradual increase and then decrease in amplitude with a specified frequency makes this loading system similar to a genuine earthquake. The harmonic excitation is represented by Eq. (3.9) and shown in Figure 3.5:

$$a_h(t) = \begin{cases} \frac{a_{\max}}{5} ft \sin(2\pi ft) & \left(t \prec \frac{5}{f}\right) \\ a_{\max} \sin(2\pi ft) & \left(\frac{5}{f} \le t \prec 3.357\right) \\ \frac{a_{\max}}{5}\left[\left(3.357 + \frac{5}{f} - t\right)\right] f \sin(2\pi ft) & \left(3.357 \le t \le 3.357 + \frac{5}{f}\right) \end{cases} \tag{3.9}$$

where, t is time, f is the frequency, and $a_{\max}$ is the acceleration amplitude. The baseline model was subjected to a reference cyclic harmonic load with increasing amplitude of the input

acceleration for a frequency of 7 Hz applied at equal time intervals of 5 s, its accelerogram was obtained using Eq. (3.9). The resulting acceleration time history was used as an input excitation in the numerical model.

3.3.9 Fundamental frequency of analysed walls

Based on one and two-dimensional (2-D) elastic theory of vibration, the fundamental frequency of a linear-elastic media of width '*B*' and height '*H*' contained between two rigid vertical boundaries and a rigid base which is subjected to excite the horizontal base, is given by Bathurst and Hatami (1998):

$$f = \frac{1}{4H}\sqrt{\frac{G}{\rho}}\sqrt{1+\left(\frac{2}{1-\nu}\right)\left(\frac{H}{B}\right)^2} \tag{3.10}$$

where, f is the frequency, G is the shear modulus, ρ is density and ν is the Poisson ratio of the soil medium. For the present model, the height of wall H was 0.6 m and the width B was 4.8 m. Considering soil density (ρ) of 1.540 kN/m^3, a shear modulus (G) of 20,000 kN/m^2 and a Poisson ratio (ν) of 0.3, the fundamental frequency of the wall was calculated as 48.53 Hz. This value is close to the frequency of the input harmonic acceleration recording (f = 7 Hz) used in the numerical simulation.

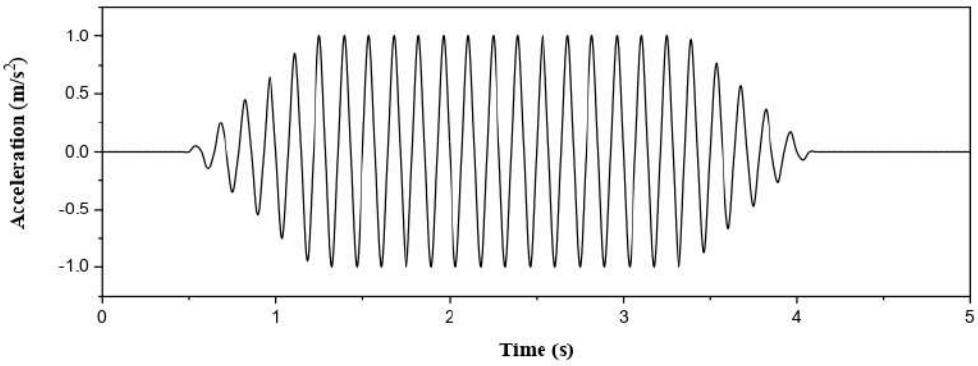

Figure 3. 5. Input sinusoidal motion with 7 Hz frequency and amplitude 0.1 g.

3.4 Model validation

The comparison of the finite element analysis with the shake table tests was firstly done for the maximum dynamic wall displacement as a function of time, at the end of 15 cycles of harmonic excitation of 0.19 g and 0.23 g accelerations at 7 Hz frequency. Figure 3.6 shows the actual response

in terms of the wall displacement time history from the shaking table test. D1, D2 and D3 represent the output points taken at the top, the middle and the bottom of the wall, respectively. The figure demonstrates an acceptable comparison between the results from the numerical and physical models to validate the numerical model in simulating the physical model shaking table tests on retaining walls.

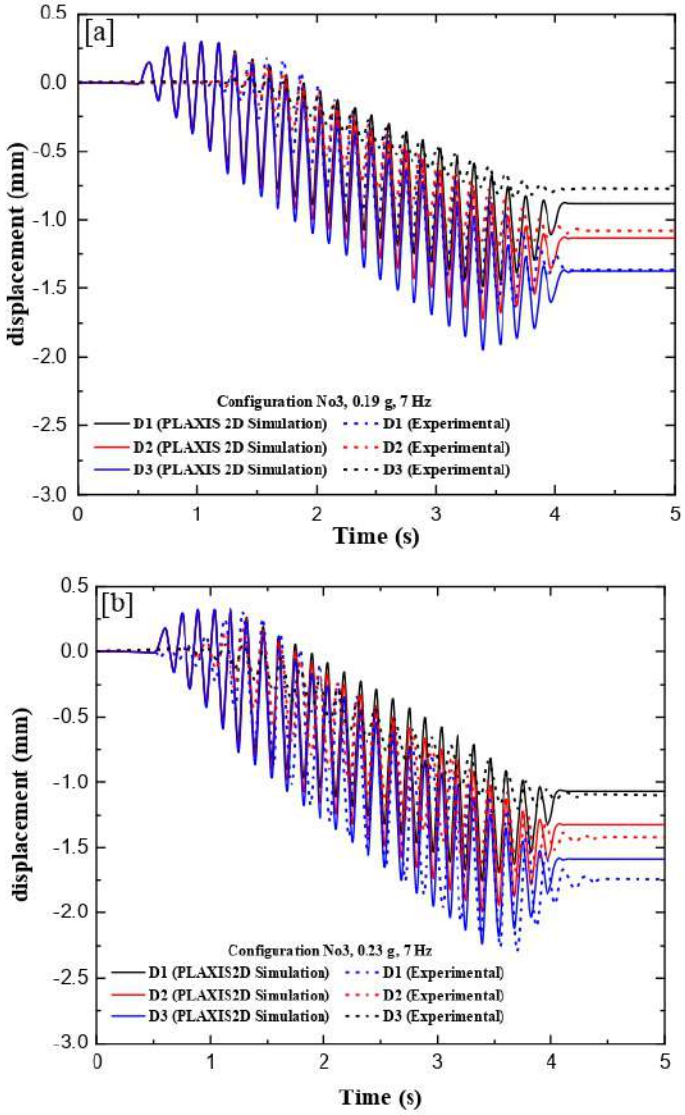

Figure 3. 6. Comparison of results from numerical and physical model tests on Configuration N°3 under sinusoidal–harmonic excitation (a = 0.19 g, 0.23 g, and f = 7 Hz): Horizontal displacement time-histories on the cantilever wall stem.

3.5 Results and Discussions

The time histories of measured horizontal dynamics operating at different elevations for the wall during sinusoidal motion excitation for both model cases (Cases A and B) are compared with Figure 3.7. The displacements at D1, D2, and D3 correspond to the elevations of 50 mm, 300 mm and 550 mm from the base, respectively. It can be seen in the figure that the direction of the displacements increases non linearly with the increase of a number of cycles. The maximum displacement recorded at the end of cycles to model without the cushion ($t/H = 0$) was about 3 mm, 2.41 mm and 1.80 mm at elevations of 550 mm, 300 mm and 50 mm, respectively. In the presence of compressible cushion ($t/H = 0.16$), the maximum displacements of about 1.36 mm, 1.31 mm and 1.26 mm were obtained at elevations of 550 mm, 300 mm and 50 mm, respectively. At the end of the simulation time, it was found that the wall reinforced with tire shreds had lower displacements in the horizontal direction as compared to the control case without the cushion.

3.5.1 Effect of base acceleration on base excitation (Case A)

The model wall subjected to end of 15 cycles of sinusoidal motion excitation with accelerations of 0.1g, 0.2g and 0.3g at a frequency of 7 Hz was considered to examine its influence on the performance of retaining walls. Figure 3.8(a) shows the influence of base acceleration on the permanent displacement response of the wall without the cushion ($t/H = 0$). The maximum displacements were observed at the top of the wall in all simulations. The maximum displacements were equal to 0.84 mm, 1.54 mm and 3.08 mm at input acceleration for 0.1, 0.2 and 0.3 g base acceleration, respectively. Figure 3.8(b) shows that the horizontal earth pressures are seen at the end of dynamic excitation with the height of the wall in different models. It can be seen that horizontal earth pressure showed an increasing trend for the control case ($t/H = 0$) with an increase in the base acceleration of 0.1g, 0.2g, and 0.3g, respectively. However, it was observed that the peak horizontal earth pressures occur at the bottom in the model wall.

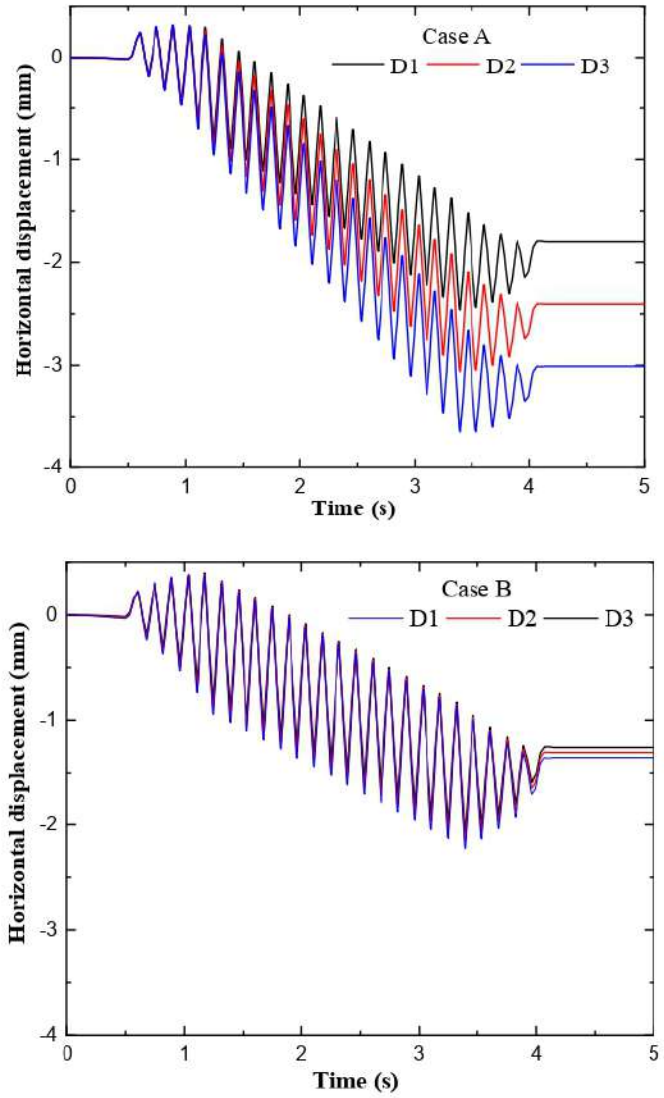

Figure 3. 7. Time histories of horizontal displacements at different elevations for Cases. A and B after 15 cycles of 0.3g at 7 Hz dynamic motion.

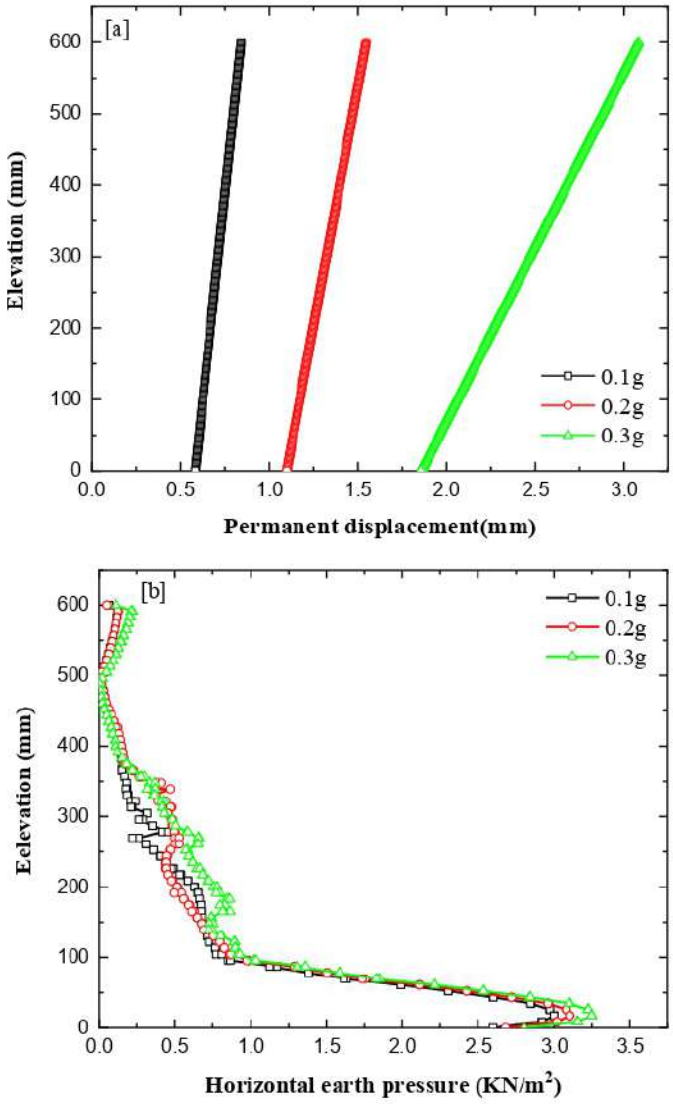

Figure 3. 8. Response of the walls under different harmonic loads for control case: (a). Permanent displacement, and (b) Horizontal earth pressure.

3.5.2 Effect of tire shreds compressible inclusion (Case B)

To study the effects of compressible inclusion, thickness on the model wall response is examined by employing different input base motions. The responses of the model wall with various compressible inclusion thicknesses were compared to those of the controlled case ($t/H = 0$) model wall at similar excitation levels.

Figure 3.9 (a) shows the displacement wall that was excited with a sinusoidal motion of 0.1 g acceleration and 7 Hz frequency, at the end of 15 cycles, showing the influence of compressible

inclusion on the permanent displacement response. It can be seen that the permanent displacements are significantly reduced with the increase in the thickness of the compressible inclusions just behind the retaining wall. The maximum displacement of 0.84 mm with the model $t/H = 0$ was reduced to 0.69 mm, 0.59 mm and 0.49 mm for models using $t/H = 0.04$, 0.08 and 0.16, respectively. A reduction of 16.9 %, 28.9 % and 40.9 % in the permanent displacements as compared to control case ($t/H = 0$) were obtained. Figure 4.9 (b) shows that the horizontal earth pressures decreased with an increase of compressible inclusion thickness along wall height for t/H ratios of 0.04, 0.8 and 0.16 models (a = 0.1 g and f = 7 Hz). The maximum horizontal earth pressure 3 kN/m² is noticed for the model $t/H = 0$ and the corresponding values for the models $t/H = 0.04$, 0.8 and 0.16 are 1.4 kN/m², 1.11 kN/m² and 0.70 kN/m², respectively. A reduction of about 52.9 % to 76.5 % in earth pressure compared to the control case ($t/H = 0$) were observed.

Figure 3.10 (a) shows the base acceleration (a) of 0.2g, dynamic motion is applied to the model wall at frequency f = 7 Hz. The maximum values of the permanent displacements were recorded for t/H ratios of 0.04, 0.8 and 0.16 at the end of 15 cycles. The model results were 1.19 mm, 1.04 mm and 0.94 mm indicating a reduction of 22.44%, 32.1% and 38.9%, respectively, compared to the control case ($t/H = 0$) with a displacement of 1.54 mm. In Figure 3.10 (b), it was observed that horizontal earth pressures exhibit a decreasing trend with an increase in compressible inclusion thicknesses (i.e., t/H ratios of 0.04, 0.8 and 0.16). The maximum earth pressures are observed in the model results were 1.66 kN/m², 1.29 kN/m² and 0.88 kN/m² which corresponds to a reduction of 46.4%, 58.2% and 71.6%, respectively, compared with the model control case with 3.10 kN/m² corresponding to 0.2g acceleration and 3 Hz frequency of base motion.

Figure 3.11 shows the effect of compressible inclusions on the model response in terms of permanent displacements and horizontal earth pressures. The base accelerations of 0.3 g and 7 Hz frequency have been applied on different model walls. As predicted, it is seen that the responses for 0.3 g acceleration are higher than of 0.2 g and 0.1 g acceleration excitation responses. From Figure 3.11(a), maximum values of the permanent displacement of 3.08 mm for the control case and the corresponding values for t/H= 0.04, 0.8 and 0.16 models are 2.51 mm, 2.02 mm and 1.55 mm, respectively. A 49 % reduction in the permanent displacements as compared with the control case ($t/H = 0$). Figure 3.11(b) shows the cushion material effectively reduces the dynamic horizontal earth pressures acting on the wall. The horizontal earth pressures of 3.25 kN/m² is observed for

model $t/H = 0$ and the corresponding values for models using $t/H = 0.04$, 0.08 and 0.16 are 42.1%, 47.2% and 62.0%, respectively.

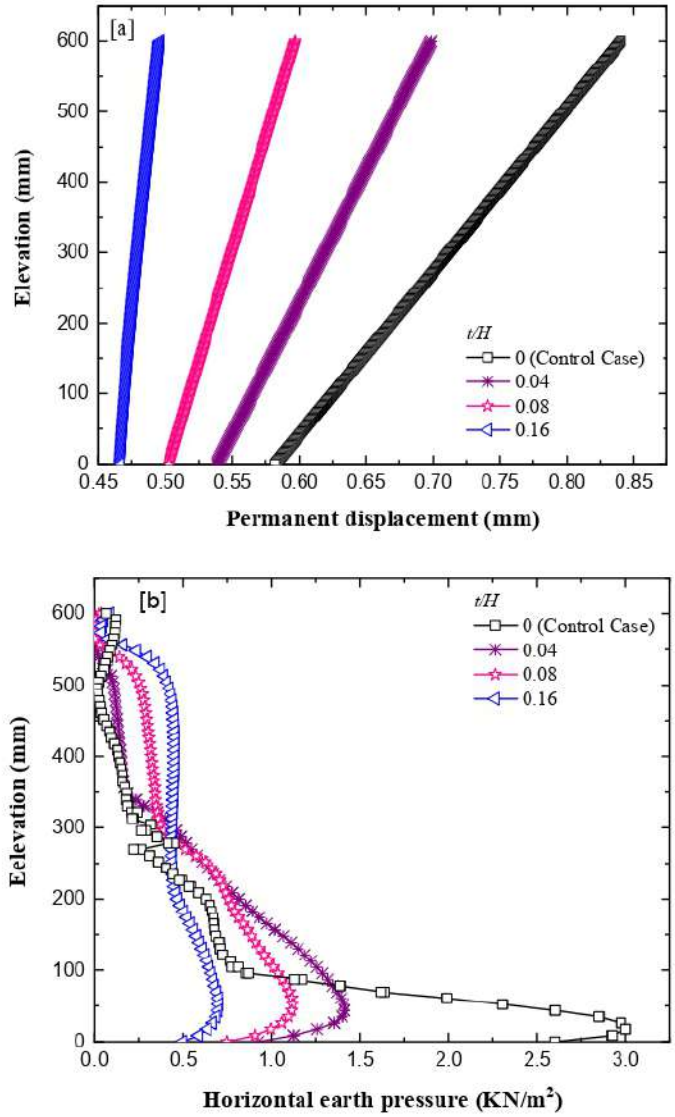

Figure 3. 9. Effect of compressible inclusion thickness under sinusoidal–harmonic excitation of 0.1 g at 7 Hz: (a) Permanent displacement, and (b) Horizontal earth pressure.

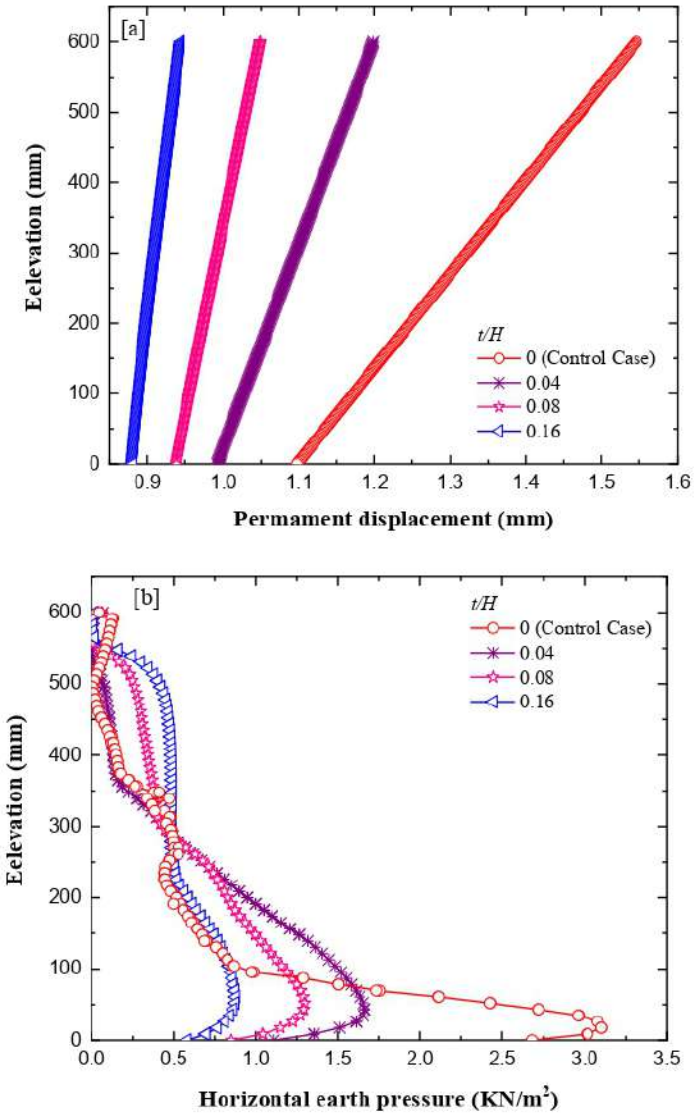

Figure 3. 10. Effect of compressible inclusion thickness under sinusoidal–harmonic excitation of 0.2 g at 7 Hz: (a) Permanent displacement, and (b) Horizontal earth pressure.

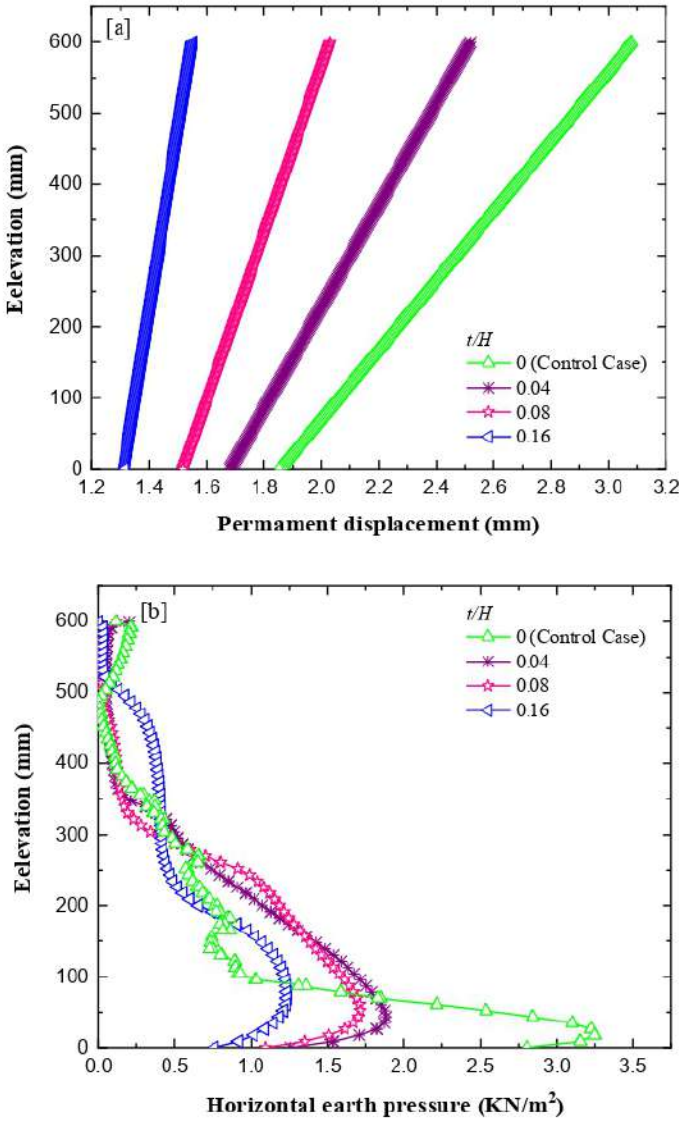

Figure 3. 11. Effect of compressible inclusion thickness under sinusoidal–harmonic excitation of 0.3 g at 7 Hz: (a) Permanent displacement, and (b) Horizontal earth pressure.

3.5.3 Effect of Backfill Friction Angle

To find the effect of friction angle of backfill soil on the harmonic response from retaining wall, dynamic horizontal earth pressure and permanent displacement of the retaining wall were tested for different friction angles of the backfill soil. It is possible to have backfill materials with possibly higher or lower friction angle than 34°, a parametric study was carried out considering the friction angles of 30° and 40°.

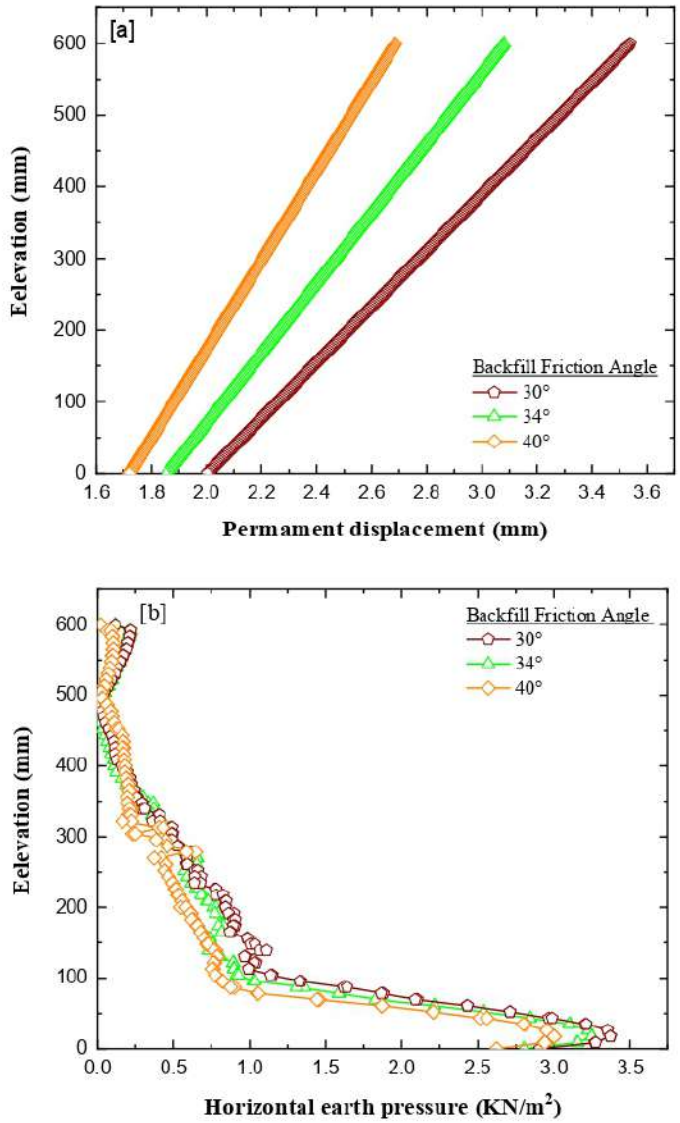

Figure 3. 12. Response of the walls with backfill friction angles 30° and 40° subjected to dynamic excitation (a = 0.3 g, f = 7 Hz) for control models: (a) Permanent displacement, and (b) Horizontal earth pressure.

The dynamic response of the retaining wall model with two different backfill friction angles of 30° and 40° were considered. The comparative results after harmonic excitation (a = 0.3 g, f = 7 Hz) for t/H = 0 cases (no inclusion). The effect of friction angle on the response of model walls without the cushion (t/H = 0) is shown in Figure 3.12. Figure 3.12(a) presents the maximum horizontal at the wall top of 3.5 mm and 2.68 mm with backfill friction angles of 30° and 40°, respectively.

The permanent displacements decrease with an increase in friction angles of the backfill soil. Figure 3.12(b) shows that the horizontal earth pressures have no appreciable variation in the wall corresponding to different friction angles of the backfill at the end of dynamic excitation. However, the horizontal earth pressures in the model without the cushion of 3.37 kN/m² and 2.99 kN/m² with backfill friction angles of 30° and 40°, respectively.

To evaluate the effects of the cushion, various thicknesses of compressible inclusions were used to analyses the effect of soil friction angle on the dynamic response is compared to the control case. As expected, an increase in the backfill soil friction angle increased the resistance of the soil. Figure 3.13(a) shows that the maximum displacements in the case of backfill friction angles of 30° and 40° for models with t/H = 0.16 are 1.67 and 1.45, indicating a reduction of 52.8% and 45.9%, respectively, compared to the control case (t/H = 0). As shown in Figure 4.13(b), the lateral earth pressures are reduced with increased thickness (t/H) of tire shreds cushion with different backfill friction angles of 30° and 40°. A reduction of approximately 55.8% to 65.7%, respectively, in earth pressures for the model t/H = 0.16 compared to the control case (t/H = 0) is observed. However, maximum displacements and earth pressures are decreased with an increasing thickness (t/H) of tire shreds cushion despite a change in the various friction angles of the backfill soil.

The results presented above indicate that recycled tire shreds acted well as compressible inclusions in reducing permanent displacements and horizontal earth pressures on the wall, of the three various thicknesses, considered the lowering is larger in the thicker compressible layer due to the lightweight and compressible nature of the tire shreds. Its absorbance characteristic can also be considered as additional damping. The calculated maximum values of the permanent displacements, horizontal earth pressures, and percentage reduction were summarized up in Table 3.5. From the table, it can be concluded that the permanent displacements were reduced in the range of 38% to 52% and horizontal earth pressures were reduced by about 55% to 76%.

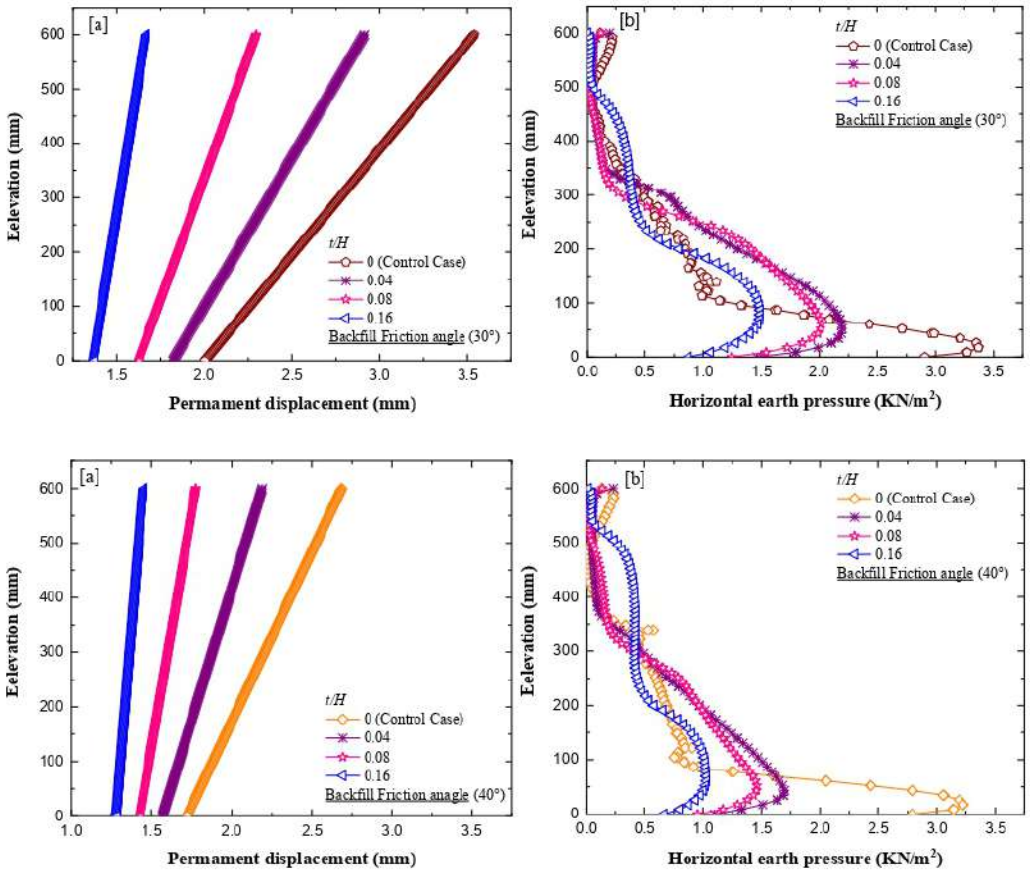

Figure 3. 13. Response of the walls with backfill friction angles 30° and 40° subjected to dynamic excitation (a = 0.3 g, f = 7 Hz) for compressible inclusion: (a) Permanent displacement, and (b) Horizontal earth pressure.

Chapter 4

Seismic performance of cantilever retaining walls with tire shreds as compressible inclusion

4.1 Introduction

This chapter discusses the use of recycled tire shreds as a compressible inclusion behind cantilever retaining wall is one of the novel ways to reduce the seismic earth pressures acting on the wall. The finite element method has been applied to analyze the response of a typical cantilever retaining wall, consisting of compressible tire shreds (CTS) as a cushion, under earthquake ground motion applied at the wall base. The parametric study is set out in this chapter to analyze and study the benefit of compressible tire shreds (CTS) as a cushion, a comparison was made in the behavior of wall without and with cushion in terms of horizontal displacement and rotation, the maximum shear force and bending moment, the seismic earth thrust, and its point of application on the wall. This chapter ends with a summary highlighting the new outcome of the current study.

4.2 Problem description

Most of the studies on the behavior of cantilever retaining wall with compressible cushion are based on experimental investigations on model retaining walls or full-scale testing on retaining walls of limited heights. Very limited studies are available on numerical modeling and analysis of cantilever walls under seismic loading with the inclusion of a cushion made up of compressible tire shreds. Additionally, the effects of various parameters on the behavior of cantilever retaining wall with the cushion in place should be clearly understood, as shown in Figure 4.1. In this study, a finite element-based numerical model was developed to study the seismic response of a cantilever wall without and with a cushion made up of compressible tire shreds between the wall and the backfill. Firstly, the behavior of cantilever walls under a strong earthquake ground motion without and with cushion were compared. Next, the influence of different factors, namely, thickness of compressible cushion, amplitude of earthquake acceleration and frequency of sinusoidal acceleration on the behavior of cantilever walls of three different heights (3 m, 6 m and 9 m) with

cushion in place was systematically studied. The maximum horizontal displacement and/or rotation, the maximum bending moment and shear force, and the total seismic earth pressure and its point of application on walls were proposed for various conditions. The results reported in the study can provide a rational and economical design of a cantilever type retaining walls in earthquake-prone areas.

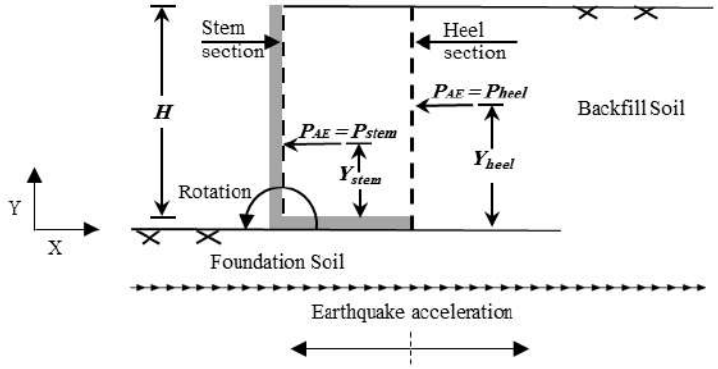

Figure 4.1. Schematic of a typical soil-retaining wall system.

4.3 Numerical modeling

In the present study, a finite element-based program, PLAXIS 2D (2018), was used to develop a plane-strain model to perform the dynamic analysis of the cantilever-type retaining wall subjected to a strong earthquake motion. In the first step, the model developed was validated by comparing the results from the present study with the experimental shake table test results reported by Kloukinas et al. (2015). A detailed parametric study was then carried out using the model developed. The effects of various parameters including (a) thickness of compressible cushion, (b) amplitude of earthquake acceleration, and (c) frequency of sinusoidal acceleration on the maximum horizontal displacements/rotations, maximum bending moments and shear forces, and seismic earth thrust on the wall were quantified.

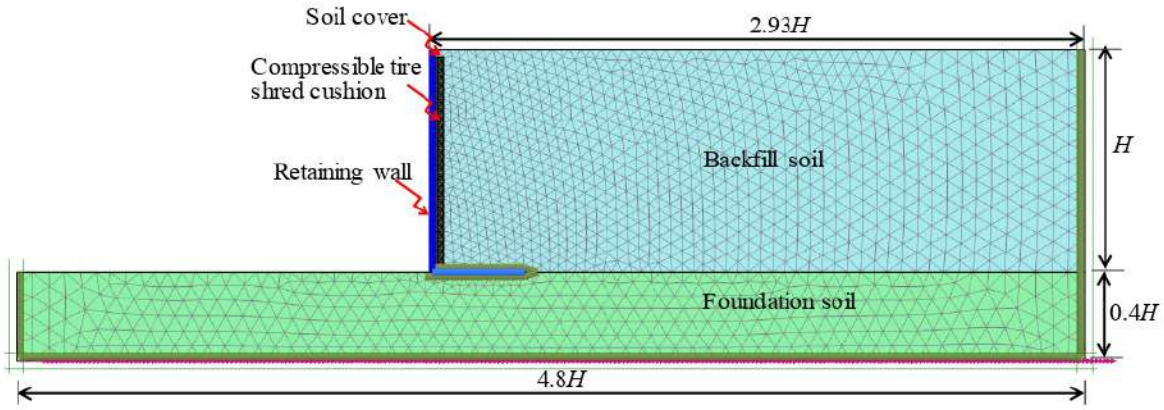

Figure 4. 2. Finite element model of a cantilever retaining wall with CTS cushion between sandy backfill and retaining wall.

4.3.1 Model geometry

Figure 4.2 shows the extents of boundaries expressed in terms of the height of wall, *H*. The selected boundary extents considered in the study were found to produce minimal interference effects [Kloukinas et al. (2015)].

The backfill, the foundation soil, and the compressible cushion as well as the retaining wall were modeled using 15-noded triangular elements in PLAXIS 2D (2018) (refer to Figure 4.2). The seismic analysis included the generation and propagation of shear waves through the wall, backfill, foundation soil, and compressible cushion. Absorbent boundaries were suitably selected to avoid distortions in numerical results (Kuhlemeyer and Lysmer (1973)). The maximum size of the element was directly linked to the maximum frequency of the wave, f_{max}, which propagates through the mesh used in the model. The maximum size of the element must not be greater than 1/8 to 1/5 of the shortest wavelength, λ_{min}, of the shear wave propagating through the soil.

4.3.2 Constitutive model and material properties

Backfill (medium dense sand) and foundation soil (dense sand) considered in the study were represented using the material properties reported by Kloukinas et al. (2015). The elastoplastic Mohr-Coulomb material model was used to represent the backfill, the foundation, and the tire shreds materials. The parameters required to define this model include cohesion *(c)*, friction angle *(φ)*, dilatancy angle *(ψ)*, Poisson's ratio *(v)*, and deformation modulus *(E)* (Table 4.1). Tire shreds material was modeled as a linear elastoplastic material. The compressible cushion consisted of pure tire shreds (particle size ranging from 50 to 150 mm). Table 4.1 gives the properties of tire shreds according to Shrestha et al. (2016).

The retaining wall was modeled as a linear elastic material. In the finite element model, the properties of the wall are defined by its elastic stiffness (*EA*), flexural rigidity (*EI*), unit weight (γ), Poisson's ratio (ν), and its weight (W). Table 4.1 gives the properties of the materials considered in the study.

Table 4. 1 Soil and retaining wall parameters considered in finite element model [Shrestha et al. (2016) and Kloukinas et al (2015)] .

Parameter	Symbol	Unit	Simulation for the shake table by Kloukinas et al (2015)		Soil and retaining wall properties and other parameters used for the present study [Shrestha et al. (2016) and Kloukinas et al (2015)].		
			Backfill	Foundation soil	Backfill	Foundation soil	Tire shreds
Relative density	D_r	%	22	60	22	60	-
Void ratio	e	-	0.72	0.61	0.72	0.61	-
Unit weight	γ_s	kN/m^3	15.1	16.1	15.1	16.1	6.3
Effective friction angle	ϕ	degrees	34	42	34	42	23
Dilatancy	ψ	degrees	4	12	4	12	0
Cohesion	c	kPa	1	1	1	1	6.8
Deformation modulus	E	kPa	52×10^3	104×10^3	52×10^3	104×10^3	1363
Poisson's ratio	ν	-	0.3	0.3	0.3	0.3	0.29
Interface	R_{inter}	-	0.67	0.6	0.67	0.6	0.64
Rayleigh coefficients	α	-	-	-	2.68	9.18	7.40
	β	-	-	-	3.35×10^{-4}	9.80×10^{-5}	1.22×10^{-3}
Retaining wall			Simulation for the shake table by Kloukinas et al (2015)		Soil and retaining wall properties and other parameters used for the present study [Shrestha et al. (2016) and Kloukinas et al (2015)].		
Unit weight	γ_{wall}	kN/m^3	27		27		
Modulus of elasticity	E_{wall}	kPa	70×10^6		70×10^6		
Poisson's ratio	ν_{wall}	-	0.3		0.3		
Elastic stiffness	EA	kN/m	2.24×10^6		22.4×10^6		
Flexural rigidity	EI	kN/m^2/m	191		191×10^3		
Thickness	d	m	0.032		0.32		
Weight of wall	W	kN/m/m	0.86		2.280		

4.4 Validation of the Model

The finite element model developed in the study was validated against the measured data from physical model testing reported in literature. The shake table tests performed by Kloukinas et al. (2015) were selected as validation experiments to compare the seismic behavior of a cantilever retaining wall from the present study. Kloukinas et al. (2015) used a 600 mm high retaining wall of 250 mm base width (Figure 4.3). The soil material used in the preparation of foundation soil and backfill consisted of dense and medium dense beds made up of Leighton Buzzard (LB) sand BS 881-131, Fraction B (average size, D_{50} = 0.82 mm, specific gravity, G_s = 2.64, and the minimum and the maximum void ratios, e_{min}= 0.486, e_{max} = 0.78). The seismic load was simulated by applying equivalent sinusoidal harmonic excitation time histories near the top, middle and bottom of the model with two accelerations of 0.19 g and 0.23 g at a frequency of 7 Hz (Figure 4.4).

Table 4.1 gives the properties of soil and retaining wall used in the model. Figures 4.5(a) and (b) compare the horizontal displacements measured from the shake table tests of Kloukinas et al. (2015) and from the numerical model of the present study. A close agreement in the results were observed. The horizontal displacements from the model were found to be within 10% of those measured from shake table experimental test results for both 0.19g and 0.23g. The validated model was further used to study the response of a typical cantilever retaining wall with and without compressible tire shreds (CTS) cushion under earthquake ground motion applied near the wall base.

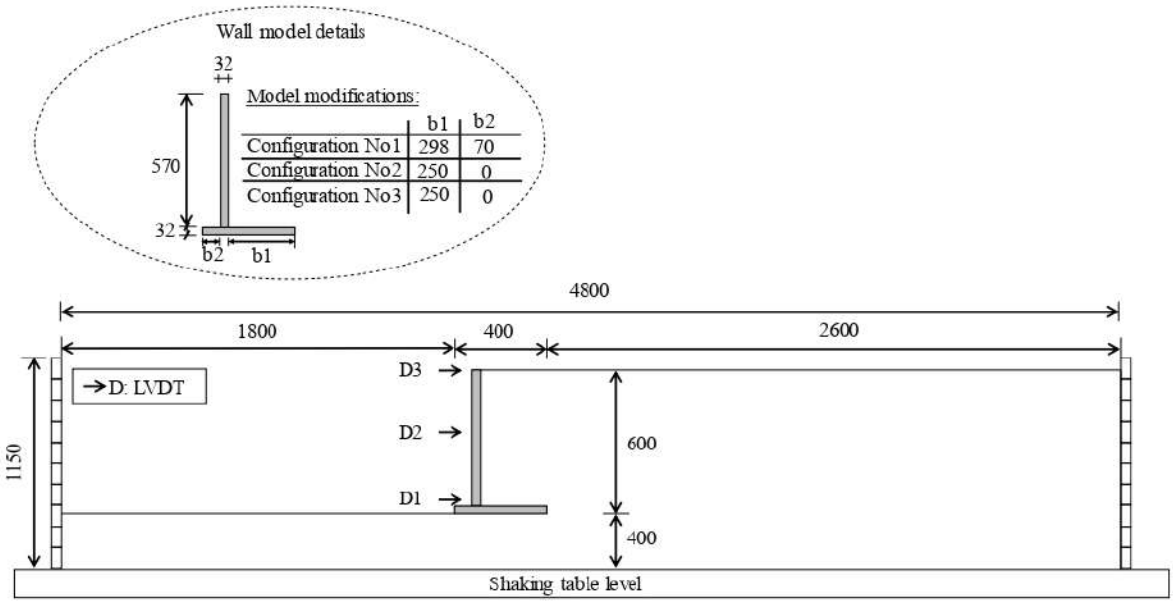

Figure 4. 3. Geometry and instrumentation during shake table testing of Kloukinas et al. (2015) (all dimensions are in mm).

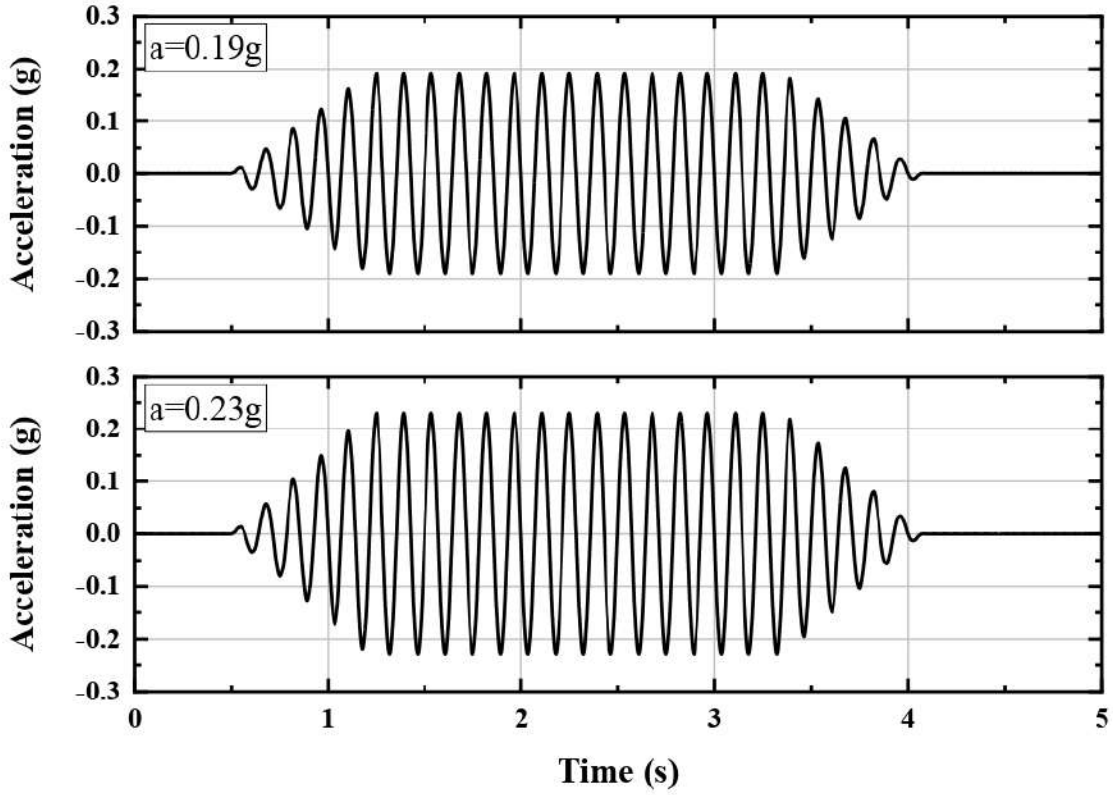

Figure 4. 4. Input sinusoidal motions corresponding to accelerations of 0.19 g and 0.23g at 7 Hz frequency.

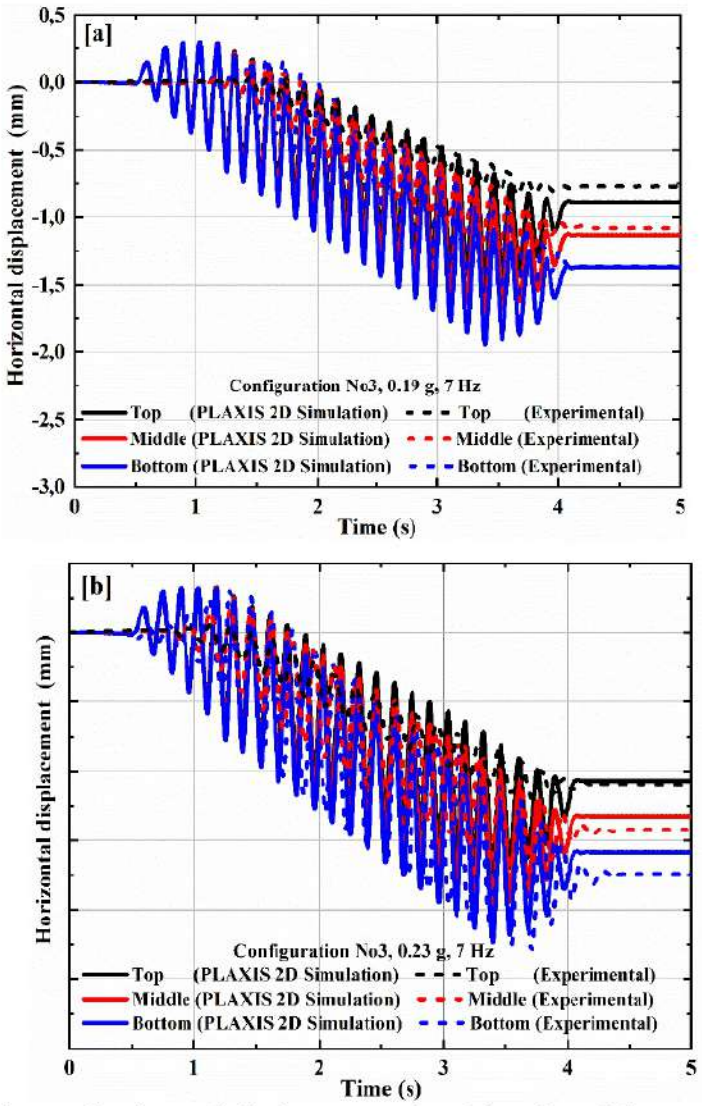

Figure 4. 5. Comparison of horizontal displacement-time histories of the retaining wall from the present study with those of Kloukinas et al. (2015) corresponding to (a) 0.19 g, and (b) 0.23 g.

4.5 Results and discussion

The acceleration recorded in East-West (E-W) direction of the Imperial Valley 1940 earthquake for the first 20 seconds was applied to the base of the model, as shown in Fig. 6, having a peak ground acceleration (PGA) of 0.28g [Fig. 6(a)] and the predominant frequency was found to be approximately 1.46 Hz [Fig. 6(b)]. The record of Imperial Valley was chosen based on its broadband frequency content which allows the submission of the model to a large range of frequencies and hence proves its robustness against broadband records. This earthquake strong-motion record was downloaded from strong-motion database of The Pacific Earthquake Engineering Research Center (PEER 2018). For the case of harmonic excitations, the applied input motion involved 10 cycles of sinusoidal acceleration, having frequencies of 1, 3and 5 Hz and amplitude of 0.2 g, 0.4 g, and 0.6g.

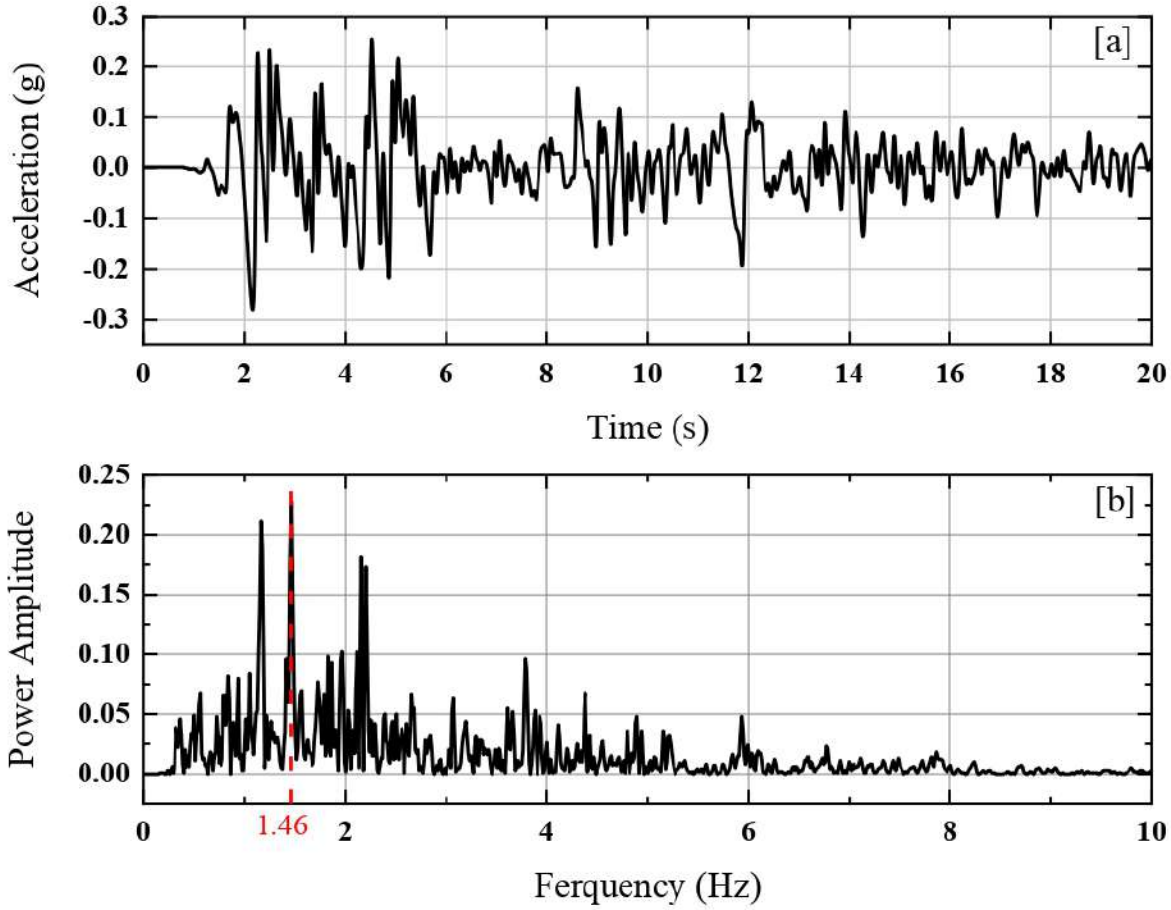

Figure 4. 6. Imperial Valley 1940 earthquake acceleration-time history.

4.5.1 Responses of cantilever wall with and without CTS cushion

4.5.1.1 Horizontal displacement and rotation of the retaining wall

The profile of maximum normalized horizontal displacements and the normalized horizontal displacement-time histories near the top of the stem during the Imperial Valley earthquake loading were analyzed for both (a) sandy backfill with CTS cushion, and (b) sandy backfill without cushion. The results show that the CTS cushion produces lower maximum displacements compared to that of the control case for the assumed seismic loading (Figure 4.7). The maximum displacement of wall with CTS cushion ($t/H = 0.05$) was reduced by about 35% when compared to the control case ($t/H = 0$).

To fully understand the mechanism of deformation of a cantilever retaining wall during the applied seismic loading, the rotation of the stem was calculated around a vertical axis, passing through the midline of the stem, expressed as

$$\theta_{stem} = \tan^{-1}\left(\frac{\Delta_{top} - \Delta_{base}}{H}\right) \tag{4.1}$$

where, θ_{stem} is the rotation of the stem, Δ_{top} is the horizontal displacement at the top of the retaining wall, and Δ_{base} is the horizontal displacement at the base of the retaining wall. Figure 4.8 shows the rotation of the stem of the cantilever wall at the end of the motion. It was observed that θ_{stem} reduced from 0.012 radian for the case without CTS cushion to 0.005 radians (about 58% decrease) for the case with CTS cushion, respectively. Therefore, it can be concluded that under the induced seismic ground motion, the tire shreds as compressible inclusion can particularly be effective in reducing the forward rotation of the cantilever retaining wall.

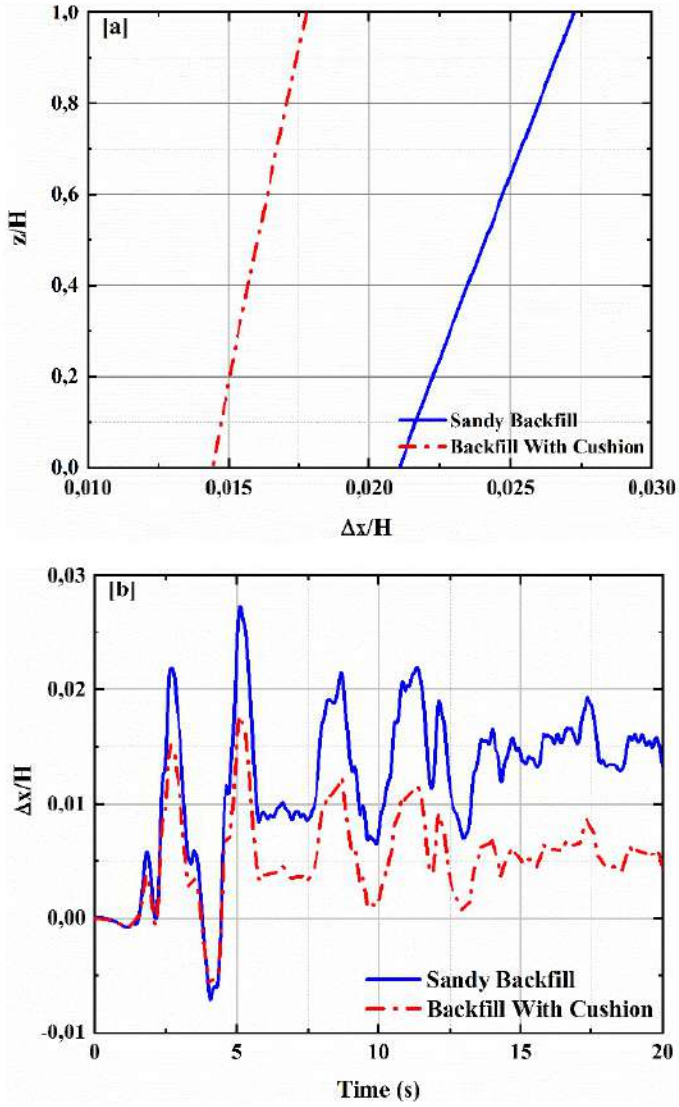

Figure 4. 7. Displacements and rotations during seismic loading with and without compressible tire shreds (CTS) cushion: (a) maximum normalized horizontal displacement profiles along the wall, and (b) normalized horizontal displacement-time history near top of stem.

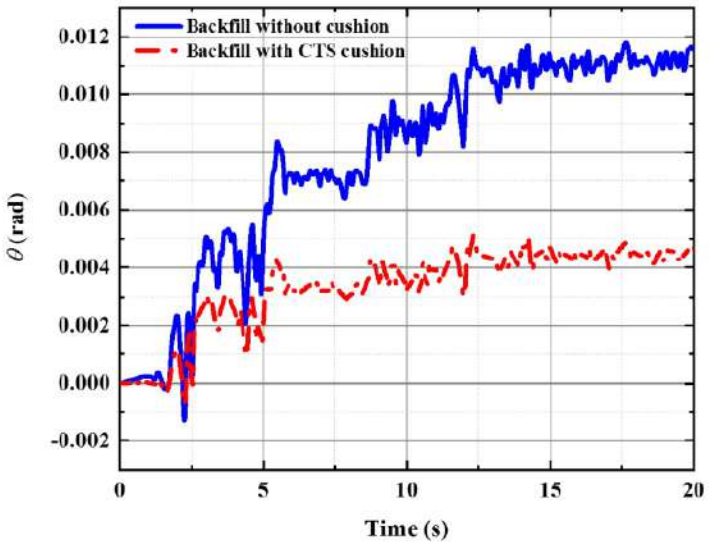

Figure 4. 8. Comparison in rotations of retaining wall with and without CTS cushion.

4.5.1.2 Bending moment and shear force

The variation in the maximum shear force and bending moment along the stem were also studied for both the conditions. The maximum values were found at the bottom of the retaining wall. The results show that the cantilever wall with CTS cushion shows a lower maximum shear force and bending moment along the stem compared to those without cushion. The shear force and bending moment (N and M) were normalized with respect to $0.5*K_{ae}*\gamma H^2$ and $1/6*K_{ae}*\gamma H^3$ (*i.e.*, $N^* = N/0.5*K_{ae}*\gamma H^2$ and $M^* = M/(1/6*K_{ae}*\gamma H^3)$). Figure 4.9 shows that the normalized maximum shear force and the bending moment reduce from 1.041 and 0.813 (for the case of without cushion) to 0.613 and 0.635 (for the case with CTS cushion). Reductions of about 41% and 22% in the maximum shear force and the bending moment were observed due to inclusion of CTS cushion.

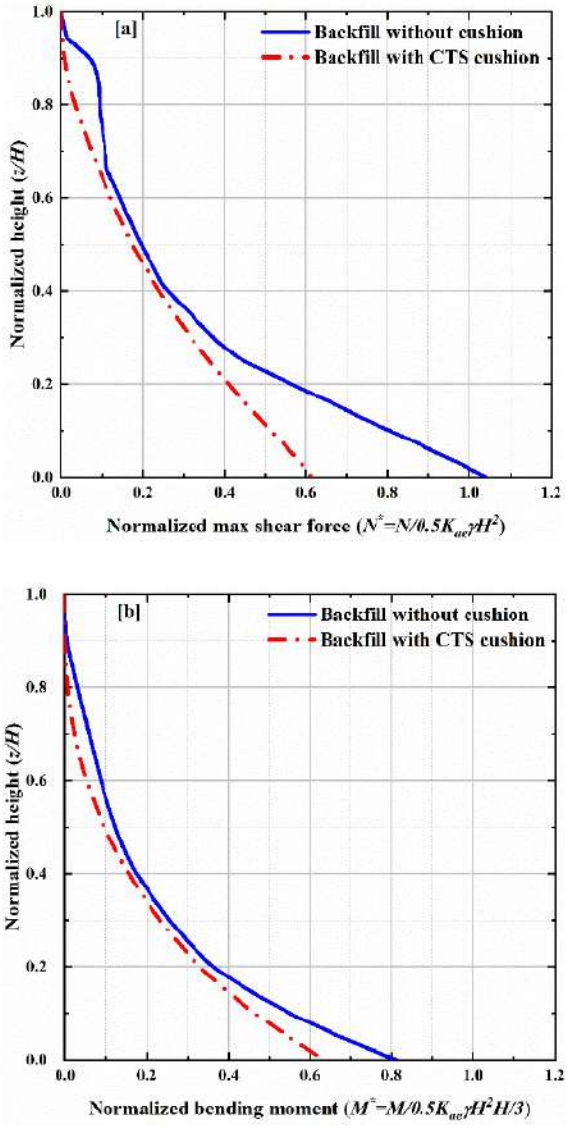

Figure 4. 9. Comparisons in the normalized maximum bending moment and normalized shear force with and without CTS cushion.

4.5.1.3 Seismic earth pressure

Figure 4.10 depicts the normalized seismic earth pressure-time histories at the mid-height behind the stem and the vertical section through the heel for with and without CTS cushion cases. The seismic earth pressure was normalized with respect to γH (*i.e.*, $\sigma^*_E = \sigma_h / \gamma H$). It can be seen that the seismic earth pressure behind the stem and the vertical section through the heel were considerably reduced due to the presence of compressible inclusions. Figure 4.10(a) shows that the normalized maximum seismic earth pressure at the mid-height of the stem reduced from about 0.239 for the case without CTS to 0.168 for the case with CTS cushion, reduction of about 30%.

Likewise, the normalized maximum seismic earth pressure at mid-height of the section through the heel, $\sigma^*_{E\_heel}$, reduced from 0.248 to 0.231, a relatively small 7% reduction [Figure 4.10(b)].

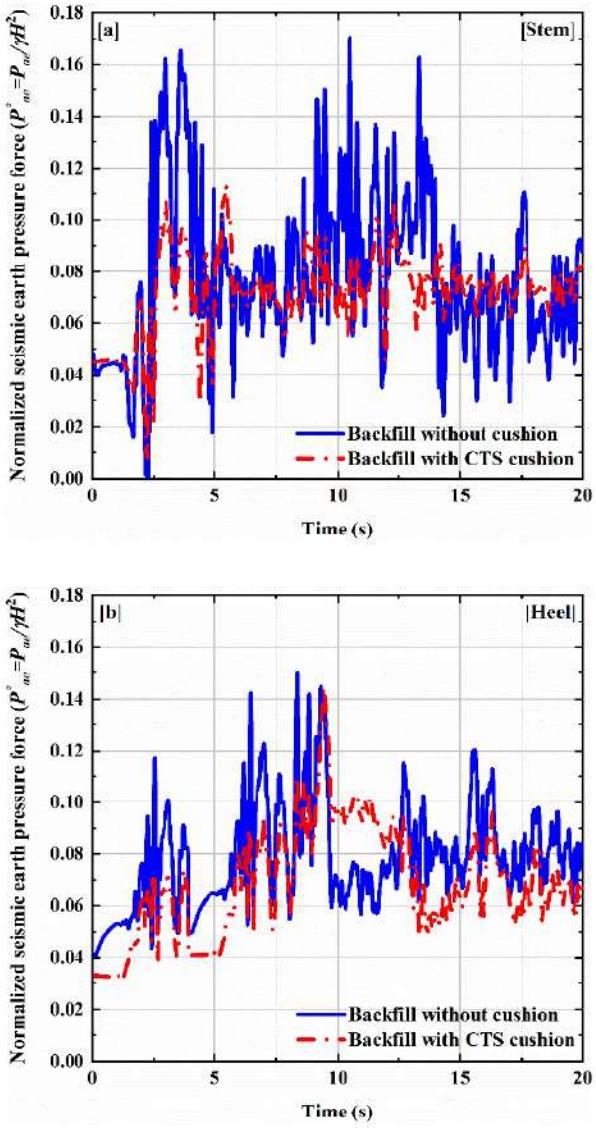

Figure 4. 10. Normalized seismic earth pressure-time histories at mid-height of (a) stem portion, and (b) section through the heel portion.

4.5.1.4 Distribution of seismic earth pressure

Figures 4.11(a) and (b) show the variations of the seismic earth pressures at the end of the earthquake across the stem and section through the heel. Figure 4.11 clearly shows that the inclusion of CTS cushion between the wall and the soil backfill provided a significant reduction in the lateral pressure distribution, especially near the wall base (*i.e.*, at z/H=0). It was observed that

the seismic earth pressures with CTS cushion were very close to the Coulomb's earth pressure, and the earth pressures were significantly less than the earth pressures on the wall without CTS cushion behind the wall. Additionally, the dynamic earth pressures obtained were found to be less than those obtained from M-O method. The maximum value of σ_h/σ_v near the wall base was found to decrease from 0.39 without cushion (t/H = 0) to about 0.22 in the presence of a compressible inclusion with t/H = 0.05 (about 44% reduction). The reduction was about 11% across the section through the heel.

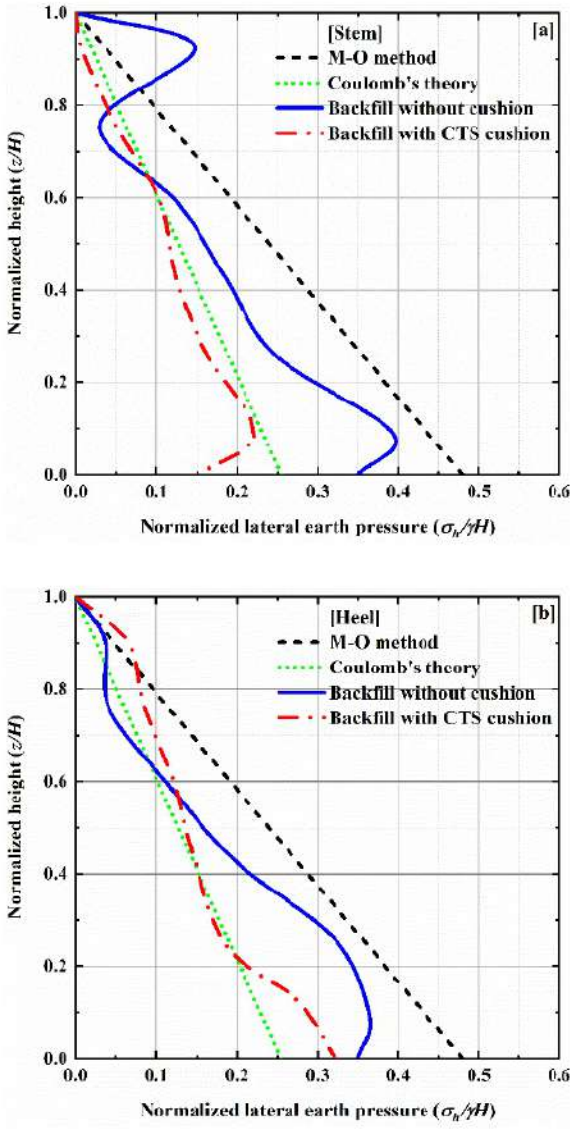

Figure 4. 11. Distribution of lateral dynamic pressures along the height of retaining walls across (a) the stem portion, and (b) the section passing through the heel.

The results presented in this section indicated clearly that recycled tire shreds acted well as a compressible cushion in improving the performance of the cantilever retaining wall under seismic loading. The effects of different parameters on the response of cantilever wall with CTS cushion are detailed in the following section.

4.5.2 Influence of various parameters on response of cantilever wall with CTS cushion

To study the influence of various factors, namely, thickness of compressible cushion, amplitude of earthquake acceleration, and frequency of sinusoidal motion, the behavior of cantilever walls was systematically studied with cushion in place. In the analysis, cantilever wall heights of 3m, 6m, and 9m and thicknesses of CTS cushion of 75mm, 150mm, and 300mm were considered. These typical values were chosen according to the studies available in the literature [Hazarika et al. (2008); Reddy and Krishna (2017); Lee and Roh (2007) and Kim et al. (2018)].

4.5.2.1 Effect of height of retaining wall

Three heights of retaining walls equal to 3 m, 6 m, and 9 m were considered. The maximum displacements increase with the increasing height of the retaining wall, and the rotations of the wall decrease with the increasing height of the retaining wall (Table 4.2). The maximum shear force and bending moment of the retaining wall, and the seismic earth pressure thrusts for each case were found to increase significantly with an increase in the height of the retaining wall. In addition, it was noted that the M-O method over predicts the seismic earth pressure thrusts for all the heights of the retaining wall. It can be seen that the inclusion of CTS cushion leads to a significant decrease in displacements and rotations of the wall. The values given in the parenthesis of Table 4.2 present the percent differences in values with respect to the control case. The seismic earth thrust across the stem was found to reduce by about 13% to 33% for t/H ranging from 0.033 to 0.1 for the three heights considered in the study while the maximum reduction across the section through the heel was about 8%.

Table 4. 2. Effect of the height of the retaining wall on the wall behavior*.

Case (mm)	Maximum displacement (m)	Rotation (degrees)	Maximum shear force (kN/m)	Maximum moment (kNm/m)	Seismic earth thrust from present study (kN/m)				Seismic earth thrust on stem from M-O theory (kN/m)	
					Stem		Heel			
					P_{stem}	h/H	P_{heel}	h/H	P_{M-O}	h/H
Height of the retaining wall = 3 m										
t=0	0.14	1.44	35.65	28.08	25.03	0.29	24.88	0.36		
t=300	0.1	0.69	25.71	24.39	21.1	0.28	22.91	0.34	32.59	0.33
(t/H=0.1)	(28.6%)	(52.1%)	(27.9%)	(13.1%)	(15.7%)		(7.9%)			
Height of the retaining wall = 6 m										
t=0	0.16	0.67	135.5	211.6	92.53	0.29	81.34	0.37		
t=300	0.11	0.29	79.8	165.2	61.6	0.33	78.51	0.36	130.34	0.33
(t/H=0.05)	(31.3%)	(56.7%)	(41.1%)	(21.9%)	(33.4%)		(3.5%)			
Height of the retaining wall = 9 m										
t=0	0.22	0.94	270.1	681.6	209.6	0.3	196.6	0.34		
t=300	0.15	0.62	214.5	623.3	181.8	0.31	198	0.34	293.27	0.33
(t/H=0.033)	(31.8%)	(34.0%)	(20.6%)	(8.6%)	(13.3%)		(-0.7%)			

** Values in the parenthesis give the differences in values with respect to the control case*

4.5.2.2 Effect of thickness of compressible cushion

The effect of the thickness of compressible cushion on the response of the wall were examined for three heights of the wall (3 m, 6 m, and 9 m) corresponding to the Imperial Valley earthquake loading. Table 4.3 gives the results obtained from the finite element analysis. It was observed that the horizontal displacement and the maximum rotation were considerably reduced with the increase in the thickness of the compressible cushion for all the wall heights compared to the control case. It was observed that the seismic earth thrust behind the stem, P_{stem}, and seismic earth thrust at the vertical section through the heel, P_{heel}, exhibit a decreasing trend with increase in compressible cushion thickness. For instance, the reduction in seismic earth thrust across the stem t/H increasing from 0.012 to 0.05 was about 27% and 33% for a wall height of 6m.

Table 4. 3. Effect of tire shreds compressible inclusion of different thicknesses on the wall behavior corresponding to various wall heights.

Case (mm)	Maximum displacement (m)	Rotation (degrees)	Maximum shear force (kN/m)	Maximum moment (kNm/m)	Seismic earth thrust from present study (kN/m)				Seismic earth thrust on stem from M-O theory (kN/m)	
					Stem		Heel			
					P_{stem}	h/H	P_{heel}	h/H	$P_{M\text{-}O}$	h/H
Height of the retaining wall = 3 m										
t=0	0.14	1.44	35.65	28.08	25.03	0.29	24.88	0.36		
t=75	0.13	1.12	28.15	25.88	23.00	0.31	25.16	0.35		
(t/H=0.025)	(7.1%)	(22.2%)	(21.0%)	(7.8%)	(8.1%)		(-1.1%)			
t=150	0.11	1.16	25.86	25.73	22.73	0.24	23.42	0.35	32.59	0.33
(t/H=0.05)	(21.4%)	(19.4%)	(27.5%)	(8.4%)	(9.2%)		(5.9%)			
t=300	0.1	0.69	25.71	24.39	21.1	0.28	22.91	0.34		
(t/H=0.1)	(28.6%)	(52.1%)	(27.9%)	(13.1%)	(15.7%)		(7.9%)			
Height of the retaining wall = 6 m										
t=0	0.16	0.67	135.5	211.6	92.53	0.29	81.34	0.37		
t=75	0.15	0.52	98.22	188.8	67.06	0.32	80.43	0.37		
(t/H=0.012)	(6.3%)	(22.4%)	(27.5%)	(10.8%)	(27.5%)		(1.1%)			
t=150	0.13	0.48	92.07	183.3	65.87	0.32	78.85	0.36	130.34	0.33
(t/H=0.025)	(18.8%)	(28.4%)	(32.1%)	(13.4%)	(28.8%)		(3.1%)			
t=300	0.11	0.29	79.8	165.2	61.6	0.33	78.51	0.36		
(t/H=0.05)	31.25%	(56.7%)	(41.1%)	(21.9%)	(33.4%)		(3.5%)			
Height of the retaining wall = 9 m										
t=0	0.22	0.94	270.1	681.6	209.6	0.3	196.6	0.34		
t=75	0.18	0.78	227.7	640.4	185.2	0.31	199.8	0.34		
(t/H=0.083)	(18.2%)	(17.0%)	(15.7%)	(6.0%)	(11.6%)		(-1.6%)			
t=150	0.18	0.74	233.5	635.1	184	0.3	197.4	0.35	293.27	0.33
(t/H=0.017)	(18.2%)	(21.3%)	(13.6%)	(6.8%)	(12.2%)		(-0.4%)			
t=300	0.15	0.62	214.5	623.3	181.8	0.31	198	0.34		
(t/H=0.033)	(31.8%)	(34.0%)	(20.6%)	(8.6%)	(13.3%)		(-0.7%)			

** Values in the parenthesis give the differences in values with respect to the control case*

4.5.2.3 Effect of amplitude of earthquake acceleration

To study the effect of amplitude of earthquake acceleration, the seismic input motion of the actual earthquake from the Imperial Valley earthquake (1940) was scaled between 0.1 and 0.6 g. These acceleration levels were applied to all the three heights of the retaining walls considered. As shown in Table 4.4, it was observed that the maximum displacements and rotations increase significantly with increase in the acceleration level for all the three wall heights. It was seen that the presence of the compressible CTS cushion leads to a decrease in displacement and rotation despite an increase in the level of acceleration, compared to the control case. On the other hand, the maximum shear and the moment along the stem increase drastically for acceleration levels up to about 0.5g. A noticeable decrease in the maximum shear and the moment were observed with the application of the compressible cushion. The seismic earth pressure thrust remains almost constant with a change in the acceleration level, the opposite of what the M-O theory suggests-an increase in the seismic earth pressure thrust with an increase in the acceleration level. It can be observed that the inclusion of compressible layer results in reduction of the seismic earth pressure thrust behind the stem and across a section through the heel with an increase in the acceleration level for the three heights of the retaining wall; however, the increment in the seismic earth pressure thrust was insignificant.

Table 4. 4. Effect of the amplitude of seismic input motion on the wall behavior for different wall heights.

Case (mm)	*a* (g)	Maximum displacement (m)	Rotation (degrees)	Maximum shear force (kN/m)	Maximum moment (kNm/m)	Seismic earth thrust from present study (kN/m)				Seismic earth thrust on stem from M-O theory (kN/m)	
						Stem		*Heel*			
						P_{stem}	*h/H*	P_{heel}	*h/H*	P_{M-O}	*h/H*
Height of the retaining wall = 3 m											
	0.1	0.04	0.13	26.47	22.61	21.18	0.31	22.75	0.34	21.57	
t=0	0.2	0.09	0.65	30.96	25.47	23.75	0.3	25.11	0.35	27	
	0.3	0.16	1.7	37.67	28.76	25.18	0.29	24.73	0.36	34.09	
	0.6	0.69	8.01	43.44	32.84	26.61	0.29	23.43	0.33	82.26	
	0.1	0.03	0.07	20.91	20.5	18.47	0.31	23.18	0.33	21.57	
		(25.0%)	(46.2%)	(21.0%)	(9.3%)	(12.8%)		(-1.9%)			
t=300	0.2	0.07	0.32	23.58	23.61	20.28	0.31	24.7	0.35	27	

(*t*/*H*=0.1)		(22.2%)	(50.8%)	(23.8%)	(7.3%)	(14.6%)		(1.6%)			
	0.3	0.11	0.79	25.72	24.6	21.82	0.31	25.24	0.36	34.09	
		(31.3%)	(53.5%)	(31.7%)	(14.5%)	(13.3%)		(-2.1%)			0.33
	0.6	0.4	4.25	34.29	29.26	24.41	0.28	23.82	0.34	82.26	
		(42.0%)	(46.9%)	(21.1%)	(10.9%)	(8.3%)		(-1.7%)			
Height of the retaining wall = 6 m											
	0.1	0.06	0.14	87.43	142.4	69.39	0.31	68.72	0.36	86.29	
	0.2	0.11	0.36	117.5	189.6	83.25	0.3	78.63	0.36	108.03	
t=0	0.3	0.18	0.76	138.1	214.9	93.15	0.28	80.97	0.38	136.37	0.33
	0.6	0.53	3.3	155.9	233.7	107.4	0.28	90.42	0.38	329.05	
	0.1	0.04	0.06	58.2	110.1	51.31	0.36	64.98	0.35	86.29	
		(33.3%)	(57.1%)	(33.4%)	(22.7%)	(26.0%)		(5.4%)			
	0.2	0.08	0.16	70.14	141.8	57.31	0.36	64.98	0.36	108.03	
		(27.3%)	(55.6%)	(40.3%)	(25.2%)	(31.2%)		(17.4%)			0.33
t=300	0.3	0.11	0.3	81.69	170.3	62.25	0.38	78.3	0.37	136.37	
(*t*/*H*=0.05)		(38.9%)	(60.5%)	(40.9%)	(20.8%)	(33.2%)		(3.3%)			
	0.6	0.25	1.37	97.96	202	74.25	0.38	87.63	0.39	329.05	
		(52.8%)	(58.5%)	(37.2%)	(13.6%)	(30.9%)		(3.1%)			
Height of the retaining wall = 9 m											
	0.1	0.06	0.17	200.9	546.7	177.1	0.32	192.7	0.33	194.15	
	0.2	0.13	0.55	244.4	637.6	195.7	0.31	196.7	0.34	243.06	
t=0	0.3	0.24	1.03	275.3	692.3	213	0.31	197.5	0.34	306.83	0.33
	0.6	0.63	2.78	321.4	771.7	243	0.29	202.4	0.35	740.35	
	0.1	0.05	0.12	177.1	502.6	166.1	0.31	197.6	0.34	194.15	
		(16.7%)	(29.4%)	(11.8%)	(8.1%)	(6.2%)		(-2.5%)			
	0.2	0.1	0.34	201	582.6	176.7	0.31	196.5	0.34	243.06	
		(23.1%)	(38.2%)	(17.8%)	(8.6%)	()9.7%		(0.1%)			0.33
t=300	0.3	0.16	0.67	216.9	631.4	182.8	0.31	199.9	0.34	306.83	
(*t*/*H*=0.033)		(33.3%)	(34.9%)	(21.2%)	(8.8%)	(14.2%)		(-1.2%)			
	0.6	0.44	1.89	237.4	700.8	197	0.31	196.4	0.36	740.35	
		(30.2%)	(32.0%)	(26.1%)	(9.2%)	(18.9%)		(3.0%)			

** Values in the parenthesis give the differences in values with respect to the control case*

4.5.2.4 Effect of frequency of sinusoidal motion

To evaluate the effect of frequency on the performance of the wall of height 6m with and without cushion, the wall was subjected to 10 cycles of excitation of sinusoidal motion with amplitudes of 0.2 g, 0.4 g, and 0.6g at three frequencies of 1, 3and 5 Hz. It was observed that for the three chosen acceleration amplitudes, the maximum displacements and rotation of the retaining wall decrease with an increase in the frequency of the sinusoidal input motion (Table 4.5). However, the results show that the CTS cushion produces lower maximum displacements and rotations with an increase in the frequency and acceleration amplitudes compared to that of the control cases. It was also observed that the seismic earth pressure thrust behind the stem and at the vertical section through the heel reduced with the frequency of seismic acceleration for both cases for a given acceleration amplitude.

Table 4. 5. Effect of the frequency of seismic input motion on the wall behavior for different amplitudes corresponding to 6 m-high wall.

Case (mm)	*f* (Hz)	Maximum displacement (m)	Rotation (degrees)	Maximum shear force (kN/m)	Maximum moment (kNm/m)	Seismic earth thrust from present study (kN/m)				Seismic earth thrust on stem from M-O theory (kN/m)	
						Stem		Heel			
						P_{stem}	*h/H*	P_{heel}	*h/H*	$P_{M\text{-}O}$	*h/H*
	Seismic input motion amplitude, a=0.2g										
	1	0.18	1.04	109.5	164.3	61.4	0.29	60.08	0.36		
	3	0.05	0.32	114.5	198.7	67.75	0.36	76.58	0.37	108.03	0.33
	5	0.02	0.15	86.97	164.9	70.84	0.34	69.18	0.4		
	Seismic input motion amplitude, a=0.4g										
	1	0.56	3.26	148.2	209.1	61.38	0.26	59.9	0.34		
t=0	3	0.15	1.02	152.0	252.6	73.61	0.38	89.72	0.42	174.9	0.33
	5	0.05	0.40	119.4	228.6	84.7	0.37	77.86	0.43		
	Seismic input motion amplitude, a=0.6g										
	1	0.95	5.41	177.3	237.3	61.5	0.28	55.94	0.33		
	3	0.24	1.72	168.7	268.8	74.95	0.38	101.0	0.44	329.05	0.33
	5	0.09	0.67	144.4	262.7	95.41	0.36	81.02	0.44		
	Seismic input motion amplitude, a=0.2g										
	1	0.11	0.55	72.73	144.8	50.12	0.29	61.74	0.36		
		(38.9%)	(47.1%)	(33.6%)	(11.9%)	(18.4%)		(-2.8%)			

Chapter 5

Earthquake response of connected and unconnected back-to-back geosynthetic reinforced soil walls

5.1 Introduction

There are very limited numerical modeling and experimental studies on the behavior of back-to-back mechanically stabilized earth (BBMSE) walls in seismic conditions. This chapter critically discusses the results of the seismic responses of reinforcement in back-to-back walls for both connected and unconnected BBMSE walls were investigated under seismic loading using real-time earthquake data. The parametric study presented in this chapter includes investigating the effect of earthquake ground motion on seismic earth pressures, total seismic earth thrust coefficients (K_{AE}), incremental seismic earth thrust coefficients (ΔK_{AE}), the locations of the point of action of resultant seismic earth thrust (P_{AE}), and the acceleration amplifications at the end of the reinforcement zone and the facing of the wall were mainly analyzed. These results were compared with the results from the analytical methods. The findings reported in the study can provide a rational and economical design of back-to-back mechanically stabilized earth walls (MSE) in earthquake-prone areas.

5.2 Numerical modeling

In the present study, a finite element-based program, PLAXIS 2D (2018), was used to develop a plane-strain model to perform the dynamic analysis of the BBMSE walls subjected to strong earthquake motion. A 6 m-high wall resting on a 2 m-thick soil foundation was considered. Figure 5.1 represents a finite element model of connected and unconnected back-to-back MSE walls. The length of the reinforcements for the two walls was considered as L = 4.2 m (the typical reinforcement length recommended by the FHWA design guidelines (FHWA 2009), i.e., L=0.7H). In the unconnected walls, the ends of reinforcement of both the walls were considered very near each other with D = 0.1 m. Reinforcements in the connected back-to-back walls case extend from one wall facing to the other wall facing (i.e., D = 0). Thus, the distance between the facing of the walls was 8.4 m. The foundation soil was modeled as Mohr-Coulomb material with very high

deformation modulus (E=200 MPa) to simulate it as a rigid material. The model involves six input parameters, namely, deformation modulus (E), Poisson ratio (ν), cohesion (c), friction angle (φ), and dilatancy angle (ψ). Table 1.6 presents the values of the material properties considered in the study. The soil-reinforcement interaction was modeled by relating the nonlinear elastic behavior of the soil to the linear elastic response of the reinforcement. For this purpose, the geogrids are selected from the elastoplastic elements with stiffness and tensile strength. The interaction between the geogrid and soil was simulated using interface element. In PLAXIS, interface can be specified as strength reduction factor (R_{int}). This factor relates the interface strength to the backfill strength. Strength reduction factor was given as 0.6 for the interaction between soil and reinforcement. Table 5.2 gives the properties of the reinforcement - uniaxial geogrid (UX-1400 type) -considered in the study [Benmebarek et al. (2016)]. Geogrids were placed at typical pacing of 0.75 m (AASTHO 2012). The well-known segmental precast concrete panels were considered in the current study to simulate the wall. Each wall contains 4 segmental concrete panels of 1.5 m in width and height and 0.14 m in thickness. The concrete panel facia was modeled as a linear-elastic material. In the present model, the facing panel was hinged to a horizontal plate which is 0.5m embedded in the foundation soil. Hence the panel had the flexibility to move in horizontal direction. Therefore, in the both wall cases (unconnected and connected) lateral displacements were observed at the bottom of the walls for the seismic loading condition. However, the panel cannot be moved in vertical direction. The boundary condition applied in the model, simulates the real situation of embedment with nominal footing at the bottom of the concrete panel. Hence, nominal lateral displacements can be expected in the real time scenario for the seismic loading. In the finite element model, the properties of the facing panel were defined by its Young's modulus, E = 25 GPa and the unit weight γ_c= 23.5 kN/m^3 (Benmebarek et al. (2016)). Table 3.6 gives the properties of the facia considered in the study.

Table 5. 1. Material properties used in numerical simulations (Benmebarek et al. 2016).

Material	Symbol	Unit	Reinforced backfill	Foundation soil
Unit weight	γ_s	kN/m^3	18	22
Angle of shearing resistance	ϕ	degrees	35	30
Dilatancy angle	ψ	degrees	5	0
Deformation modulus	E	kPa	30×10^3	200×10^3
Cohesion	c	kPa	0	200
Poisson's ratio	ν	-	0.3	0.2
Rayleigh coefficients	α	-	1.87	4.54
	β	-	4.82×10^{-4}	1.98×10^{-4}

Table 5. 2. Reinforcement properties.

Identification	Model	Ultimate tensile strength	Allowable tensile strength, T_a	Axial stiffness
Uniaxial geogrid	Elastoplastic	70 kN/m	25.6 kN/m	1,100 kN/m

Table 5. 3. Material properties of concrete panel facing elements.

Identification	Elastic stiffness (EA)	Flexural rigidity (EI)	Thickness (d)	Weight of panel (W_c)	Poisson ratio (ν_c)
Concrete panel facia	3.5×10^6 kN/m	5,717 kN/m^2/m	0.14 m	3.29 kN/m/m	0.2

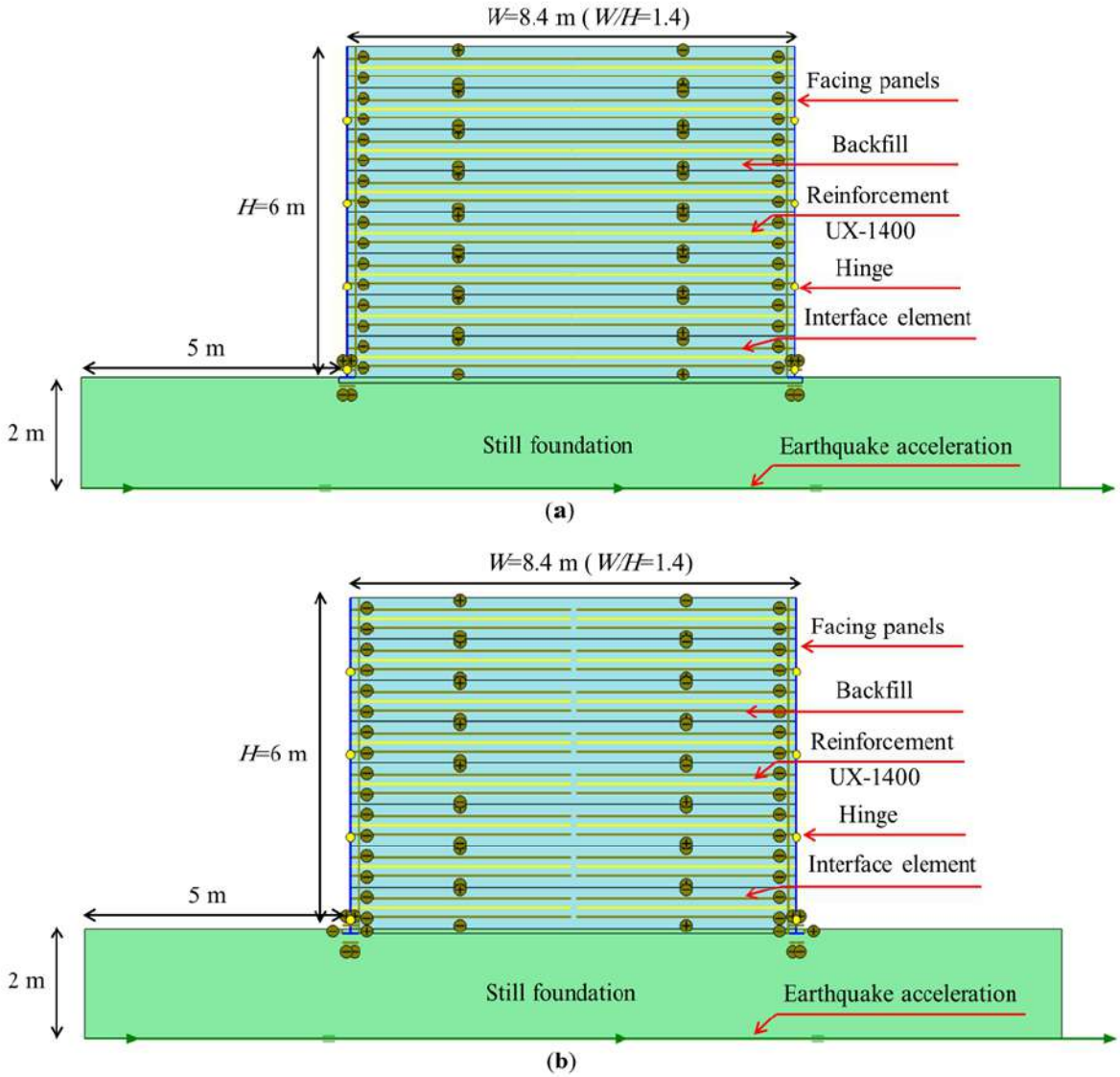

Figure 5.1 Finite element models of back-to-back MSE walls: (a) connected case; and (b) unconnected case.

5.3 Validation of the Model

The finite element model was validated against the measurements from centrifuge tests of geosynthetic-reinforced retaining walls conducted using facilities available at the Tokyo Institute of Technology (Takahashi et al. 1999; Takemura and Takahashi 2003). Figure 5.2(a) shows the geometry and instrumentation of the model wall. The physical models in the centrifuge testing simulated prototype wall of height equal to 7.5m. They considered five tests with different reinforcement lengths and spacing of geogrid reinforcements. For validation, results from two

Tests designated as Test 3 and Test 4 with reinforcement lengths of 0.6H and 0.8H with reinforcement spacing's as 0.2H and 0.1H were considered. Rubber boards were placed at the front and back ends of the test walls for absorbing reflective waves. Figure 5.2(b) shows the finite element model developed. The model walls were subjected to 20 cycles of sinusoidal seismic excitation of 0.2 g base acceleration for a period of 12 s, as reported by Ling et al. (2004).

Figure 5.3(a) shows the comparison between the results from present model and measured horizontal displacements of the wall facing at the end of shaking. Through the validation assessment, it can be inferred that the results from the numerical model of the present study agree quite well with the measured displacements from centrifuge testing, although only two experimental values were given for each wall.

Crest settlements of the backfill (refer to Figure 5.3(b)) were also compared in this study. The validation results from two Tests designated as Test 3 and Test 4 with reinforcement lengths of 0.6H and 0.8H with reinforcement spacing as 0.2H and 0.1H were considered. Validation of Test 3 wall crest settlements was not satisfactory, which might be due to soil densification and also due to the sliding out of the reinforced soil mass behind the reinforced zone.

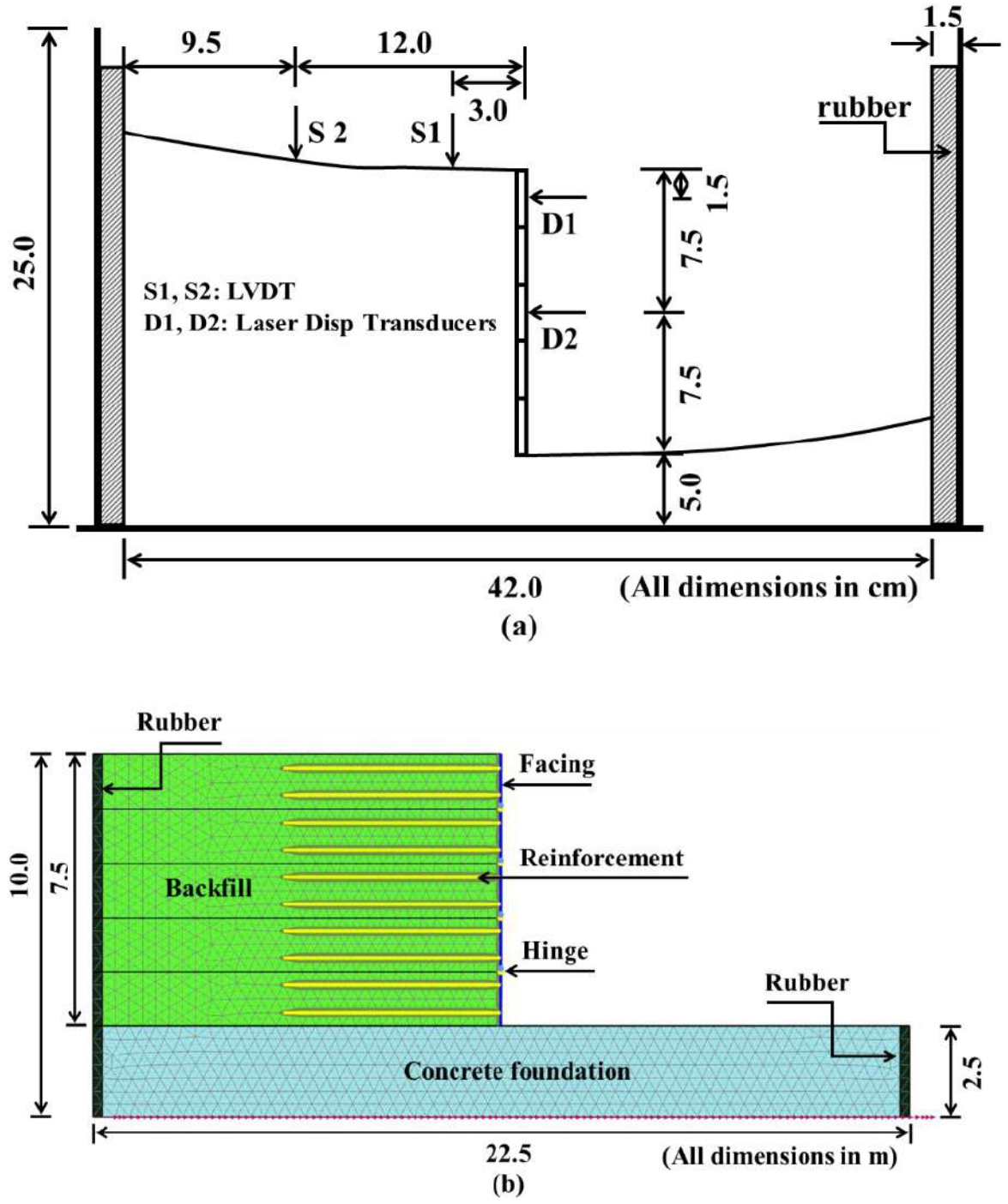

Figure 5.2. Model details: (a) layout and instrumentation details of centrifuge model (Takahashi et al. 1999; Takemura and Takahashi 2003), and (b) dynamic finite element model used to simulate Test 4.

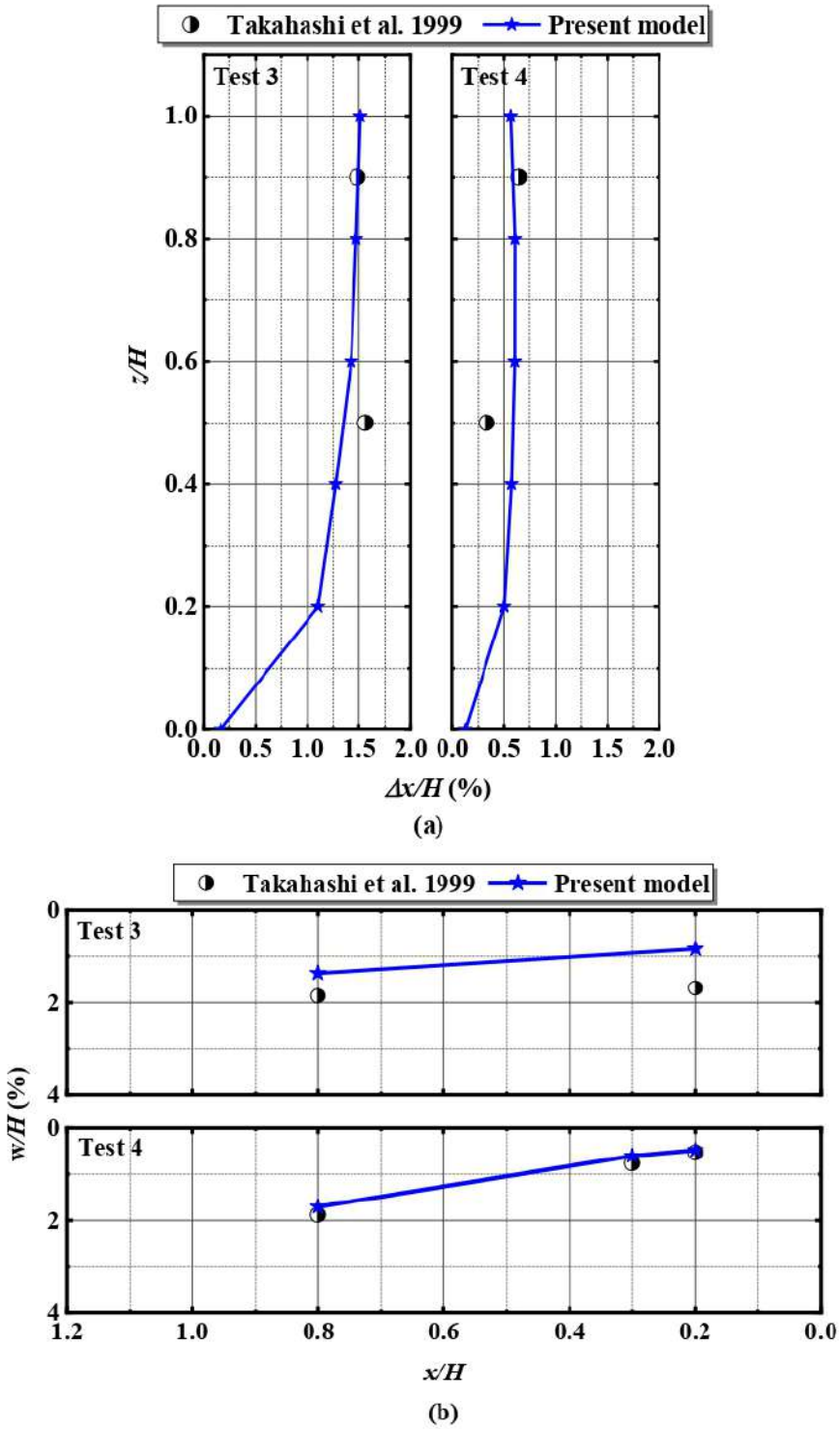

Figure 5.3. Comparison between the numerical model results and measured values for (a) horizontal wall facing displacements, and (b) wall crest settlements.

5.4 Results and Discussions

Using the validated numerical model, a detailed parametric study was carried out for lateral displacements of the wall, seismic earth pressures, and tensile forces mobilized in the reinforcements of connected and unconnected BBMSE walls under acceleration-time history of the 1995 Kobe CUE90 earthquake (Pacific Earthquake Engineering Research Center (PEER) Strong Motion Database) at the foundation level in the model (Figure 5.4). The peak ground acceleration (PGA) of this ground seismic motion was 0.345g. The acceleration history shown in Figure 5.4 is the baseline corrected and frequency filtered using the program SeismoSignal (Seismosoft 2013).

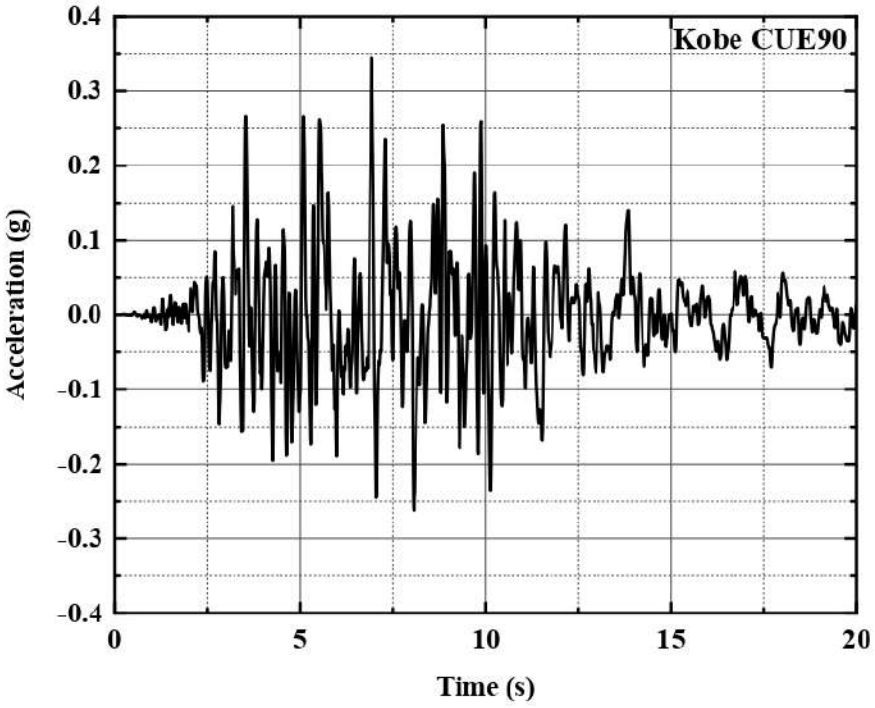

Figure 5.4. Input acceleration time history for Kobe CUE 90.

In order to check whether the input motion is consistent with the time history of the original Kobe earthquake motion, Figure 5.5 shows the comparison between the acceleration and displacement time histories of the original input motion and the acceleration and displacement histories obtained from the numerical simulation at the base of the model. The comparisons show that a significant agreement between the two-time histories can be observed; therefore, it can be

concluded that the proposed model was able to represent the behavior of the numerical simulations under earthquake loading reasonably and reliably.

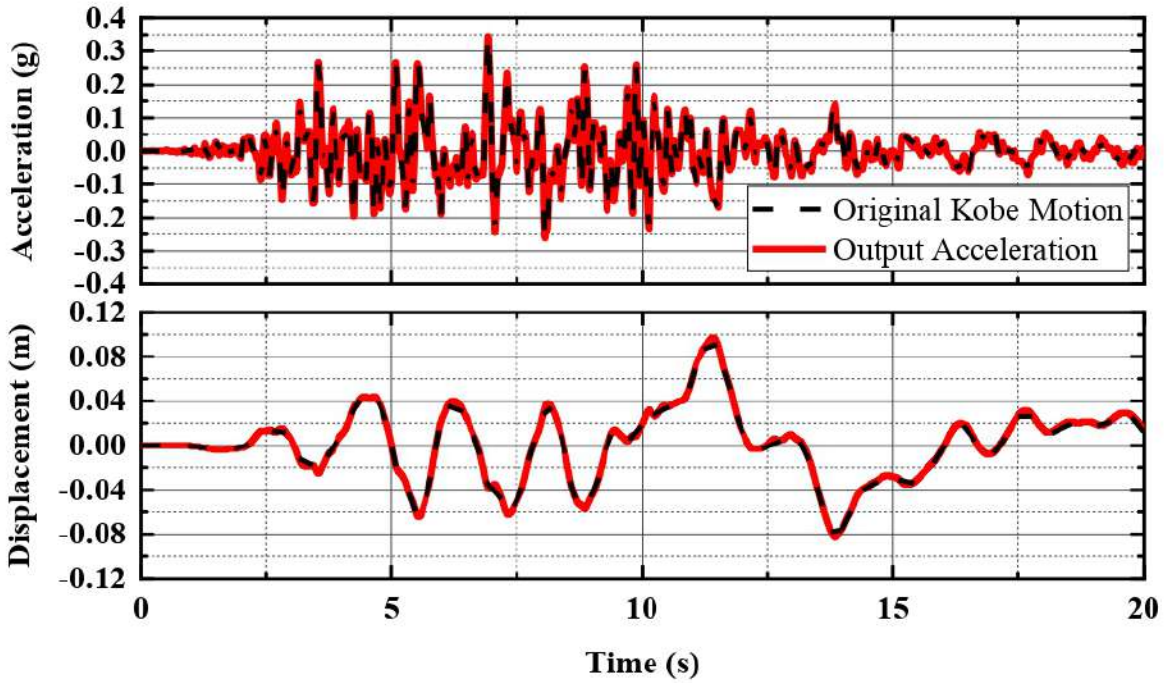

Figure 5. 5. Comparison of the ground response analyses obtained with input and output acceleration and displacement time histories.

The baseline correction was conducted to make sure the integral of earthquake acceleration time history, velocity, and residual displacement to be zero for frequency filtering. Next, the elastic simulation was made without damping to estimate the dominant the frequency range for the natural response of the system and the maximum cyclic shear strains for the given site conditions. Velocity was recorded at different locations in the model to calculate frequencies. The frequency range for the natural response of the system was observed to be relatively uniform throughout the model. Figure 5.6 presents a typical power spectrum of velocity for this simulation, the predominant frequency was found to be approximately 0.6 Hz. After that, a series of simulations with representative damping were carried out focusing on maximum displacements of the wall, tensile forces mobilized in geogrids and lateral earth pressures.

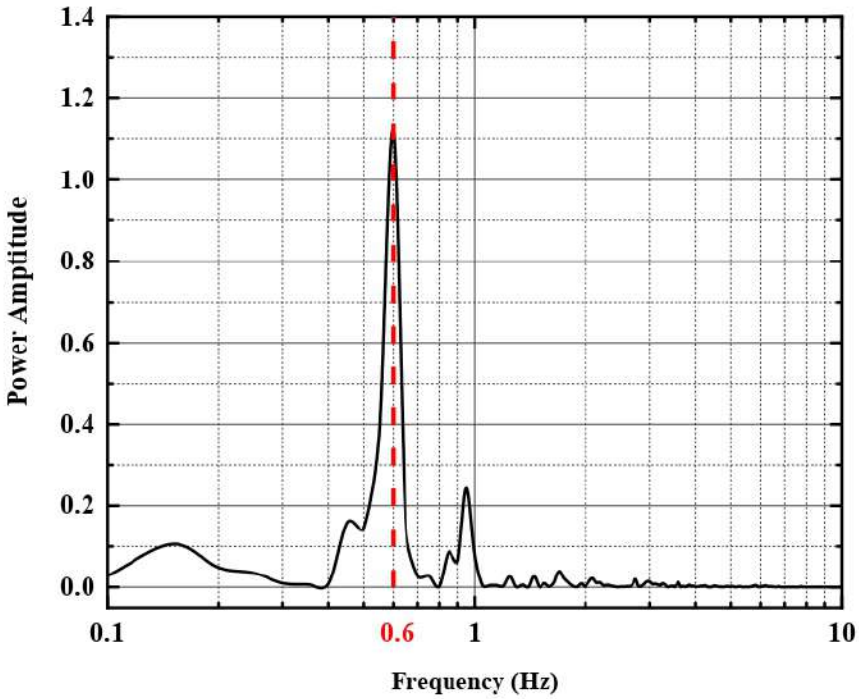

Figure 5. 6. Response spectrum from velocity history of predominant frequency model.

5.4.1 Lateral displacements of the wall

Figure 5.7 shows the variations of the maximum normalized displacements at the facing and the normalized horizontal displacement - time histories of the middle point of the wall in both connected and unconnected walls for the case of W/H=1.4 during the Kobe earthquake motion. As expected, maximum displacement, $\Delta x_{max}/H$, occurred in the middle, not at the top of the walls as the maximum displacement values for both connected and unconnected walls about 0.021 and 0.026, respectively. It can be observed that the maximum displacements due to seismic loading in the connected walls were 19% less compared with those of unconnected walls. On the other hand, studies reported in the literature showed that the effect of the distance between the ends of the reinforcement for the two walls has a significant influence on the maximum displacements of the wall models under seismic conditions (Benmebarek and Djabri (2017a)). In addition, in the case of connected walls, bottom displacement is higher than the top displacement. From the displacement profile, it is observed that bulging of the walls is seen near the bottom of the walls. Due to higher lateral pressures at the bottom of the wall than that of the top of the walls, the lateral displacements were also high at the bottom. However, at the top of the walls, the lateral deformations were constrained by the tie back effect of the reinforcement.

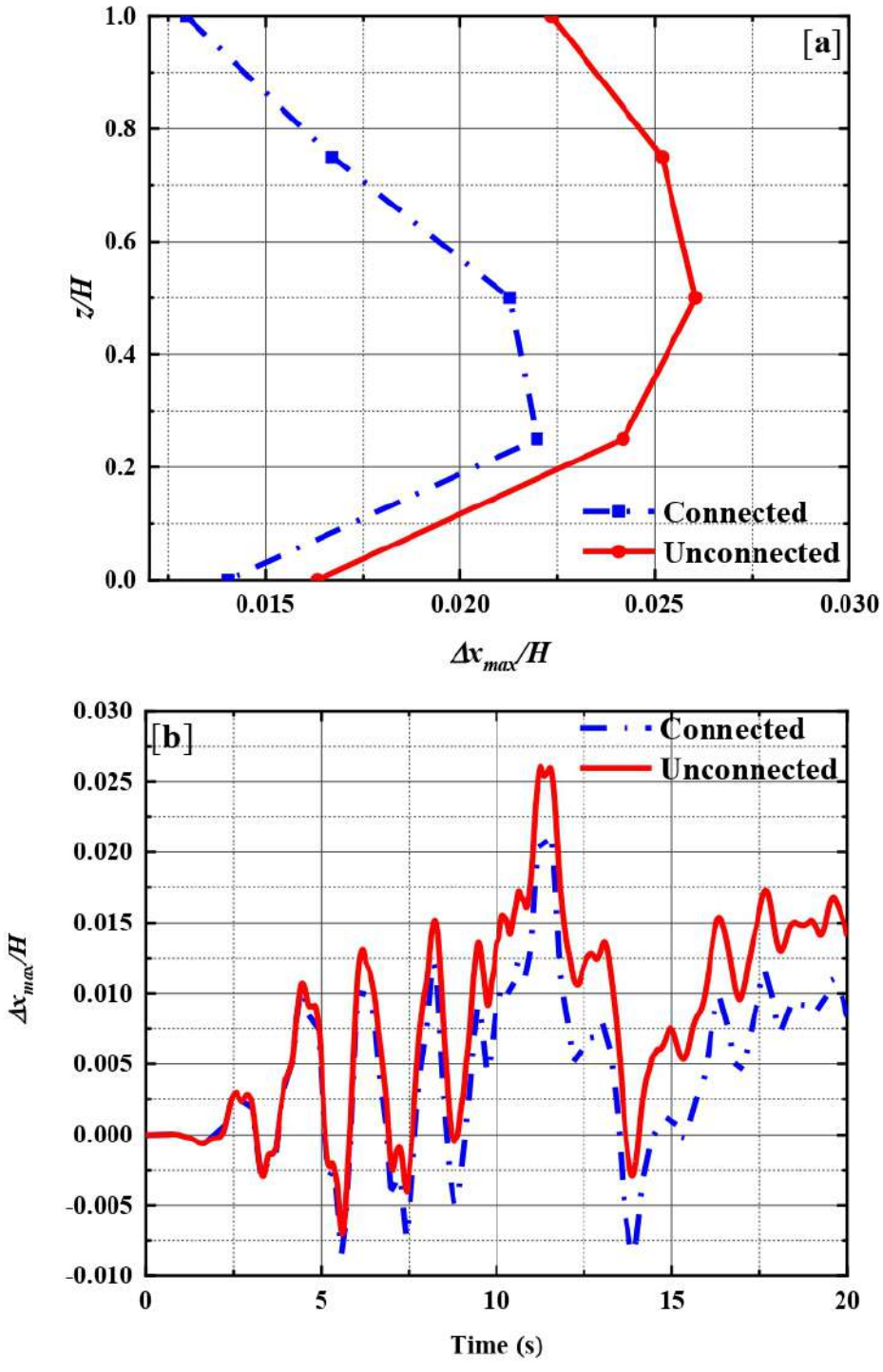

Figure 5. 7. Lateral displacements of connected and unconnected walls showing (a) the maximum normalized displacement profiles, and (b) history of normalized horizontal displacements at middle point of the walls.

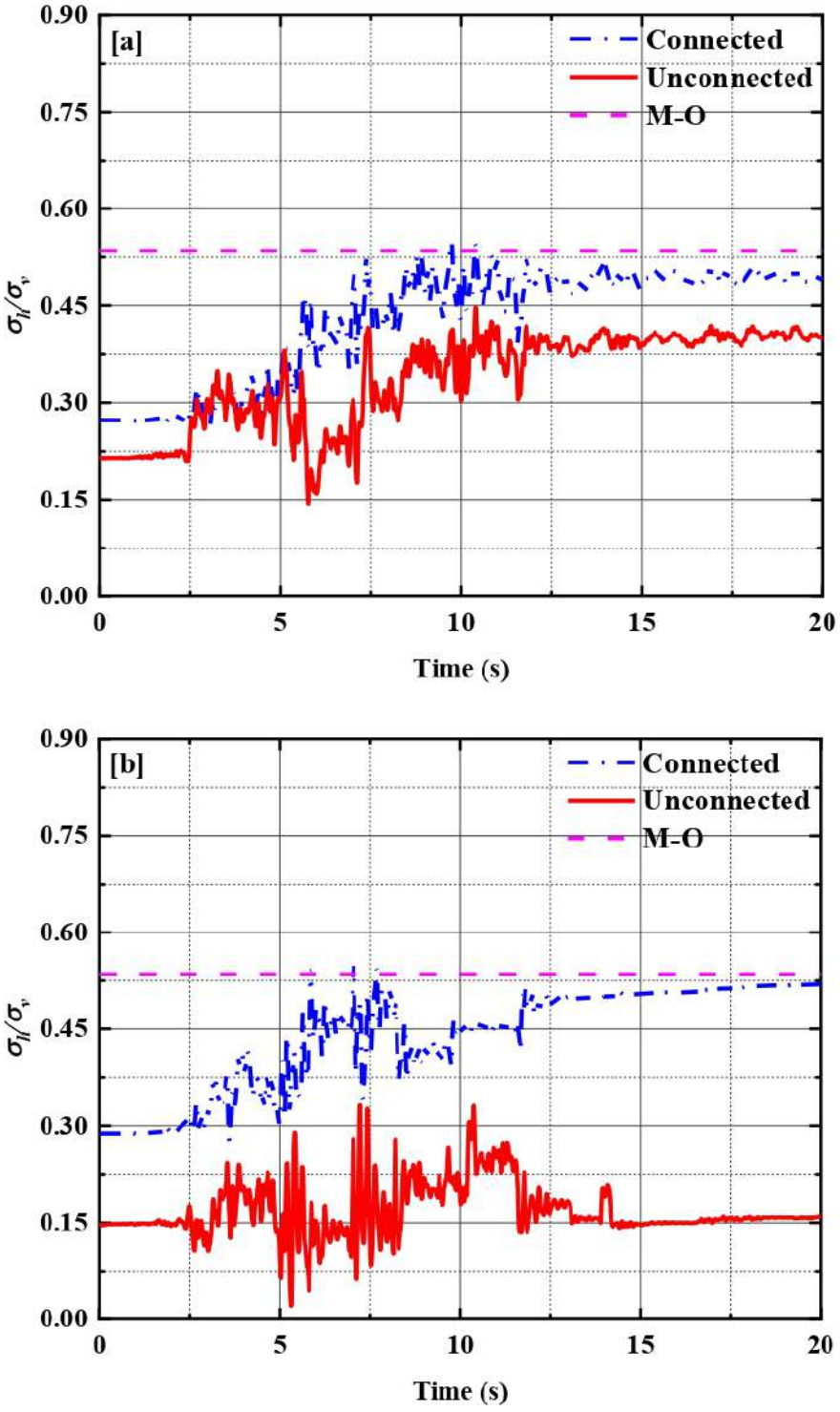

Figure 5. 8. Time-histories of total earth pressures at mid-height of walls at the (a) facing and (b) end of reinforcement zone.

5.4.2 Seismic earth pressures behind the wall and end reinforcement zone

Based on the FHWA design guidelines (Berg et al. 2009), the lateral earth pressures behind the end of the reinforced zone for the external stability analysis depend on the *D/H* ratio; no active earth trust from the backfill needs to be considered for external stability calculation for connected reinforcement. In this section, normalized lateral earth pressures at mid-height of the wall behind the wall facing and at the end of the reinforcement zone were evaluated in terms of time history in both connected and unconnected walls under earthquake motion (Figure 5.8). The results in terms of the normalized lateral earth pressures were compared with the widely used Mononobe-Okabe method. It can be seen from Figure 5.8(a) that the maximum peak of total earth pressures behind connected and unconnected walls were approximately 0.56 and 0.44, respectively. In addition, the peak of normalized earth pressures in connected walls were close to the M-O method, and slightly higher than the normalized earth pressures in the unconnected walls. It should be noted that the dynamic loading increases lateral pressures for both cases compared to the static state. However, in the middle of the connected and behind end reinforcement zone (Figure 8.6(b)), differences in response can be observed particularly at the last part of dynamic loading. The case of connected reinforcement displays an increase of the normalized lateral earth pressures conversely to the case of unconnected where no increase was noted. Clearly, the M-O method was found to be conservative for both connected and unconnected BBMSE walls.

5.4.3 Tensile forces mobilized in geogrids

Figure 5.9 shows the tensile forces along the geogrid layers in connected and unconnected walls at the end of the dynamic analyzes subjected to Kobe seismic loading. The tensile forces at the time of peak ground acceleration were presented as maximum tensile forces (T_{max}). These tensile forces correspond to the maximum forces in the entire time history of the earthquake. The maximum tensile forces in the geogrid layers were normalized with the product of soil unit weight (γ), the geogrid vertical and horizontal intervals (S_V and S_H) and the wall height (H). The results indicate that, near the wall facing, the tensile forces in both connected and unconnected reinforcement increased with depth due to the effect of the overburden stress. Furthermore, connected reinforcement exhibited slightly higher tensile force than unconnected reinforcement due to the tie-back effect of the other wall. At the free end of all unconnected reinforcements, the tensile forces were attenuated as inspected. However, the tensile forces in connected walls were

uniform in the top reinforcements (z/H = 0.81 and z/H = 0.56). This means that in the top wall, the connection limited the divergence of facing walls and allowed a uniform lateral expansion of the backfill without generating a sliding surface. At the bottom reinforcement, z/H = 0.31, the tensile forces for connected and unconnected walls were close. The tensile force where a peak was observed near the facing for connected and unconnected walls decreased to null tension at the middle. The null tensile force in connected case affirms the absence of deformation in the middle bottom of the connected walls. The same behavior was reported in Sravanam et al. (2020) for static loading cases.

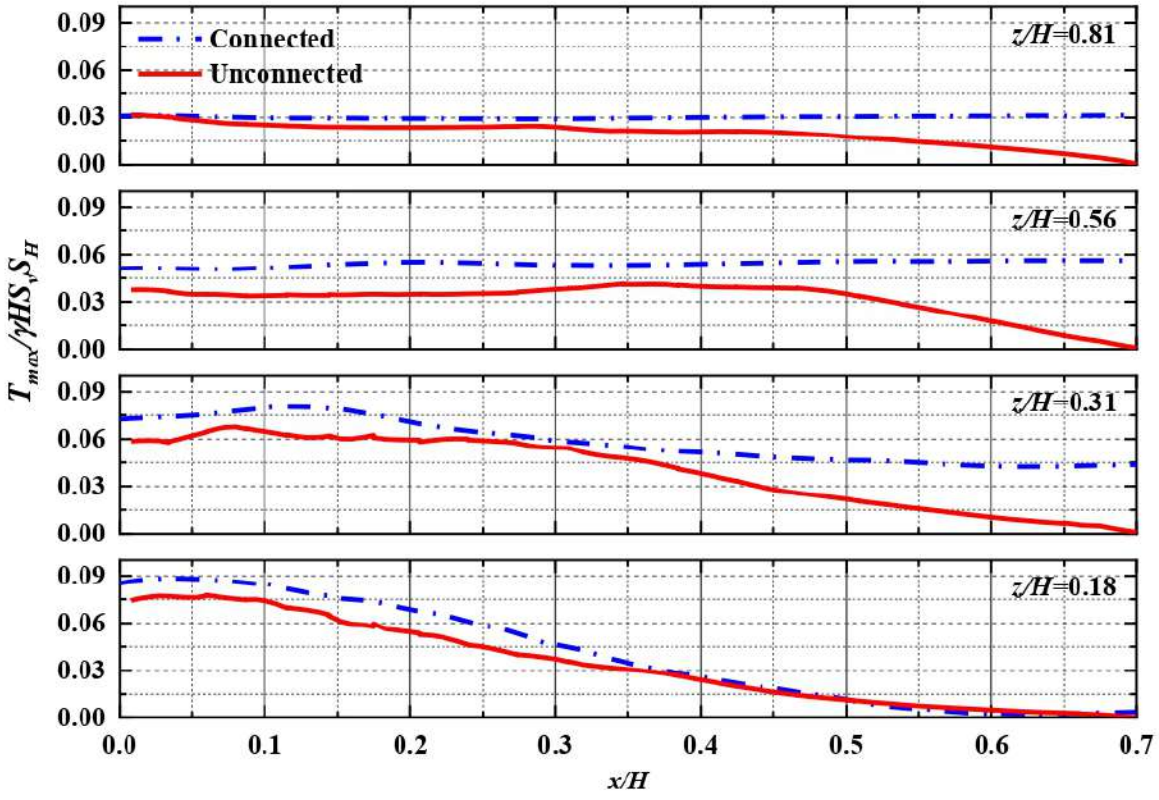

Figure 5.9. Distribution of maximum tensile forces along the reinforcements under seismic excitations.

5.4.4 Distribution of seismic earth pressure

The calculations for active earth thrust against mechanically-stabilized earth walls under earthquake loads used in internal and external stability design checks is typically obtained from the Mononobe-Okabe method (an extension of Coulomb's approach), given by the following expression:

$$P_{AE} = \frac{1}{2} K_{AE} \gamma H^2 (1 - k_v) \tag{5.1}$$

where, γ = unit weight of the soil, and H = height of the wall. The total (static plus dynamic) earth pressure coefficient (K_{AE}) is calculated using the Mononobe-Okabe equation given by:

$$K_{AE} = \frac{\cos^2(\varphi - \theta - \beta)}{\cos^2\theta \cos\beta \cos(\delta + \theta + \beta)\left[1 + \sqrt{\frac{\sin(\delta + \varphi)\sin(\varphi - \alpha - \beta)}{\cos(\delta + \theta + \beta)\cos(\theta - \alpha)}}\right]^2} \tag{5.2}$$

where, φ = peak soil friction angle, α = backfill surface slope angle from the horizontal, δ = interface friction angle at the back of the wall-soil (or back of the reinforced soil zone), β = seismic inertial angle given by $\beta = tan^{-1}(k_h/1 \pm k_v)$, and k_h and k_v are the peak horizontal and vertical seismic coefficients, respectively.

Equation (5.1) denotes the total active thrust on the wall during seismic loading and the point of application of the resultant thrust to beat $1/3H$ from the bottom of the wall. Seed and Whitman (1970) (S-W method) simplified the calculation by separating the total thrust (static and dynamic), P_{AE}, into two components representing the static earth force component, P_A, and the incremental dynamic earth thrust due to seismic load, ΔP_{AE}, where $P_{AE} = P_A + \Delta P_{AE}$, $K_{AE} = K_A + \Delta K_{AE}$, and $\Delta K_{AE} = 3/4 k_h$. However, the S-W method uses $0.6H$ from the base of the wall for dynamic thrust as the point of application. Thus, the point of application of the total thrust under seismic conditions is calculated using the subsequent equation:

$$h = \frac{P_A\left(\frac{H}{3}\right) + \Delta P_{AE}\left(0.6H\right)}{P_{AE}} \tag{5.3}$$

Figure 5.10 shows the variations in the normalized total earth pressure thrust ($K_{AE} = P_{AE}/0.5\gamma h^2$) and the normalized incremental seismic earth pressure thrust ($\Delta K_{AE} = \Delta P_{AE}/0.5\gamma h^2$) at the facing and at the end of the reinforcement zone in both connected and unconnected walls. The results were also compared with those of conventional methods (Mononobe-Okabe (1929) and Seed and Whitman (1970) earth pressure methods) with peak ground accelerations (PGA) was scaled between 0.1 and 0.6 g. Numerical results show that the variations of K_{AE} and ΔK_{AE} with the PGA for both at the facing and at the section passing through the end of the reinforcement zone were higher at connected compared to unconnected walls. K_{AE} and ΔK_{AE} at the end of reinforcement zone were not affected by PGA in the unconnected walls. Hence, the values for the total and incremental dynamic earth pressure coefficients, K_{AE} and ΔK_{AE}, at the facing for connected walls are in a linear trend and were found to be closer to those of S-W prediction.

5.4.5 Location of the point of application of the dynamic earth thrust

Figure 5.11 shows the effect of the application point of the dynamic thrust, h/H, with various PGA for both connected and unconnected walls at the facing and end of the reinforcement zone of the walls. The results were compared with the M-O method which uses one-third of the wall height and with the S-W method which uses 0.6 H for the point of application of dynamic thrust. For connected and unconnected walls for both facing panel and end of the reinforcement zone for walls, the point of action of the resultant remains approximately constant at one-third of the height of the wall for various PGA. At the end of the reinforcement zone for connected and unconnected walls, the point of action of P_{AE} progressively shifts from $0.33H$ to $0.2H$ when PGA varies from 0 to 0.1 g. With the further increase in PGA from 0.1 g to 0.6 g, the point of action reaches the constant value which is approximately one-third of the height of the wall.

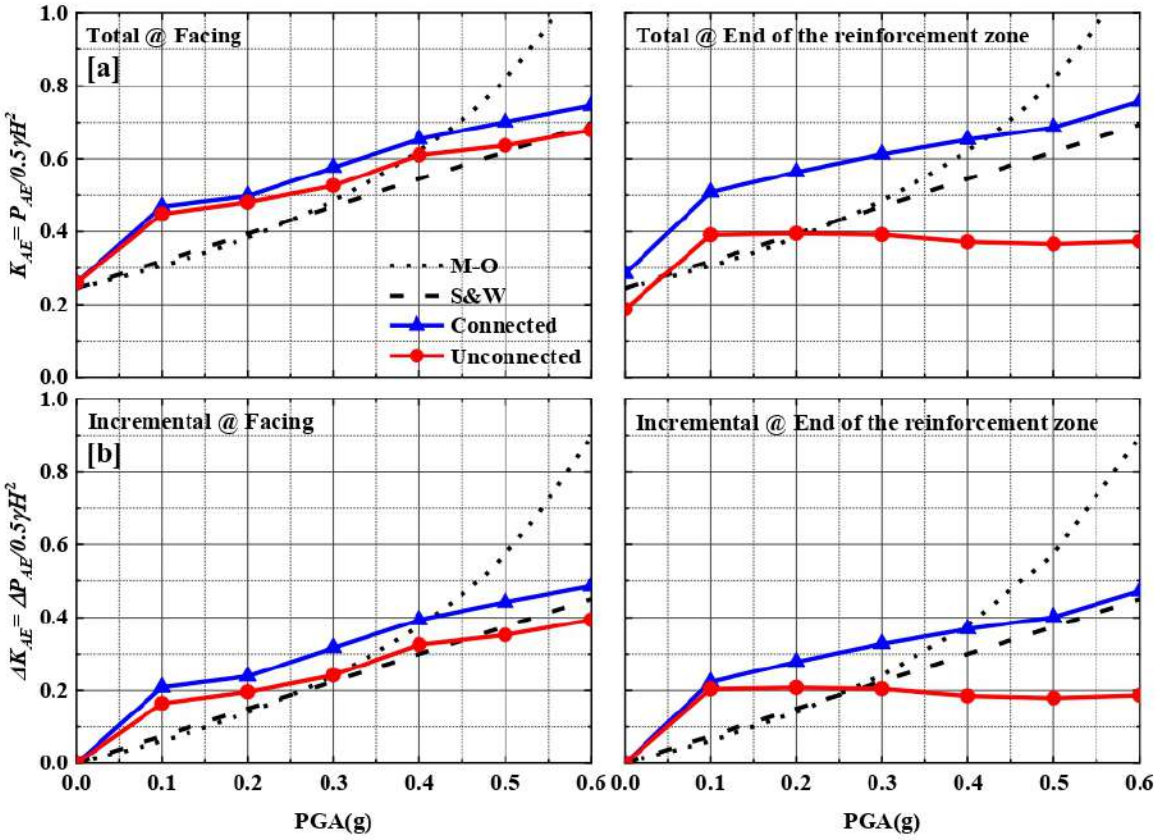

Figure 5.10. Variations in normalized total earth pressures at facing and at end of reinforcement zone of connected and unconnected walls showing (a) total, and (b) incremental values.

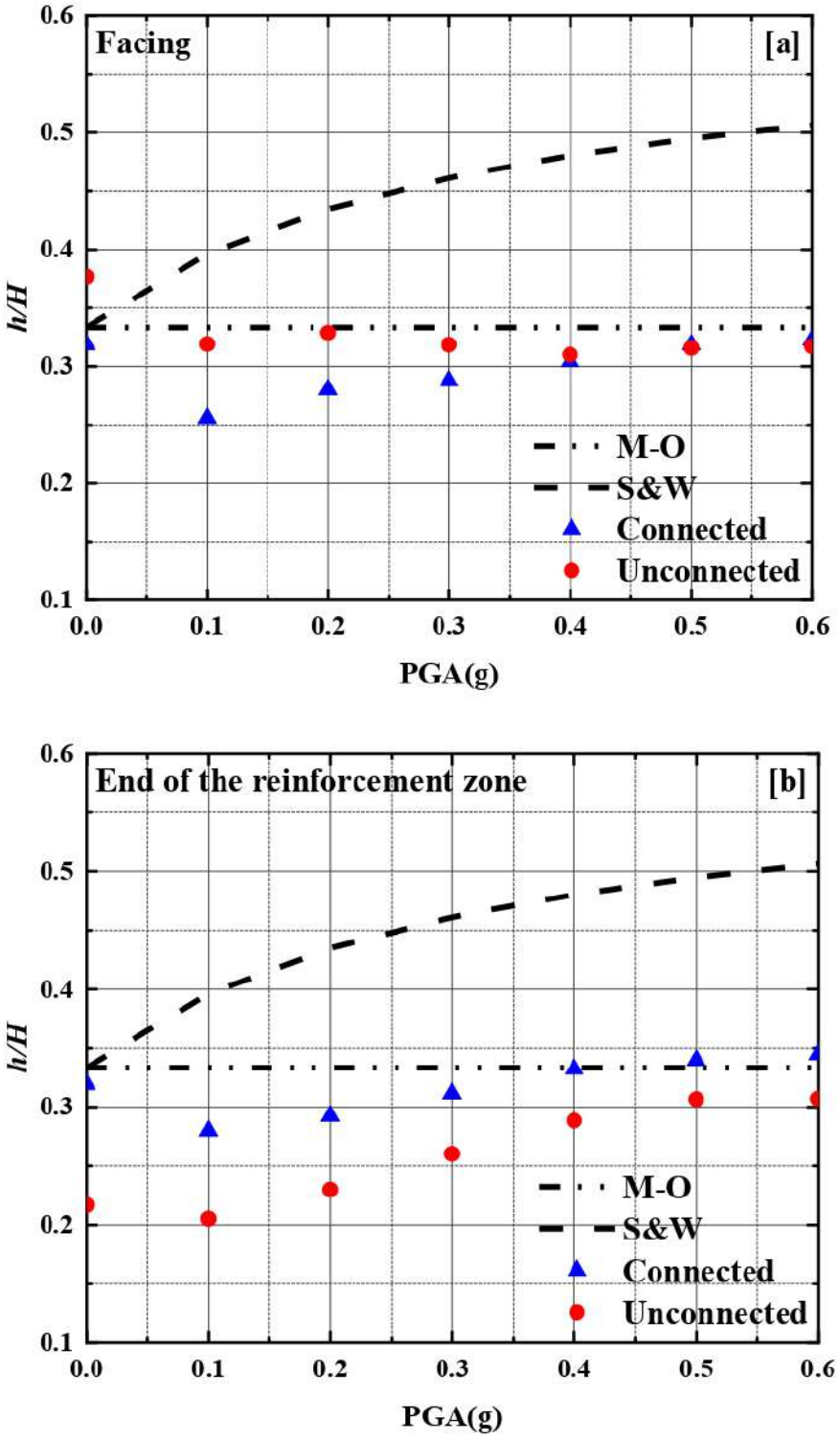

Figure 5.11. Variation of h/H for facing and end of the reinforcement zone of connected and unconnected walls.

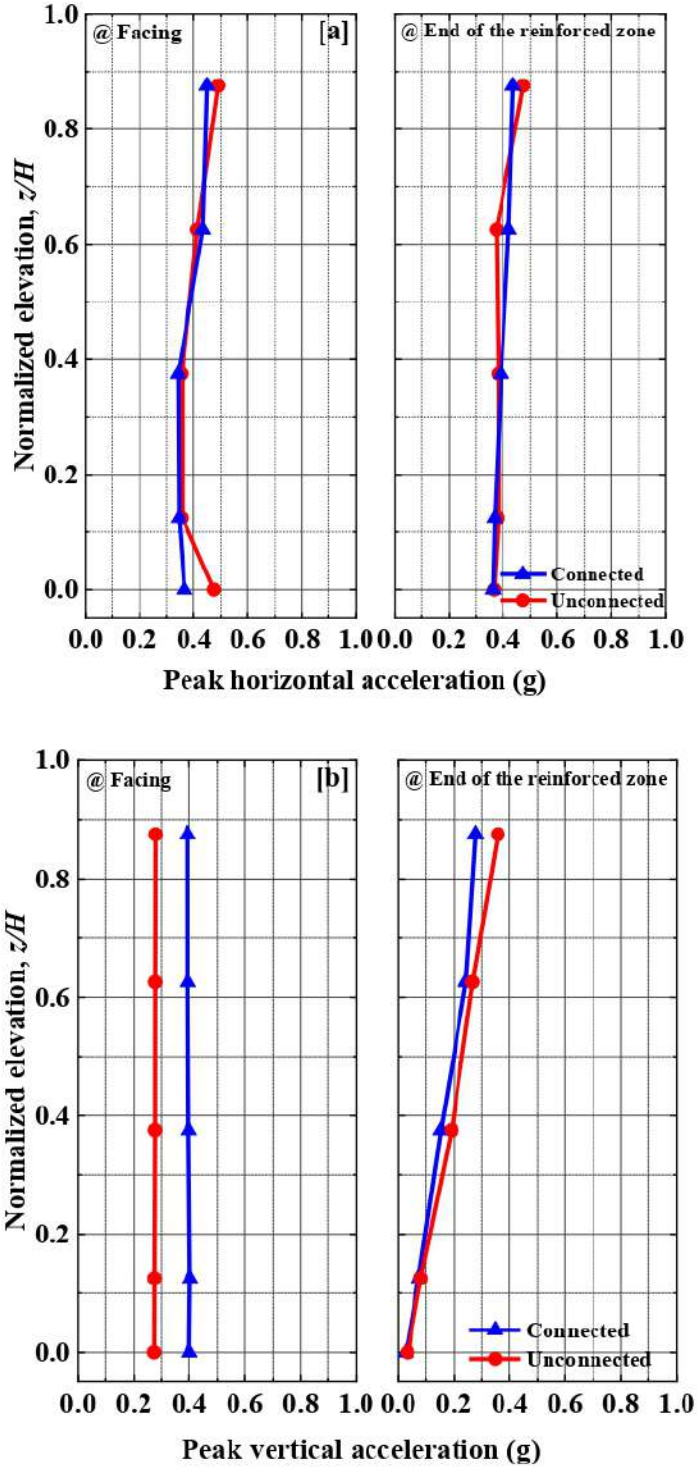

Figure 5.12. Responses walls during Kobe earthquakes at facing and at end of reinforced soil zone in terms of (a) peak horizontal acceleration, and (b) peak vertical accelerations.

5.4.6 Wall acceleration response

The amplification studies of horizontal and vertical accelerations during seismic loading play an important role in the estimation of the seismic performances of reinforced soil retaining walls. Figure 5.12 shows the horizontal and vertical acceleration responses along the wall height ratio (h/H) for both the connected and unconnected walls at the facing and at the end of the reinforced zone. Responses at the end of the reinforced zone implies that acceleration responses were considered at a horizontal distance of 4.2m from the facing. This is the zone at which the reinforcement ends in the unconnected walls. However, the reinforcement does not end in the connected walls. It was noted that the walls recorded similar values for horizontal accelerations at the facing and at the end of the reinforced zone. However, unconnected walls tend to give greater amplification of about 0.48 at the bottom compared to the connected walls of 0.37 at the facing wall, respectively. It was also observed that the vertical acceleration at the end of the reinforced zone was amplified roughly linear along the height of both the connected and unconnected walls. However, no amplification was noted as expected at the facing due to the high vertical stiffness of the wall.

5.4.7 Mechanisms of potential failure

Figure 5.13 shows the distribution of plastic points and of shear strain increment contours in both connected and unconnected walls at the end of the dynamic analyzes subjected to Kobe seismic loading. The Mohr-Coulomb plastic points indicate that the Coulomb failure is reached for these points. Shear strain increment contours visualize more clearly the localization of potential failure mechanism than the distribution of plastic points. For both cases, shear strain bands were developed from the bottom of the two facings and spread with angle close to the angle of shearing resistance of the backfill. Therefore, a trapped triangular soil, observed in the middle bottom of the BBMSE walls, was not affected by shear strain bands. This state is in perfect agreement with the reduction until zero of the tensile force in the connected reinforcement layers in this area (Figure 5.9). In the case of unconnected walls, the interception of shear bands from the two walls created a triangular failure zone in the middle top of the BBMSE walls. However, in the case of connected walls, the tie back effect hampered the spread of shear strain bands to the top of the reinforced backfill. In fact, the connection of reinforcements in the middle ensures the mobilization of the full strength and length of the reinforcement and reduces the maximum required tensile

GENERAL CONCLUSIONS

The main aim of this thesis was to investigate the seismic performance of a cantilever-type retaining wall and back-to-back mechanically stabilized earth walls with the addition of lightweight and compressible materials with a high vibration absorption capacity. In order to achieve this aim, numerical models were developed and validated to simulate the studies on retaining walls using the PLAXIS 2D geotechnical finite element software. The validation of our models is considered a major step that can only be carried out from real experimental data.

This thesis consists of two main parts:

The first part is devoted to a bibliographic summary containing two chapters, the first behavior of estimating dynamic pressures on retaining walls, and the second generality of scrap tire-derived and geosynthetic geomaterials for geoengineering applications.

The second part consists of three numerical applications were presented. The first application is on the behavior of cantilever retaining walls with a compressible inclusion of waste tire shreds placed behind the retaining wall under harmonic excitation. The seismic response of wall models was studied in terms of horizontal displacement and lateral earth pressures to demonstrate the effectiveness of tire chips as compressible inclusions. The second application is a numerical investigation of response of a typical cantilever retaining wall, consisting of compressible tire shreds (CTS) as a cushion under earthquake ground motion. To quantify the benefit of CTS cushion, a comparison was made in the behavior of wall without and with cushion in terms of horizontal displacement and rotation, the maximum shear force and bending moment, the seismic earth thrust and its point of application on the wall. Finally, an application on the behavior of connected and unconnected back-to-back BBMSE walls in soil reinforced with geogrids.

The bibliographical study carried out by the first part made it possible to highlight the following points:

- The most common methods used for the design of retaining structures under seismic conditions are force-based design methods; pseudo-static analysis (Mononobe-Okabe 1926, 1929), pseudo-dynamic analysis (Steedman and Zeng 1990), and Displacement-based design method on the sliding block method (Richards and Elms 1979).
- Scrap tire-derived fills showed excellent performance benefits when compared to conventional sand fills.
- The use of scrap tire-derived are low-cost, lightweight, recycled and this research combined with previous studies and field trials shows that they are as alternative materials in civil engineering applications, especially in geotechnical applications, has been practiced on several occasions.
- There are very limited numerical modeling and experimental studies on the behavior of back-to-back mechanically stabilized earth walls in seismic conditions.

The first two numerical applications are made to cantilever retaining walls with a compressible inclusion made up of waste tire shreds placed behind the retaining wall. The main conclusions of this study are:

- The horizontal displacements and earth pressures are low when compressible tire shreds as a cushion were provided behind the wall.
- The horizontal displacements and earth pressures were decreased with an increase in the thickness of the cushion made up of compressible tire shreds.
- The rotation of the stem of the cantilever retaining wall was reduced as compared to the control case.
- It was found that the maximum shear force and bending along the stem reduced significantly when a compressible cushion was provided behind the wall.
- It is also noted that the seismic earth thrust at the stem and along a section through the heel showed a reduction in the seismic earth pressure thrusts, due to the inclusion of 300 mm-thick cushion compared to the control case.

- An increase in the thickness of the cushion showed a favorable effect on the dynamic behavior of walls of different heights with the inclusion of compressible tire shreds cushion.
- The compressible cushion led to a decrease in results despite an increase in the acceleration level, compared to the control case.
- The behavior of three different heights of the retaining wall considered in the study showed that the dynamic earth thrust against the retaining wall can be considerably reduced using the proposed method, which justified that the wall with the shredded compressible cushion of the tires could work well during earthquake loading of different magnitudes.
- The results from numerical model proposed in the study can be very helpful to design cantilever retaining walls of different heights without and with a compressible cushion of tire shreds of varying thicknesses and subjected to different amplitudes of earthquake acceleration and frequencies of sinusoidal acceleration.
- The numerical model was used to quantify the effects of friction angle on the dynamic response in terms of the horizontal displacements and earth pressures and showed much superior performance to that of a granular backfill.
- The parametric study of the friction angle variation of the granular backfill material showed that a decrease in friction angle a more positive effect on performing compressible inclusions.

The third numerical study conducted, provides information on the behavior of reinforcement in back-to-back walls for both connected and unconnected BBMSE walls were investigated under seismic loading using real-time earthquake data. The following points emerged from the present investigation:

- The maximum displacements in the connected walls were lower than those of the unconnected walls.
- The total earth pressure the facing and at end reinforcement zone in connected walls were found to be slightly more than the total earth pressure obtained in unconnected walls under seismic loading. Also, the peak of normalized earth pressures in connected walls was close to the M-O method.

- Results showed that the maximum tensile forces in connected walls were slightly higher and uniform than those for the unconnected walls. In addition, high tensile forces were observed in the reinforcements near the base.
- At the facing, the values of the total and the increased dynamic ground pressure parameters (K_{AE} and ΔK_{AE}) for both the connected and unconnected walls were under predicted by S-W and M-O methods. At the end of the reinforcement zone, the K_{AE} and ΔK_{AE} for connected walls with the increased PGA followed the linear trend of S&W prediction compared to the connected walls.
- The point of application of dynamic thrust obtained was approximately constant located at the one-third of the height from the base with the increase in the PGA in both connected and unconnected walls.
- It was observed that the horizontal and vertical accelerations increase with the increase in the amplitude of peak acceleration. Also, the most acceleration amplification occurred at the facing and at the end of the reinforced zone for both connected and unconnected walls, respectively.
- The results of the lateral wall displacements, distribution of maximum tensile forces along the reinforcements, and shear strain increment contours demonstrate that connection of reinforcement is more beneficial than the case of unconnected in limitation of lateral displacement at the top of the walls and spread of potential failure to backfill surface.

BIBLIOGRAPHIC REFERENCES

AASTHO. 2012. AASHTO LRFD Bridge design specifications, 6th edn. American Association of State Highway and Transportation Officials (AASHTO), Washington DC.

Ahmed, I., & Lovell, C. (1993). Rubber soils as lightweight geomaterials. Transportation research record(1422).

Ahn, I.-S., & Cheng, L. (2014). Tire derived aggregate for retaining wall backfill under earthquake loading. Construction and Building Materials, 57, 105-116.

Ahmad, S. M. & Choudhury, D. 2008a. Pseudo-dynamic approach of seismic design for waterfront reinforced soil-wall. Geotextiles and Geomembranes, 26, 291-301.

Ahmad, S. M. & Choudhury, D. 2008b. Stability of waterfront retaining wall subjected to pseudo dynamic earthquake forces and tsunami. Journal of Earthquake and Tsunami, 2, 107-131.

Aggour, M. S., and Brown, C. B. 1973. Retaining walls in seismic areas. Proceedings, 5th World Conference on Earthquake Engineering, Rome, Italy, 2624-2627.

Al Atik, L., Sitar, N. (2010). Seismic earth pressures on cantilever retaining structures. Journal of Geotechnical and Geoenvironmental Engineering, Vol. 136, No. 10, pp. 1324-1333.

Al Atik, L. & Sitar, N. (2008). Experimental and analytical study of the seismic performance of retaining structures. PEER Report 2008/104, Pacific Earthquake Engineering Research Center, College of Engineering, University of California, Berkeley.

Anubhav, S., & Basudhar, P. (2011). Numerical modelling of surface strip footings resting on double-faced wrap-around vertical reinforced soil walls. Geosynthetics International, 18(1), 21-34.

ASTM D6270 (2012). Standard practice for use of scrap tires in civil engineering applications. American Society for Testing and Materials, West Conshohocken, PA.

Balunaini U, Yoon S, Prezzi M, Salgado R (2009) Tire shred backfill in mechanically stabilized earth wall applications. Final report FHWA/IN/JTRP-2008/17. West Lafayette, USA: purdue university.

Balunaini, U., S. M. Sravanam, and M. R. Madhav. 2017. "Effect of compaction stresses on performance of back-to-back retaining walls." In Proc., 19th Int. Conf. Soil Mechanics and Geotechnical Engineering, Seoul, South Korea, edited by W. Lee, J.-S. Lee, H.-K. Kim, and D.-S. Kim, 1951–1954.

Bathurst, R., & Hatami, K. (1998). Seismic response analysis of a geosynthetic-reinforced soil retaining wall. Geosynthetics International, 5(1-2), 127-166.

Bakr, J. and Ahmad, S. M. (2018). A finite element performance-based approach to correlate movement of a rigid retaining wall with seismic earth pressure. Soil Dynamics and Earthquake Engineering, 114, 460-479

Bakr, J., Ahmad, S. M., & Lombardi, D. (2019). Finite-element study for seismic structural and global stability of cantilever-type retaining walls. International Journal of Geomechanics, 19(10), 04019117.

Bakr, J. A. (2018). Displacement-based approach for seismic stability of retaining structures: The University of Manchester (United Kingdom).

Baziar, M. H., Sanaie, M., Amirabadi, O. E., Khoshniazpirkoohi, A., & Azizkandi, A. S. (2020). Mitigation of hunchbacked gravity quay wall displacement due to dynamic loading using shaking table tests. Ocean Engineering, 216, 108056.

Bellezza, I., D'Alberto, D., & Fentini, R. (2012). Pseudo-dynamic approach for active thrust of submerged soils. Proceedings of the Institution of Civil Engineers-Geotechnical Engineering, 165(5), 321-333.

Benmebarek, S., Attallaoui, S., & Benmebarek, N. (2016). Interaction analysis of back-to-back mechanically stabilized earth walls. Journal of Rock Mechanics and Geotechnical Engineering, 8(5), 697-702.

Benmebarek, S., & Djabri, M. (2017a). FE Analysis of Back-to-Back Mechanically Stabilized Earth Walls Under Cyclic Harmonic Loading. Indian Geotechnical Journal. Benmebarek, S., & Djabri, M. (2017b). FEM to investigate the effect of overlapping-reinforcement on the performance of back-to-back embankment bridge approaches under self-weight. Transportation Geotechnics, 11, 17-26.

Berg, R. R., Christopher, B. R., & Samtani, N. C. (2009). Design of mechanically stabilized earth walls and reinforced soil slopes–Volume I: United States. Federal Highway Administration.

Bhattacharjee, A. & Krishna, A. M. (2009). Study of Seismically Induced Permanent Displacement Of Gravity Wall.

Bolton M.D., and Steedman, R.S. (1985). The behavior of fixed cantilever walls subject to lateral loading. Application of Centrifuge Modeling to Geotechnical Design, Craig (ed.), Balkema, Rotterdam.

Candia, G. (2013). Experimental and Numerical Modeling of Seismic Earth Pressure on Retaining Walls with Cohesive Backfills. Ph.D. thesis, Department of Civil & Environmental Engineering, University of California, Berkeley.

Candia, G., Mikola, R.G., Sitar, N. (2013). Seismic earth pressures on braced wall and displacing retaining wall in clay (GC01). Network for Earthquake Engineering Simulation (database), Dataset, DOI: 10.4231/D37W67572

Candia, G., Sitar, N. (2013). Seismic Earth Pressures on Retaining Structures in Cohesive Soils. Report No. UCB GT 13-02, August 2013, p. 161.

Cecich, V., Gonzales, L., Hoisaeter, A., Williams, J., & Reddy, K. (1996). Use of shredded tires as lightweight backfill material for retaining structures. Waste Management & Research, 14(5), 433-451.

Choudhury, D., & Nimbalkar, S. (2005). Seismic passive resistance by pseudo-dynamic method. Geotechnique, 55(9), 699-702.

Choudhury, D., & Nimbalkar, S. S. (2006). Pseudo-dynamic approach of seismic active earth pressure behind retaining wall. Geotechnical & Geological Engineering, 24(5), 1103-1113.

Choudhury, D., & Nimbalkar, S. S. (2008). Seismic rotational displacement of gravity walls by pseudodynamic method. International Journal of Geomechanics, 8(3), 169-175.

Choudhury, D., Sitharam, T., & Rao, K. S. (2004). Seismic design of earth-retaining structures and foundations. Current science, 1417-1425.

Conti, R., Madabhushi, G. S. P. & Viggiani, G. M. B. 2012. On the behaviour of flexible retaining walls under seismic actions. Géotechnique [Online], 62.

Conti, R., Madabhushi, G., Mastronardi, V., & Viggiani, G. (2015). Centrifuge dynamic tests on gravity retaining walls: an insight into bearing vs sliding failure mechanisms. Paper presented at the Proceedings of the 6th International Conference on Earthquake Geotechnical Engineering, Christchurch, New Zealand.

Corigliano, M., C.G., L. & R, P. (2011). Displacement-based seismic design of gravity walls using double-support excitation. Proceedings of the 8th International Conference on Structural Dynamics, EURODYN 2011.

Coulomb, C. A. (1973). Essai sur une application des regles de maximis et minimis a quelques problemes de statique relatifs a l'architecture (essay on maximums and minimums of rules to some static problems relating to architecture).

Corigliano, M., Lai, C., & Pasquali, R. (2011). Displacement-based seismic design of gravity walls using double-support excitation. Paper presented at the 8th International Conference on Structural Dynamics, Eurodyn.

Dammala PK, Sodom BR, Adapa MK (2015). Experimental investigation of applicability of sand tire chip mixtures as retaining wall backfill. IFCEE 2015, pp 1420-9.

Djabri, M., & Benmebarek, S. (2016). FEM Analysis of Back-to-Back Geosynthetic-Reinforced Soil Retaining Walls. International Journal of Geosynthetics and Ground Engineering, 2(3).

Djabri, M., & Benmebarek, S. (2020). Numerical Investigations on the Behavior of Back-to-Back Mechanically Stabilized Earth Walls: Effect of Structural Components. Jordan Journal of Civil Engineering, 14(3).

Djadouni, H., Trouzine, H., Gomes Correia, A., & Miranda, T. F. d. S. (2019). 2D numerical analysis of a cantilever retaining wall backfilled with sand–tire chips mixtures. European Journal of Environmental and Civil Engineering, 1-17.

Dram, A., Benmebarek, S., & Balunaini, U. (2020). Performance of Retaining Walls with Compressible Inclusions under Seismic Loading. Civil Engineering Journal, 6(12), 2474-2488.

El-Emam, M., & Bathurst, R. (2005). Facing contribution to seismic response of reduced-scale reinforced soil walls. Geosynthetics International, 12(5), 215-238.

El-Emam, M. M., & Bathurst, R. J. (2007). Influence of reinforcement parameters on the seismic response of reduced-scale reinforced soil retaining walls. Geotextiles and Geomembranes, 25(1), 33-49.

El-Sherbiny, R., Ibrahim, E., & Salem, A. (2013). Stability of back-to-back mechanically stabilized earth walls. Paper presented at the Geo-Congress 2013: Stability and Performance of Slopes and Embankments III.

Gazetas, G., Psarropoulos, P. N., Anastasopoulos, I. & Gerolymos, N. (2004). Seismic behaviour of flexible retaining systems subjected to short-duration moderately strong excitation. Soil Dynamics and Earthquake Engineering, 24, 537-550.

Geraili, R., Candia, G. & Sitar, N. (2016). Seismic earth pressures on retaining structures and basement walls in cohesionless soils. Journal of Geotechnical and Geoenvironmental Engineering, 142, 04016047.

Ghazavi M, and Sakhi MA. (2005). Influence of optimized tire shreds on shear strength parameters of sand. International Journal of Geomechanics 5(1):58-65.

Ghosh, S. (2010). Pseudo-dynamic active force and pressure behind battered retaining wall supporting inclined backfill. Soil Dynamics and Earthquake Engineering, 30(11), 1226-1232.

Ghosh, P. (2007). Seismic passive earth pressure behind non-vertical retaining wall using pseudo-dynamic analysis. Geotechnical and Geological Engineering, 25(6), 693.

Green, R.A., Ebeling, R.M. (2002). Seismic analysis of cantilever retaining walls, Phase I. Report ERDC/ITL TR-02-3, Information Technology Laboratory, US Army Corps of Engineers, Engineer Research and Development Center, Vicksburg, MS

Green, R. A., Olgun, C. G., Ebeling, R. M. & Cameron, W. I. (2003). Seismically induced lateral earth pressures on a cantilever retaining wall P.The sixth US conference and workshop on lifeline earthquake engineering (TCLEE2003), ASCE.

Green, R. A., Olgun, C. G. & Cameron, W. I. (2008). Response and modeling of cantilever retaining walls subjected to seismic motions. Computer-Aided Civil and Infrastructure Engineering, 23, 309-322.

Han, J., and D. Leshchinsky. 2010. Analysis of back-to-back mechanically stabilized earth walls. Geotext. Geomembr. 28 (3): 262–267.

Hardianto, F. S., and K. M. Truong. 2010. Seismic deformation of back-to-back mechanically stabilized earth (MSE) walls. In Earth Retent. Conf. 3, Geotechnical Special Publication 208, edited by R. Finno, Y. M. A. Hashash, and P. Arduino, 704–711. Bellevue, WA: ASCE.

Hashash, Y. M., & Park, D. (2002). Viscous damping formulation and high frequency motion propagation in non-linear site response analysis. Soil Dynamics and Earthquake Engineering, 22(7), 611-624.

Hatami, K., & Bathurst, R. (2000). Effect of structural design on fundamental frequency of reinforced-soil retaining walls. Soil Dynamics and Earthquake Engineering, 19(3), 137-157.

Hazarika H, Yasuhara K, Karmokar AK and Mitarai Y (2008b) Shaking table test on liquefaction prevention using tire chips and sand mixture, Hazarika & Yasuhara (eds), Taylor & Francis Group, London, ISBN 978-0-415-46070- 5,CRC Press, USA, 215-222

Hudson, M., Idriss, I., & Beirkae, M. (1994). QUAD4M User's manual. A computer program to evaluate the seismic response of soil structures using finite element procedures and incorporating a compliant base.

Humphrey DN., and Sandford TC. (1993). Tire chips as lightweight subgrade fill and retaining wall backfill. In: Proceedings of the symposium on recovery and effective reuse of discarded materials and by-products for construction of highway facilities. Us department of transportation, federal highway administration, pp 5-87.

Humphrey D, Cosgrove T, Whetten N, Hebert R (1997) Tire chips reduce lateral earth pressure against the walls of a rigid frame bridge. In: Proceeding of the Conference on Renewal, Rehabilitation and Upgrades in Civil and Environmental Engineering. Maine Section ASCE Technical Seminar, 11p1997.

Ibrahim, K. M. H. I. (2015). Seismic displacement of gravity retaining walls. HBRC Journal, 11(2), 224-230.

Ishibashi, I., and Fang, Y.S. (1987). Dynamic earth pressures with different wall movement modes. Soils and Foundations, Vol. 27, No. 4, 11-22.

Jadhav, P. R., & Prashant, A. (2020). Computation of seismic translational and rotational displacements of cantilever retaining wall with shear key. Soil Dynamics and Earthquake Engineering, 130, 105966.

Jo, S.-B., Ha, J.-G., Lee, J.-S. & Kim, D.-S. 2017. Evaluation of the seismic earth pressure for inverted T-shape stiff retaining wall in cohesionless soils via dynamic centrifuge. Soil Dynamics and Earthquake Engineering, 92, 345-357.

Jung, C., Bobet, A. (2008). Seismic Earth Pressures Behind Retaining Walls: Effects of Rigidbody Motions, Proceedings of Geotechnical Earthquake Engineering and Soil Dynamics IV, D. Zeng, M. Manzari & D. Hiltunen, eds., ASCE, Sacramento, CA.

Katkar, B. H., & Viswanadham, B. V. S. (2011). SOME STUDIES ON THE BEHAVIOUR OF BACK-TO-BACK GEOSYNTHETIC REINFORCED SOIL WALLS. In Proceedings of Indian Geotechnical Conference (IGC 2011) (Vol. 15).

Kim S.R., Kwon O.S., Kim M.M., (2004). Evaluation of Force Components Acting on Gravity Type Quay Walls During Earthquakes. Soil Dynamics and Earthquake Engineering 24 (2004) 853–866.

Kim S.R., Kwon O.S., Kim M.M. (2004). Evaluation of Force Components Acting on Gravity Type Quay Walls During Earthquakes. Soil Dynamics and Earthquake Engineering 24 (2004) 853–866.

Kloukinas, P., Scotto di Santolo, A., Penna, A., Dietz, M., Evangelista, A., Simonelli, A. L., . . . Mylonakis, G. (2015). Investigation of seismic response of cantilever retaining walls: Limit analysis vs shaking table testing. Soil Dynamics and Earthquake Engineering, 77, 432-445.

Koseki, J., Munaf, Y., Sato, T., Tatsuoka, F., Tateyama, M., & Kojima, K. (1998). Shaking and tilt table tests of geosynthetic-reinforced soil and conventional-type retaining walls. Geosynthetics International, 5(1-2), 73-96.

Kramer, S. L. (1996). Geotechnical earthquake engineering: Pearson Education India.

Kuhlemeyer, R. L., & Lysmer, J. (1973). Finite element method accuracy for wave propagation problems. Journal of Soil Mechanics & Foundations Div, 99(Tech Rpt).

Lee, H. J., & Roh, H. S. (2007). The use of recycled tire chips to minimize dynamic earth pressure during compaction of backfill. Construction and Building Materials, 21(5), 1016-1026. doi: 10.1016/j.conbuildmat.2006.02.003

Li, L., Yang, J., Xiao, H., Zhang, L., Hu, Z., & Liu, Y. (2020). Behavior of tire-geogrid–reinforced retaining wall system under dynamic vehicle load. International Journal of Geomechanics, 20(4), 04020017.

Ling, H. I., Liu, H., Kaliakin, V. N., & Leshchinsky, D. (2004). Analyzing dynamic behavior of geosynthetic-reinforced soil retaining walls. Journal of engineering mechanics, 130(8), 911-920.

Ling, H. I., and D. Leshchinsky. 2003. Finite element parametric study of the behavior of segmental block reinforced-soil retaining walls. Geosynth. Int. 10 (3): 77–94.

Liu, H., Wang, X., & Song, E. (2010). Centrifuge testing of segmental geosynthetic-reinforced soil retaining walls subject to modest seismic loading GeoFlorida 2010: Advances in Analysis, Modeling & Design (pp. 2992-2998).

Madabhushi, S., & Zeng, X. (1998). Seismic response of gravity quay walls. II: Numerical modeling. Journal of Geotechnical and Geoenvironmental Engineering, 124(5), 418-427.

Matsuo, O., Yokoyama, K., & Saito, Y. (1998). Shaking table tests and analyses of geosynthetic-reinforced soil retaining walls. Geosynthetics International, 5(1-2), 97-126.

Mikola, R.G., Sitar, N. (2013). Seismic earth pressures on retaining structures in cohesionless soils. Report No. UCB GT 13-01, March 2013, p. 217.

Moghadam, A.M., Ghalandarzadeh, A., Towhata, I., Moradi, M., Ebrahimian, B., Hajialikhani, P. (2009). Studying the Effects of Deformable Panels on Seismic Displacement of Gravity Quay walls. Ocean Engineering, 36 (2009) 1129–1148.

Mohajeri, M., Ichii, K., and Tamura, T. (2004). Experimental Study on Sliding Block Concept for Caisson Walls. Journal of Waterway, Port, Coastal and Ocean Engineering, ASCE / MAY/JUNE 2004.

Mouli, S. S., & Umashankar, B. (2019). Behavior of Back-to-Back Reinforced Earth Retaining Walls (Doctoral dissertation, Indian institute of technology Hyderabad).

Murali Krishna, A., & Bhattacharjee, A. (2017). Behavior of rigid-faced reinforced soil-retaining walls subjected to different earthquake ground motions. International Journal of Geomechanics, 17(1), 06016007.

Murali Krishna, A., & Madhavi Latha, G. (2009). Seismic behaviour of rigid-faced reinforced soil retaining wall models: reinforcement effect. Geosynthetics International, 16(5), 364-373.

Murthy, V. (2002). Geotechnical engineering: principles and practices of soil mechanics and foundation engineering: CRC press.

Nadim, F., & Whitman, R. V. (1983). Seismically induced movement of retaining walls. Journal of Geotechnical Engineering, 109(7), 915-931.

Nakamura, S. (2006). Reexamination of Mononobe-Okabe theory of gravity retaining walls using centrifuge model tests. Soils and foundations, 46(2), 135-146.

Newmark, N. M. (1965). Effects of earthquakes on dams and embankments. Geotechnique, 15(2), 139-160.

Nova-Roessig, L., & Sitar, N. (2006). Centrifuge model studies of the seismic response of reinforced soil slopes. Journal of Geotechnical and Geoenvironmental Engineering, 132(3), 388-400.

Nimbalkar, S., & Choudhury, D. (2007). Sliding stability and seismic design of retaining wall by pseudo-dynamic method for passive case. Soil Dynamics and Earthquake Engineering, 27(6), 497-505.

Ortiz, L. A., Scott, R. F. & Lee, J. (1983). Dynamic centrifuge testing of a cantilever retaining wall. Earthquake Engineering and Structural Dynamics 11, 251–268.

Ostadan, F. (2005). Seismic soil pressure for building walls-An updated approach" J.Soil dynamic and earthquake Engineering and Engineering Vibration, 25, 785-793.

Pathmanathan (2007). Numerical modelling of seismic behaviour of earth-retaining walls. MSc Dissertation. Pavia University.

PEER. (2018). PEER ground motion database. https://peer.berkeley.edu/peer-strong-ground-motion-databases.

Rao, G. V., & Dutta, R. (2006). Compressibility and strength behaviour of sand–tyre chip mixtures. Geotechnical & Geological Engineering, 24(3), 711-724.

Ravichandran N, Huggins L (2014) Applicability of shredded tire chips as a lightweight retaining wall backfill in seismic regions. Geo-Congress 2014: Geo-characterization and Modeling for Sustainability, pp 3496-505.

Reddy SB, Krishna A.M (2015) Recycled Tire Chips Mixed with Sand as Lightweight Backfill Material in Retaining Wall Applications: An Experimental Investigation. International Journal of Geosynthetics and Ground Engineering. http://dx.doi.org/10.1007/s 40891-015-0036-0.

Reddy, S.B., & Krishna, A.M. (2017). Tyre chips as compressible inclusions in earth-retaining walls. Proceedings of the Institution of Civil Engineers - Ground Improvement, 170(3), 137-148. doi: 10.1680/jgrim.16.00034

Reddy, S.B., & Krishna, A. M. (2019). Sand–scrap tyre chip mixtures for improving the dynamic behaviour of retaining walls. International Journal of Geotechnical Engineering, 1-13.

Ren, F., Zhang, F., Wang, G., Zhao, Q., & Xu, C. (2018). Dynamic assessment of saturated reinforced-soil retaining wall. Computers and Geotechnics, 95, 211-230. doi: 10.1016/j.compgeo.2017.08.020

Richards Jr, R., & Elms, D. G. (1979). Seismic behavior of gravity retaining walls. Journal of the Geotechnical Engineering Division, 105(4), 449-464.

Richardson, G. N., & Lee, K. L. (1975). Seismic design of reinforced earth walls. Journal of the Geotechnical Engineering Division, 101(2), 167-188.

Saberian, M., Li, J., Nguyen, B. T., & Boroujeni, M. (2020). Experimental and analytical study of dynamic properties of UGM materials containing waste rubber. Soil Dynamics and Earthquake Engineering, 130, 105978.

Sadrekarimi, A. (2011). Seismic displacement of broken-back gravity quay walls. Journal of waterway, port, coastal, and ocean engineering, 137(2), 75-84.

Saito, Y., Mastuo, O., Tustsumi, T. & Nakamura, S. (1999). Dynamic Centifuge model tests on Seismic Stability of Retaining Wall. Part 4, Proc. 54th Annual Conf. of the Japan Society of Civil Engineer.

Salem, A. N., Ezzeldine, O. Y., & Amer, M. I. (2020). Seismic loading on cantilever retaining walls: Full-scale dynamic analysis. Soil Dynamics and Earthquake Engineering, 130, 105962.

Sakaguchi, M. (1996). A study of the seismic behavior of geosynthetic reinforced walls in Japan. Geosynthetics International, 3(1), 13-30.

Seed, H. (1970). Design of earth retaining structures for dynamic loads. Paper presented at the ASCE Specialty Conf.-Lateral Stress in the Ground and Design of Earth Retaining Structures, 1970.

Shrestha, S., & Ravichandran, N. (2018). Performance of retaining wall backfilled with tire aggregate under static and dynamic loading conditions: conventional designs and finite element simulations. International Journal of Geotechnical Engineering, 1-13.

Shrestha, S., Ravichandran, N., Raveendra, M., & Attenhofer, J. A. (2016). Design and analysis of retaining wall backfilled with shredded tire and subjected to earthquake shaking. Soil Dynamics and Earthquake Engineering, 90, 227-239. doi: 10.1016/j.soildyn.2016.08.034

Shukla, S., & Zahid, M. (2011). Analytical expression for dynamic active earth pressure from c-&ϕ soil backfill with surcharge. International Journal of Geotechnical Engineering, 5(2), 143-150.

Shukla, S. K., Gupta, S. K., & Sivakugan, N. (2009). Active earth pressure on retaining wall for c-ϕ soil backfill under seismic loading condition. Journal of Geotechnical and Geoenvironmental Engineering, 135(5), 690-696.

Shukla, S. K., & Habibi, D. (2011). Dynamic passive pressure from c–ϕ soil backfills. Soil Dynamics and Earthquake Engineering, 31(5-6), 845-848.

Sravanam, S. M., Balunaini, U., & Madhav, M. R. (2019). Behavior and design of back-to-back walls considering compaction and surcharge loads. International Journal of Geosynthetics and Ground Engineering, 5(4), 31.

Sravanam, S. M., Balunaini, U., & Madhira, R. M. (2020). Behavior of Connected and Unconnected Back-to-Back Walls for Bridge Approaches. International Journal of Geomechanics, 20(7), 06020013.

Steedman, R., & Zeng, X. (1990). The influence of phase on the calculation of pseudo-static earth pressure on a retaining wall. Geotechnique, 40(1), 103-112.

Steedman, R.S. (1984). Modeling the behavior of retaining walls in earthquakes. PhD Thesis, Cambridge University, Cambridge, England.

Subba Rao, K., & Choudhury, D. (2005). Seismic passive earth pressures in soils. Journal of Geotechnical and Geoenvironmental Engineering, 131(1), 131-135.

Siddharthan, R., and Maragakis, E. M. 1989. Performance of flexible retaining walls supporting dry cohesionless soils under cyclic loads. International Journal for Numerical and Analytical Methods in Geomechanics 13: 309-326.

Takahashi, A., Takemura, J., and Izawa, J. 1999. ‘‘Dynamic behavior of vertical geogrid-reinforced soil during earthquake.’’ Proc., Int. Symp. on Slope Stability Engineering, N. Yagi, T. Yomagami, and J.-C. Jiang, eds., Balkema, Rotterdam, The Netherlands, Vol. 2, 991–996.

Takemura, J., and Takahashi, A. 2003. “Centrifuge modeling of seismic performance of reinforced earth structure.” In Reinforced Soil Engineering (pp. 414-438). CRC Press.

Tiznado, J. C. & Rodríguez-Roa, F. (2011). Seismic lateral movement prediction for gravity retaining walls on granular soils. Soil Dynamics and Earthquake Engineering, 31, 391-400.

Tweedie JJ, Humphrey DN, Sandford TC (1998) Tire chips as lightweight backfill for retaining walls-Phase II. New England transportation consortium, University of Maine.

Umashankar, B., Sravanam, S. M., & Madhav, M. R. (2017). Effect of Compaction Stresses on Performance of Back-to-Back Retaining Walls.

Wagner, N. B. (2016). Seismic earth pressure on basement walls with cohesionless backfill. UC Berkeley.

Watanabe, K., Munaf, Y., Koseki, J., Tateyama, M., Kojima, K. (2003). Behavior of several types of model retaining walls subjected to irregular excitation. Soils and Foundations, Japanese Geotechnical Society, Vol. 43, No. 5, pp. 13-27.

Watanabe, K., Koseki, K., Tateyama, M. (2011). Seismic earth pressure exerted on retaining walls under a large seismic load. Soils and Foundations, Japanese Geotechnical Society, Vol. 51, No. 3, pp. 379-394.

Wood, J. H. 1973. Earthquake induced soil pressures on structures. PhD Thesis, California Institute of Technology, Pasadena, CA.

Xiao, M., Bowen, J., Graham, M., & Larralde, J. (2012). Comparison of Seismic Responses of Geosynthetically Reinforced Walls with Tire-Derived Aggregates and Granular Backfills. Journal of Materials in Civil Engineering, 24(11), 1368-1377.

Xu, C., Luo, M., Shen, P., Han, J., & Ren, F. (2020). Seismic performance of a whole Geosynthetic Reinforced Soil–Integrated Bridge System (GRS-IBS) in shaking table test. Geotextiles and Geomembranes, 48(3), 315-330.

Xu, P., Hatami, K., & Jiang, G. (2020). Shaking table study of the influence of facing on reinforced soil wall connection loads. Geosynthetics International, 1-15.

Yang, S., Gao, Y., Cui, K., Zhang, F., & Wu, D. (2020). Three-dimensional internal stability analysis of geosynthetic-reinforced earth structures considering seismic loading. Soil Dynamics and Earthquake Engineering, 130, 105979.

Yazdandoust, M. (2017). Investigation on the seismic performance of steel-strip reinforced-soil retaining walls using shaking table test. Soil Dynamics and Earthquake Engineering, 97, 216-232.

Yazdandoust, M. (2018a). Laboratory evaluation of dynamic behavior of steel-strip mechanically stabilized earth walls. Soils and foundations, 58(2), 264-276.

Yazdandoust, M. (2018b). Seismic performance of soil-nailed walls using a 1 g shaking table. Canadian Geotechnical Journal, 55(1), 1-18.

Yazdandoust, M. (2019a). Assessment of horizontal seismic coefficient for three different types of reinforced soil structure using physical and analytical modeling. International Journal of Geomechanics, 19(7), 04019070.

Yazdandoust, M. (2019b). Shaking table modeling of MSE/soil nail hybrid retaining walls. Soils and foundations, 59(2), 241-252.

Yazdandoust, M., Panah, A. K., & Ghalandarzadeh, A. (2019). Effect of reinforcing technique on strain-dependent dynamic properties of reinforced earth walls. Soils and foundations, 59(4), 1001-1012.

Zarnani, S. (2011). Seismic performance of geosynthetic-soil retaining wall structures.

Zarrabi-Kashani, K. (1979). Sliding of gravity retaining wall during earthquakes considering vertical acceleration and changing inclination of failure surface. Massachusetts Institute of Technology.

Zeng, X., & Steedman, R. (2000). Rotating block method for seismic displacement of gravity walls. Journal of Geotechnical and Geoenvironmental Engineering, 126(8), 709-717.